

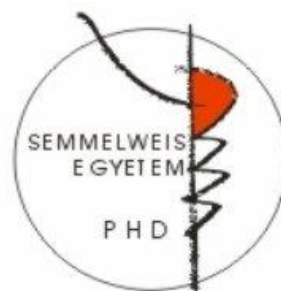
STUDY OF THE EFFECT OF P2X7 RECEPTOR PROTEIN FUNCTIONAL EXPRESSION IN THE PHENCYCLIDINE MURINE MODELS FOR SCHIZOPHRENIA

PhD thesis

Stefano Calovi

János Szentágothai Doctoral School of Neurosciences

Semmelweis University



Supervisor: Beáta Sperlágh, DSc, senior researcher
Official reviewers: László G. Hársing, DSc, scientific advisor
Maria Domercq, PhD, senior researcher
Head of the Complex Examination Committee:
Nándor Nagy, DSc, associate professor, habilitate
Members of the Complex Examination Committee:
Erzsébet Kató, PhD, assistant professor
Judit Lazáry, PhD, senior physician

Budapest

2021

Table of contents

List of abbreviations	5
1.0. Introduction structure	8
1.1. Philosophical Introduction	8
1.1.1. Upon the research in neuropsychopharmacology	8
1.1.2. Upon the research of treatments for schizophrenia	10
1.1.3. Upon the preclinical research of the Sperlagh Laboratory	11
1.1.4. Biological Question and Biological model	12
1.2. The purinergic signaling system and P2X7 receptor (P2X7R)	13
1.2.1. Extracellular ATP is a signaling molecule	13
1.2.2. Extracellular ATP and purines have specific receptors	14
1.2.3. There are three subfamilies of Purinergic Receptors	14
1.3. The research about P2X7R	16
1.3.1. From structure to function	16
1.3.2. P2X7R triggers a non-desensitizing non-selective current	17
1.3.3. P2X7R: from the gene to the functional protein	19
1.4. P2X7R as a neuropharmacological target	21
1.4.1. P2X7R cellular expression, where is the target?	22
1.4.2. P2X7R immunological functions as targets to silence inflammation	22
1.4.3. Microglia and the brain immunity	23
1.4.3.1. Microglia and extracellular ATP	23
1.4.3.2. Microglia express different purinergic receptors	24
1.4.3.3. Ramified microglia is characterized by P2Y ₁₂ R expression	25
1.4.4. The P2X7R and microglia: roles and hypothesis	26
1.4.4.1. The P2X7R and microglia <i>in vivo</i>	28
1.4.4.2. The P2X7R and microglia <i>ex vivo</i>	29
1.5. Modeling schizophrenia: the effects of phencyclidine (PCP)	31
1.5.1. The pathology of schizophrenia	31
1.5.2. Schizophrenia and PCP	32
1.5.2.1. Schizophrenia and PCP: historical overview: historical overview	33
1.5.2.2. PCP: from pharmacology to the models for schizophrenia	34

1.5.3.	Proposed models for the neurological substrate of schizophrenia	36
1.5.3.1.	Dopamine in the PCP model: positive and cognitive symptoms	38
1.5.3.2.	The glutamatergic hypothesis: search for the PCP target	39
1.5.3.2.1.	PCP and the rodents cognitive functions: the medial PFC	40
1.5.3.2.2.	Prefrontal cortex: anatomical overview	40
1.5.3.2.3.	PCP and the cortical parvalbumin (PV) interneurons	43
1.5.3.2.4.	PCP effects on mPFC: connectivity hypothesis	45
1.6.	Schizophrenia and P2X7R: the neuroinflammatory hypothesis	47
1.6.1.	P2X7 Receptor: the immunological bridge to psychiatric disorders	49
1.6.2.	Purinergic Receptors in animal models for schizophrenia	50
2.	Aims	52
3.	Materials and methods	54
3.1.	Animals	54
3.2.	Treatments	54
3.3.	Real-time qPCR	55
3.4.	Behavioral studies	56
3.4.1.	Acute treatments	56
3.4.2.	Subchronic Treatment	57
3.5.	Histology	58
3.5.1.	Acute treatment	58
3.5.2.	c-Fos DAB immunohistochemistry	59
3.5.3.	Fluorescence immunohistochemistry	58
3.6.	Confocal microscopy	59
3.7.	[³ H]-Dopamine release experiment	60
3.8.	Electrophysiology	61
3.9.	Two-photon microscopy imaging of fluorescent microglia ex vivo	61
3.10.	Two-photon fluorescent microglia movie analysis	62
3.11.	Cytokine quantification	62
3.12.	Statistics	63

4.	Results	64
4.1	P2rx7 gene expression in C57Bl/6 Prefrontal cortex	64
4.2	Acute PCP treatment-induced hyperactivity was alleviated in P2rx7 ^{-/-} mice	64
4.3	P2rx7 ^{-/-} layer-specific neuronal activation in the mPFC is lower	65
4.4	P2X7R deficiency does not affect PCP-related changes in PV interneurons	68
4.5	The PFC and dopamine release from the striatum	69
4.6	P2X7R gene deficiency may play a role in microglial contacts with hyperactive neuronal soma	70
4.7	Intrinsic properties of P2rx7 ^{-/-} mPFC layer V pyramidal neurons	74
4.8	P2X7R-EGFP overexpressing reporter mice displayed higher sensitivity to acute low-dose PCP treatment	76
4.9	Acute PCP treatment-induced hyperactivity and layer-specific neuronal activation in the mPFC was exacerbated in P2rx7 ^{tg/+} mice	77
4.10	Subchronic PCP did not induce detectable prefrontal neuroinflammation, and PCP-induced working memory deficit is absent in P2X7R deficient animals	79
4.11.	Single-cage housing condition is necessary to induce cognitive-like symptoms in the current PCP model	82
4.12.	Long-lasting effects of subchronic PCP treatments	84
4.13.	Immunohistochemical study of the P2rx7 ^{+/+} and P2rx7 ^{-/-} PFC after subchronic PCP treatment	85
4.14.	Histological profile of glial cell types in subchronically treated PCP animals	87
4.15.	Effects of P2X7R inhibition on CX3CR1 ^{+/+} -GFP ^{+/+} microglia dynamics in <i>ex vivo</i> slices, analyzed with two-photon microscopy	89
4.16.	Effect of 3 mM ATP on fluorescent microglia in <i>ex vivo</i> acute slices	93
5.	Discussion	95
5.1	Acute effect of PCP in P2rx7 genetically modified animals	95
5.2	Mechanisms involved in the acute effect of PCP in P2rx7 ^{-/-} animals	95
5.3	Hypothesis of P2X7R role in the mPFC microglial cells	98
5.4	Acute effect of PCP in animals overexpressing P2X7R	100
5.5	Subchronic PCP treatment in P2rx7 ^{-/-} young adult mice	101
6.	Conclusions	104
7.	Summary	105

8.	Összefoglalás	106
9.	References	107
10.	List of publications	147
11.	Acknowledgements	148

List of abbreviations:

[³ H]-DA	Dopamine enriched with tritium isotopes
5-HT; 5-HT _{1A/2A/2C}	Serotonin, and serotonin receptor subtypes 1A, 2A, 2C
A10 nucleus, or VTA	Ventral tegmental area
ACC	Agranular cingulate cortex
ACSF	Artificial cerebrospinal fluid
ADP	Adenosine 5'- diphosphate
AMP	Adenosine 5'- monophosphate
ASD	Autism spectrum disorder
ATP	Adenosine 5'- triphosphate
BBB	Blood-brain barrier
BBG	Organic dye, and P2X7R antagonist, brilliant blue G
bp	Base-pairs, unit of nucleic acid sequences
CNS	Central nervous system
CX3CL1	Fractalkine receptor protein ligand
CX3CR1	Fractalkine receptor protein
CX3CR1 ^{-/+} EGFP ^{+/-}	Fluorescent microglia mouse strain (213)
D2R	Dopamine receptor D2
DAB	3,3'-Diaminobenzidine, chromogen for immunostainings
dIPFC	Dorsolateral prefrontal cortex, primates
DSM	Diagnostic and Statistical Manual of Mental Disorders
EC ₅₀	Concentration of a drug that gives half-maximal response
EEG	Electro-encephalogram
FDA	Food and Drug Administration
GFAP	Glial fibrillary acidic protein, astrocytic marker
GFP, EGFP	Green fluorescent protein, and enhanced GFP
IL	Infralimbic cortex or area
IL-1β	Interleukin-one beta
<i>i.p.</i>	intra-peritoneal
IR	Infrared, light source
I _{step}	Current injection step, in patch clamp experiments

I/V	Current/voltage relationship
KO	Knock-out, P2rx7 ^{-/-} C57Bl/6J strain
LPS	Bacterial lipopolysaccharide
M1, M2	Pro-inflammatory, or anti-inflammatory/resolutive, microglial phenotypic shift.
mdTh	Mediodorsal nuclei of the thalamus
mPFC	Medial prefrontal cortex, rodents
MRI	Magnetic resonance imaging
NDS	Normal donkey serum
NMDA	N-methyl D-aspartate
NMDA-R	N-methyl D-aspartate glutamate receptor
NMDG	N-methyl D-glucamine
NO	Nitric oxide
P1, P2X, P2Y	Purinergic receptor type 1 adenosine receptor, and 2: X ionotropic type and Y metabotropic type
P2rx7	Gene sequence encoding the P2X7 purinergic receptor subunit
P2rx7 ^{+/+} , ^{-/-} , ^{tg/+}	Mouse strains genetically modified for P2rx7 gene, wild-type, knock-out (35), and heterozygous overexpressing a fusion P2X7R-EGFP protein (36)
P2X7R	P2rx7r gene products forming trimeric ATP receptors P2X7
P2Y12R	P2ry12r gene products forming metabotropic ADP receptors P2Y12
PAMPs	Pathogen-associated molecular pattern
PFA	Paraformaldehyde
PB, PBS	Phosphate buffer, and with 0.9% saline solution
PCP	Phencyclohexyl piperidine, or phencyclidine
PCR	polymerase chain reaction
PET	Positron Emission Tomography
PFC	Prefrontal cortex
PL	Prelimbic cortex or area
PNN	Perineuronal Net (Parvalbumin interneurons specialized extracellular matrix).

PRRs	Pattern recognition receptors
PV	Parvalbumin, GABAergic interneurons population marker
ROI	Regions of interest
Rt	Reticular nucleus of the thalamus
RT	Room temperature, 18-23 °C
RT-qPCR	Real-time quantitative PCR
ROS	Reactive oxygen species
SNPs	Single nucleotide polymorphisms
TG/+	Heterozygous mice overexpressing a fusion P2X7R-EGFP protein (36)
TH	Tyrosine Hydroxylase
TLR	Toll-like receptor family
Tx	Triton-x, detergent
UDP	Uridine 5' - diphosphate
V _m	Resting membrane potential
WT	wild-type, P2rx7 ^{+/+} C57Bl/6J strain

1.0. Introduction structure

The Introduction is organized in sections, describing topics from the generic to the specific. It will first introduce the history and philosophy of the research field, the approach of our laboratory and of the current work, concluding with the biological models and questions. The second part will review the purinergic signaling system and the ATP receptor P2X7 (P2X7R), main expertise of the Sperlagh laboratory, and molecular target of the current work. It will provide general knowledge about P2X7R protein, the related genetic mouse strains, its role in the brain and its potential as a neuropharmacological target. The following section will introduce the employed pharmacological model, treatments with the drug phencyclidine (PCP) that mimics various aspects of schizophrenia. Eventually, the focus will narrow on the relationship between P2X7R and the schizophrenia animal models, reviewing studies at the base of the current doctoral thesis.

1.1. Philosophical Introduction

The current dissertation encounters the need to converge two apparently unrelated topics, the purinergic signaling system and the PCP murine model for schizophrenia. The following section will introduce general concepts and provide some basic notions upon the history and development of the research field, about the idea and aim behind the clinical and preclinical neuropharmacological research. Eventually will be overviewed the culture and expertise of the laboratory run by Prof. Beáta Sperlág, where the PhD studies have been performed.

1.1.1. Upon the research in neuropsychopharmacology

The medical research field of neuropsychopharmacology has a peculiar history. The understanding of the biochemical interactions that few specific small molecules perform to maneuver the psychological status of an individual always raised deep fascination. Yet, with the development of modern medicine, it has progressively suffered from scientific skepticism among the medical community. Along the second half of the XXth century, clinical prescription of psychoactive drugs became slowly stigmatized and considered pseudo-scientific. The main reason probably lies in the series of trials and errors, of which, the field of psychiatry, failed to a great extent in predicting harmful side effects. Poor medical and pharmaceutical choices capitulated into socio-political and economic distrust. Eventually, the influence of non-science-based opinion started to weigh more

than the science-based one, often worsening legal and illegal psychoactive drug-related issues. The nature of the psychiatric investigation itself is determinant in such recurrence of misconceptions: there has never existed an objective biological measurement that allows to determine a “pathological” psychology. The concept of mental health was defined many times in different places, and was fundamentally related to the cultural background of those who are defining it. The struggle of psychiatry in constituting a unified view is well reflected along the evolution of the Diagnostic and Statistical Manual of Mental Disorders (DSM). This text is an example of the effort of the western psychiatry community (coordinated by the American Psychiatry Association) to discipline the matter. The first DSM edition was published in 1952, but its redefinition is still taking place, the latest edition being published in 2013. The aim of the DSM was to provide a universal glossary for describing the diagnostic categories of mental disorders, and to standardize clinical practices specific for the disorders (1). Interestingly, 1952 was also the year of the discovery of chlorpromazine, the very first effective neuroleptic drug, which opened the way to a novel type of neuropharmacological research. Along the DSM history, several mental disorders have been heavily misdiagnosed, and the manual has always been subject to many critiques. Both medical and non-medical communities often questioned the historical approach of psychopharmacology, which prioritized psychiatric rather than biological data. Treatments for psychiatric disorders such as schizophrenia, from the 60s, remain poorly updated today, due to the difficulties in finding clear cut benefits over side effects, with more recent drugs. Many approved treatments are typically based on the well-known dopaminergic and serotonergic pharmacology. However, along the last couple of decades, the research in neuropsychopharmacology definitively shifted towards massive collection of biological and molecular data. The development of genetics and biotechnology launched a sort of “gold rush”, to find novel drugs and molecular pathways that provide benefits against the most insidious and subtle traits of psychiatry disorders. The case of the negative and cognitive symptoms of schizophrenia, for example, happened to be historically, almost neglected. One of the paramount concerns in novel drug development is the drug safety. This reinforced preclinical research on animal models, which became the context for developing new hypotheses and biological questions. The following work contributes to answering some questions regarding two apparently independent systems: the PCP mouse model for schizophrenia, and a receptor

of the purinergic signaling system. It will be shown that, in mice, some detrimental effects associated with the symptoms of schizophrenia are modulated by the functional presence of the P2X7R protein. Curiously, P2X7R is more related to immune and glial functions, rather than to classical synaptic neurotransmission. Drugs acting on the purinergic receptors have shown repeatedly a good level of safety, but have never been tested on schizophrenic patients, making it worth the study about potential benefits.

1.1.2. Upon the research of treatments for schizophrenia

Antipsychotics, formerly known as neuroleptic drugs, are defined as drugs clinically used to control positive symptoms inside the broad spectrum of psychosis, including schizophrenia, bipolar disorder, dementia and other conditions. Neuroleptics are a category of chemically unrelated drugs, namely phenothiazine (chlorpromazine), thioxanthene (flupentixol), diphenylbutylpiperidine (pimozide) and butyrophenones (haloperidol). Many neuroleptics are still adopted as first line therapies today, all sharing a tendency to block the D2 dopamine receptor (D2R) in the brain. The D2R blockade, which accounts for variable effectiveness in counteracting the psychotic symptoms, if chronically present, often leads to undesirable side effects. These may affect motor abilities, appetite and weight, hormonal equilibrium, mental and mood state, and rarely, as well as unpredictably, development of a neuroleptic malignant syndrome can be lethal (2). The second generation of antipsychotics, carrying a mixed dopaminergic and serotonergic pharmacological activity, gained worldwide popularity during the 90s. However, beyond the lower impact on motor functions, meta-analyses have been regularly reporting no differences in the benefits between first and second generation antipsychotics (3). The pharmacology of drugs for treating psychosis was often revealed years after the introduction to clinical practice. Haloperidol, one of the most prescribed antipsychotics ever, was approved by the FDA in 1967 in the United States, yet its dopaminergic antagonism was not identified till the mid 70s (4, 5). The hypothesis of a dopaminergic dysfunction at the core of schizophrenia was proposed prior to the pharmacological discoveries on antipsychotics (6), and later endorsed by the scientific community (7). During that time, new findings established the pharmacology of phencyclidine (PCP) and ketamine, well-known for provoking acute psychosis. These drugs block the pore of the glutamate receptor N-methyl-D-aspartate (NMDA-R) (8, 9), and opened the way to the NMDA-R hypofunction hypothesis of schizophrenia, generally

referred as the glutamate hypothesis, shifting part of the research attention from dopaminergic to glutamatergic signaling (10, 11).

1.1.3. Upon the preclinical research of the Sperlágh Laboratory

From the late 90s, the murine models for schizophrenia involving PCP have been greatly exploited (Figure 1).

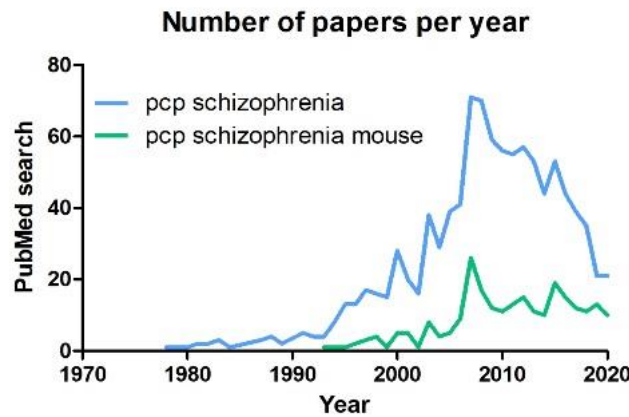


Figure 1. PubMed results of publications relating PCP with schizophrenia raised from the ‘90s.

The progressive build up of data is providing a basic understanding of the action of the drug. In the following study, the purinergic receptor P2X7 was studied in relation with the acute and subchronic PCP murine model of schizophrenia. The original idea came from Beáta Sperlágh, the director of the thesis, pioneering researcher of the purinergic signaling system neurobiology. She opened her career by widening the knowledge on the effects of ATP on the release of different neurotransmitters (12, 13, 14, 15). Later, her work focused on the study of a truly puzzling purinergic receptor, the one composed by homo-trimers of the P2X7 subunit (16), providing the initial evidence of its neuronal functional expression (17, 18). Under her direction, the Laboratory of Pharmacology of the Institute of Experimental Medicine, IEM (KOKI) contributed with several findings to basic neuropharmacology, beyond the purinergic system (19, 20, 21). The laboratory is internationally recognised for contributing to the study of the relationships between the brain purinergic signaling and mouse models for psychiatric disorders or conditions, keeping an eye of regard for the P2X7R (22, 23, 24). The strategy developed to tackle complex, and sometimes abstract, biological questions, is a multi-disciplinary approach that includes experiments on behavior, biochemistry, electrophysiology, genetics, and

molecular biology. The laboratory produced original research and reviews dedicated to the comprehension of the P2X7R functions in models of mania (25), depression (25, 26, 27, 28), autism (29) and schizophrenia (30, 31), employing a mouse line genetically lacking the receptor's full-length expression (P2rx7^{-/-}) and several antagonist drugs. Moreover, other studies explored cellular actions potentially underlying the role of P2X7R in psychiatric disorders (32, 33, 34). The line of research regarding the P2X7R in the context of the PCP model for schizophrenia sprouts from previous publications. Early indications, showing that P2X7R loss-of-function lowers the effect of amphetamines (25), suggested some P2X7R-related interactions with psychotomimetic drugs. The first study using PCP on P2X7R antagonists and genetically modified mice (30) shed lights on possible protective effects of P2X7R loss-of-function. Differences were found in the transcription levels of several neurotransmitter receptor proteins, between wild-type and P2rx7^{-/-} mice (30). At this point, we set up the biological questions and models in which to further confirm, or dismiss, the protective role of P2X7R loss-of-function in schizophrenia PCP models.

1.1.4. Biological Question and Biological model

Before any strategy and plan is in place, it is good practice in scientific research to define and justify the aim and ambition of the study. The biological question goes necessarily with the biological model, from which the experimental data will be obtained. In the case of the following dissertation, the biological question is fairly unambiguous: we asked whether PCP acts in different ways in mice genetically modified for the P2rx7 gene, and if so, to identify the underlying neurobiological mechanism. We set out that behavioral measurements shall represent the starting point of theory development, prior to targeted molecular and cellular experiments. In our previous publication, P2rx7^{-/-} mice and wild-type mice, treated with both P2X7R antagonists and low-dose PCP, expressed less psychotomimetic behaviors respect to PCP-treated P2rx7^{+/+} wild-type animals (30). This correlated with changes in expression of genes in the brain, encoding different neurotransmitter receptors and synaptic proteins (30). The current study (31, and other results), though employing a mouse strain already used in 30, attempted an unbiased approach, changing PCP dosage and experimental paradigms. The biological models are wild-type C57Bl/6 mice as controls, and mice lacking the functional expression of the full-length protein (P2rx7^{-/-}, 35) or overexpressing the functional protein fused with a

fluorescent green protein (in this study heterozygous P2rx7^{tg/+}, **36**) as testing subjects. The PCP models for schizophrenia in rodents are considered solid tools to reproduce arrays of positive, negative and cognitive symptoms (**37, 38, 39, 40**). Mice of the strains C57Bl/6J and 6N result valid for modeling schizophrenia-like symptoms with PCP treatments (**41**). In this study the PCP dosage, treatment schedule, and animal's age were optimized to induce cognitive symptoms (**42**). Eventually, an important feature, which characterizes the majority of preclinical studies about PCP and schizophrenia, is the use of males only. This controversial issue (**43**) represents a bias of which the discussion goes far beyond the objective of the thesis. We acknowledge the fact that sexual dimorphism was found in the study of the pathology of schizophrenia (**44, 45**), in the rodent purinergic system and neuroimmunological functions (**46, 47, 48**) and in the rodent cognitive functions relative to the PCP models for psychiatric conditions (**49, 50**). The current study is therefore limited to be potentially predictive for male subjects.

1.2. The purinergic signaling system and P2X7R

The protein subject of the current work is P2X7R. Even if our results focus mainly on the P2X7R protein, before describing its molecular and physiological features, it is important to understand that P2X7R is part of an ubiquitous and complex signaling system. Therefore, the following section of the introduction will present the basic concept of the purinergic signaling system, the expertise of our laboratory.

1.2.1. Extracellular ATP is a signaling molecule

Adenosine is one of the fundamental nucleosides composing DNA and RNA in every living cell. The adenosine 5'- triphosphate (ATP) is the basic energy exchange molecule, synthesized by mitochondria in all eukaryotic cells, and present at millimolar concentration in the cytosol (**51, 52**). ATP is unable to diffuse across the lipid bilayer of the cellular membrane by simple diffusion, thanks to its polarized nature. As a result, ATP is an ubiquitous and continuously renovated metabolite, highly compartmentalized inside the cells. Regarding the nervous system, ATP is stored as a co-transmitter in all nerve types, both by the peripheral and central nervous system (CNS) cells (**52, 53**). In physiological conditions, extracellular ATP is kept at concentrations in the nanomolar range (**54**). Nevertheless, ATP is released outside the intracellular compartment in response to physiological and pathological stimuli, via exocytosis and transporter-mediated release (**55, 56**). Exocytotic phenomena are considered to induce local transient

changes in purine concentrations. Thanks to an efficient neutralizing action, carried out by concerted metabolising and transporter proteins, intact tissue's parenchyma do not experience high-micromolar gradients of extracellular ATP (54, 55). A second pathway through which ATP pours into the extracellular milieu happens through membrane leakage. This situation is common in case of dying cells, tissue getting injured, and in general when a system is under stress (54). In these pathological cases, a surge of extracellular purines reaches concentrations of hundreds of micromolar (57, 58). The ectoenzymes are enzymes that rapidly convert ATP into Adenosine di-phosphate (ADP), Adenosine mono-phosphate (AMP), and adenosine. Extracellular nucleotide-hydrolyzing proteins are ubiquitously expressed by all cell types, and get modulated by several environmental factors (59). Extracellular adenosine is eventually transported back inside the cytosol by nucleosides transporters such as ENT1 (60). Along this journey, extracellular ATP and related metabolites exert pharmacological actions on a large family of receptors, called purinergic receptors, composing an entire intercellular communication system, highly conserved from an evolutionary point of view (61, 62).

1.2.2. Extracellular ATP and purines have specific receptors

The original identification of purine-related pharmacological activity, namely the effects of adenine compounds on the mammalian circulatory system, was originally reported in the 1920s by Drury and Szent-Gyorgyi (63). The identification and study of the ATP release from sensory nerves was first published in the 1950s (64, 65). Almost 50 years after the first publication, studies guided by Geoffrey Burnstock confirmed that extracellular nucleotides and nucleosides are transmitters and modulators of a widespread signaling system (66, 67, 68). Burnstock, with its many collaborations, greatly propelled and accompanied the research development of the whole “purinergic” field. The international purinergic community, celebrated his lifelong passion after his death in 2020, by entitling him as the “creator of the purinergic signaling” (69). Progress of biotechnologies, during the 90s, opened the way to the electrophysiological and pharmacological classification of single subunit-purinergic receptors (70, 71). Purinergic receptors are abundantly expressed in different cell types and systems, including the CNS. The endogenous agonists acting in the nervous system include adenosine, ATP, ADP, uridine diphosphate (UDP), uridine triphosphate, or UDP-glucose (72).

1.2.3. There are three subfamilies of Purinergic Receptors

Purinergic receptors are divided into three subfamilies: P2X receptors, P2Y receptors and P1 receptors. The P2X receptors subfamily are trimeric ionotropic channels, while the P2Y and P1 subfamilies are G protein-coupled metabotropic purinergic receptors. Each subfamily has seven (P2X1, 2, 3, 4, 5, 6, 7), eight (P2Y1, 2, 4, 6, 11, 12, 13, 14, 15, 16) and four (P1A1, 2A, 2B, 3) subunits, respectively (73).

The P2X receptors, phylogenetically, are the oldest family of receptors activated by purines (61, 62), reported on an algae's intracellular organelles, likewise the mammalian P2X4R (74). P2X receptors activate exclusively upon ATP-binding, sensitive from nanomolar (P2X1 and P2X3 receptors) to low micromolar ATP-concentrations (P2X2 and P2X4 receptors). As an outlier, sensitive to hundreds of micromolar ATP, stays the P2X7 receptor (72). In addition, each receptor subtype displays different desensitization dynamics (75, 76). Ligand-binding opens a nonselective pore permeable to Na⁺, K⁺, and Ca²⁺ cations (77). Moreover, some P2X subunits provide an additional pathway for the passage of large organic cations (77, 78). The diversity of P2XR trimeric ionotropic channels depends on their homomeric or heteromeric subunit composition (79). Their expression and function is scattered throughout all mammal's physiology (80).

P2Y metabotropic receptors present a diverse nucleotide selectivity (72). The P2Y11 receptor is the only P2Y receptor sensitive to and selective for ATP (EC₅₀ ≈10 μM). Interestingly, the P2Y11 receptor is expressed in humans, but its orthologous gene is absent in the murine genome (81). Receptors activated by ADP are the P2Y1R (EC₅₀ ≈10 μM), P2Y12R (EC₅₀ ≈0.01 μM) and P2Y13R (EC₅₀ ≈0.001 μM). The P2Y2R is activated by both ATP (EC₅₀ ≈0.1 μM) and UTP (EC₅₀ ≈0.01 μM). The P2Y4R recognizes UTP as an agonist (EC₅₀ ≈1 μM), while ATP acts as an antagonist in humans and a full agonist in mice (82). The receptors sensitive to UDP are the P2Y6R (EC₅₀ ≈0.3 μM) and the P2Y14R (EC₅₀ ≈0.1 μM), the latter also activated by UDP-sugars (EC₅₀ ≈0.3 μM). The EC₅₀ values were taken from the comprehensive review by Jacobson and Muller (72).

The P2Y1R, P2Y2R, P2Y4R, P2Y6R, and P2Y11R intracellularly couple to G_q/G₁₁ proteins, leading to generation of inositol-1,4,5-triphosphate, subsequently increasing intracellular Ca²⁺ by release from the endoplasmic reticulum. The P2Y12R, P2Y13R, and P2Y14R couple to G_i/G₀, inhibiting adenylyl cyclase, and thereby affecting intracellular Ca²⁺ (83).

Eventually, the family of adenosine purinergic receptors consists of four metabotropic receptors. Adenosine acts as a ligand on the extracellular surface of the cell before being transferred inside the cell. The adenosine receptors A₁ and A_{2A} are abundantly expressed in the CNS, where their roles were principally studied in the modulation of synaptic transmission. A_{2A} displays facilitating effect, by enhancing long-term potentiation, in response to high-frequency activity. It is counterbalanced by the inhibitory effect of A₁ receptor (84).

1.3. The research about P2X7 receptor

The main subject of the current dissertation is the P2X7R, therefore next is introduced the research about this protein. Nonetheless, since the purinergic receptors all share the fundamental agonist ATP, but typically present much higher affinity than P2X7R, it is important to keep in mind that P2X7R is just a small part of a large purinergic picture.

1.3.1. From structure to function

Depending on the trimeric compositions and the location of the expression, P2X receptors exert physiological processes ranging from synaptic transmission, contraction of smooth muscle, secretion of chemical transmitters and regulation of the immune responses (52, 80). In 2009 the first resolved structure of a P2X receptor ectodomain and transmembrane regions in the closed state was published (85). Three years later, the analysis of the receptor interaction with ATP definitively confirmed the P2X trimeric composition, describing the subunit shape similar to a jumping dolphin (86). Structural information on the architecture of the P2XR family was enriched by X-ray studies on an invertebrate P2X receptor (87) and a minimally truncated human P2X3 receptor (88, 89). At the end of 2016, the analysis of the crystal structures of a mammalian (*Ailuropoda melanoleuca*) P2X7 truncated receptor was published, resolving the receptor interacting with ATP and five structurally-unrelated specific antagonists (90). In this study, the tested antagonists all interacted with a single allosteric binding site, distinct from the ATP-binding pocket (90).

The shape of the P2X7R is described as three “dolphin-like” subunits, collectively resembling a chalice, with the base in the membrane and the cup extracellular. The ATP-binding pockets are extracellular, at the interface between subunits. Upon binding to ATP, the ion channel opens by conformational changes of the lower part of the receptor (86,

90). The binding site of the endogenous agonist ATP is well-conserved among the different P2XR (**91**).

The function of P2XR was shown to be allosterically modulated by divalent cations as Mg^{2+} , Ca^{2+} and Zn^{2+} (**92, 93**), steroids (**94**) and lipids (**95**).

The length of the seven P2X subtypes ranges from 384 amino acids for the P2X4R, to 595 amino acids for the P2X7R, the longest, thanks to its exceptionally extended C-terminal tail (**96**). P2X subunits have two transmembrane domains (which contributes to the pore gate), two cytoplasmic (NH_2 and $COOH$) termini and a large extracellular loop forming the ATP binding motifs, with five conserved disulfide bonds (**97, 52, 79**). While several subunits were found to form heterotrimers, the P2X7 seems to form exclusively homotrimeric channels (**98, 52**).

1.3.2. P2X7 receptor triggers a non-desensitizing non-selective current

The activation of P2X receptors triggers non-selective cationic depolarizing currents (**52**). The gating of P2X receptors channels consists of an activation phase, a desensitization phase (in continuous presence of the agonist), and a deactivation phase. The current's characteristics are determined by the subunit sensitivity and trimeric composition, which confers specific activation/desensitization rate (**77, 99**).

Interestingly, the P2XR affinities for ATP combine with three ranges of desensitization rates. The nanomolar sensitive P2X1R and P2X3R are desensitizing in the order of milliseconds. The micromolar sensitive P2X2R and P2X4R display slow desensitization, in the order of seconds. P2X7R, sensitive to hundreds of micromolar extracellular ATP, often exhibits complete lack of desensitization (**75, 76**). The rate of P2X receptor desensitization depends on the stability of the intracellular domain, termed the “cytoplasmic cap” (**88, 89**).

Recently, a cryo-electron microscopy study proposed a complete model for the full-length rat P2X7R structure, in both opened and desensitized states (**100**). In this work it is shown that P2X7R, differently from other P2XR, concedes little access to the ATP pocket, partly explaining its lower affinity. The P2X7R intracellular C- and N-termini form two unique cytoplasmic elements, the C-cys anchor and cytoplasmic ballast (**100**). Palmitoylation, known to prevent the P2X7R desensitization (**101**), was detected on five residues of the C-cys anchor. The authors also identified a novel intracellular zinc complex and a GTP/GDP binding site (**100**). It is known that extracellular zinc modulates P2X7R

functions (**102, 103**), and was recently demonstrated within hippocampal neuron-glia primary cultures (**34**).

An interesting property, which still raises scientific debates, is the so-called P2X7R dependent “macropore” formation. In addition to the persistent activation, upon sustained stimulation by millimolar ATP concentrations, P2X7R typically induces the formation of aqueous pores on the cell membrane, permeable to molecules up to 900 Da, and leading to the disruption of the ionic homeostasis of the cell (**104, 78**).

Since its first appearance in the literature, the P2X7R current, originally named “ATP⁴ receptor”, has been associated with cell permeabilization (**105**). With progress in the field, different ATP receptors, called either ATP⁴R, P2ZR or P2X7R, and recognized upon distinct affinities for ATP, emerged to be products of the same P2rx7 gene (**106**). The primary differences between these P2X7R variants concerned the threshold to trigger the macropore formation. The homologous genes P2rx7 and P2rx4 (**107, 108**) encode slowly desensitizing ion channels, and both are abundantly expressed in the CNS. Yet, the EC₅₀ values, millimolar and low micromolar respectively, suggest that they specialized to operate in different environmental conditions (**109**). The P2X7R-related non-desensitizing currents, which can mature into membrane permeabilization, are common features of both human and rodent immune cells (**110, 111**). The discrepancies, coming from early measurements of the P2X7R-ATP dissociation constant, eventually appeared to revolve around the presence of divalent cations (Ca²⁺ and Mg²⁺, **112, 105**). Divalent cations bind ATP, further reducing its affinity for P2X7R, and increasing the channel’s activation threshold (**113, 77**). There has been a long-lasting debate about the molecular substrate of the P2X7R “macropore”. Recently, a single-channel electrophysiological study demonstrated that the full-length P2X7R does not dilate intrinsically its ionotropic pore, despite strong and persistent stimulation, suggesting that the macropore must be constituted by an auxiliary channel (**114**).

An essential mechanism to understand P2X7R is called priming. The priming is the early cellular response to immune challenges (infections) and to exposure to immunity-signaling molecules (inflammation). Part of this response is the sensitization of P2X7R current, carried by a number of modulative agents (**115**), possibly acting on both the extracellular and intracellular domains (**116, 117**). Upon activation of the P2X7R aqueous macropore, the release of large-scale ATP in the extracellular milieu amplifies the

signaling, thus propelling inflammation (**118**). As a general rule, to specifically activate the P2X7R ionotropic cationic channel, it is recommended brief acute exposure to a few hundreds micromolar ATP (**119, 120, 52**). Electrophysiology suggests that, under physiological conditions, the P2X7R should remain mostly silent. A reasonable hypothesis considers that thanks to its low affinity, the P2X7R pro-inflammatory actions only take place under extraordinary conditions. Many pathophysiological functions of P2X7R are thought to depend on the macropore formation, rather than the ionotropic current (**78**). Therefore, understanding and predicting which type of P2X7R activation takes place in a determined context, may be helpful when drawing conclusions over pathological events and models.

1.3.3. P2X7R: from the gene to the functional protein

The *P2rx7* gene is located in the human chromosome 12q24.31, and in the mouse chromosome Chr.5, 62.50 cM, originating probably from *P2rx4* gene duplication (**107, 108**). While 9 splicing variants are reported in humans, 4 alternative P2X7R subunits have been identified in the mouse (**108**). In humans, the full-length gene product (P2X7A) is generally less expressed than the variant P2X7B, a COOH-truncated isoform (**121**). The functional P2X7B receptors are incapable of generating macropores, and P2X7A and B isoforms can assemble into a mixed heterotrimer (**122**). The mouse truncated variant P2X7k, on the opposite, was reported to escape the channel inactivation, acting as a gain-of-function isoform (**123**).

Since modifications of the gene lead to important functional differences, the current section will focus on genetically modified knock-out mouse lines, including the one used in this study. At least two strains of P2X7R knock-out mice are currently commercially available. GlaxoSmithKline produced a line in which, in exon 1, has been inserted the lacZ gene and neomycin cassette (or Neo, **124**). The second line, from Pfizer, and commercially available over C57Bl/6 background from the Jackson Laboratory (one of the line used in the current study, *P2rx7^{-/-}*), has a portion of the exon 13, encoding Cys506 to Pro532, deleted and replaced with a Neo-cassette, truncating the long C-terminal cytoplasmic tail (**35**). Later identification of partial-length P2X7R splicing variants disclosed the alternative P2X7R isoforms expression in T-cells from both the knock-out lines. However, the P2X7R knock-out strategies effectively abolished the protein expression in macrophages and neurons (**125, 126**). Moreover, while the

GlaxoSmithKline line derived T-cells presented a functional P2X7R activity, responses to the BzATP stimulation were not detectable with Pfizer mice T-cells (**127, 125**). Regarding the brain, cerebellar neurons and midbrain synaptosomes from the Pfizer knock-out line resulted positive for P2X7R expression and current, measured through Ca^{2+} imaging. Yet, the current's analysis indicates a loss-of-function mutation in the Pfizer P2rx7 knock-out gene (**128, 129**). Two truncated variants of the mouse P2X7R, supposed to escape the Pfizer inactivation strategy, were recently identified, both displaying lower current amplitudes than the P2X7A variant (**126**). The C57Bl/6 genetic background, over which the Pfizer P2X7R knock-out mouse line was developed, co-express the P2X7A and P2X7k isoforms in every system (**130**). The P2X7k variant harbors an alternative exon1, encoding different N terminus and TM1 domain, that in oocytes conferred an 8-fold increase for Bz-ATP sensitivity, slower deactivation and increased propensity to form macropores (**130**).

Eventually, interindividual differences may depend on mutations termed single nucleotide polymorphisms (SNPs). Several SNPs have been identified in the human and mouse P2rx7 gene. Co-presence of more than one SNP often generates entangled haplotypes excessively complex to decipher (**107, 108**). One SNP worth mentioning for the aims of this study is the mouse P2X7R P451L missense mutation (**131**). This mutation generally produces a loss-of-function P2X7R^{L451}, and resides in some classical experimental animal strains, including the C57Bl/6 mice used in the current study. The mouse P2X7R^{L451} genotype was linked to impaired glucose homeostasis and higher bone fragility (**132, 133**).

The control animals for the current study are C57Bl/6 mice, expressing a mixture of P2X7A and P2X7k splicing variants harboring the SNP P451L. They are compared with C57Bl/6 homozygotic Pfizer P2X7R knock-out mice (P2rx7^{-/-}). While not adequate to study the absolute role of the protein, it is advocated that the truncated P2X7R solve the ionotropic channel functions, but is less efficient in triggering the "macropores". This makes Pfizer P2X7R knock-out derived cells less prone to apoptosis, either through membrane blebbing (**134**) or caspase activation (**121**). The long intracellular C-terminal domain was found to be necessary for the cytolytic action of ATP (**122, 106**). It has been observed that the Pfizer P2X7R knock-out line, and the five P2X7R unrelated antagonists, are both associated with a minimization of P2X7R aqueous pores (**78, 90**).

Results from expression analysis of young-adult prefrontal cortex (PFC) P2rx7 mRNA, in controls and P2rx7^{-/-} C57Bl6 mice, will be presented and discussed (Figure 4).

1.4. P2X7R as a neuropharmacological target

The P2X7R agonist ATP is reported to have an EC₅₀ value of 2 to 4 millimolar, with BzATP as the only non-specific exogenous agonist available, effective at hundreds of micromolar (52, 72). The idea that the blockade of P2X7R should hinder the basic inflammatory process raised considerable attention towards P2X7R antagonists. In the brain, neuroinflammation is essentially described as the innate immune system activation, dependent on inflammatory-mediators signaling (22). P2X7R antagonists displayed significant levels of protection in preclinical models carrying an evident neuroinflammatory component, including pain-models (neuropathic, inflammatory, nociceptive and chronic), multiple sclerosis, neurodegenerative disorders, cerebral ischemia, brain and spinal cord injury, depression, anxiety and bipolar disorders models (135, 136). P2X7R pharmacology was also tested in oncology, including for treatments of brain cancers, displaying potential benefits (137). It is worth keeping in mind that different P2X7R antagonists are still proceeding through tens of clinical trials, usually showing high tolerability and encouraging efficacy (138, 139). About psychiatric conditions, the P2X7R antagonist JNJ-54175446 is currently tested in a Phase II clinical trial for major depressive disorder (140). Development of radioligands based on P2X7R high-affinity antagonists is emerging as a diagnostic tool for neuroinflammatory events (141; 142). All considered, the research on P2X7R produced an array of specific antagonists, which, though promising, still need refinements before becoming solid therapies (22, 72). The scattered efficacy of P2X7R-related drugs throughout individuals is partly explained by the genetics of P2X7R (143). The detection of one common allosteric site for five different antagonists, different from the ATP-binding pocket, and with higher affinity in the absence of ATP binding, is indicative of a few considerations (90). For example, in case of a pathological insult involving high levels of extracellular ATP, the P2X7R antagonist pre-treatment, rather than co-treatment, may be more effective.

For the current study, we considered that P2X7R-pharmacological studies would imply an overwhelming enrichment in complexity, therefore we have limited experiments on genetic models. Comprehensive reviews about the latest progress in purinergic

pharmacology of the central nervous system are Gunosewoyo and Kassiou (144) and Jacobson and Muller (72).

1.4.1. P2X7R cellular expression, where is the target?

The P2X7R expression, in mammals, distributes throughout the whole body (80). The protein is abundantly expressed by innate and adaptive immune cells, namely monocytes, macrophages, neutrophils, lymphocytes and mast cells among others. It is also found in epithelial cells, fibroblasts, osteoblasts and pituitary cells (52, 80, reviewed in 145, 146). In the CNS, P2X7R outlines the membrane of both microglial and oligodendroglia lineage cells (36). As for neurons, while several pieces of indirect evidence were provided, a proof beyond doubt is still missing (17, 18, 147, 148). The publication that exhibited the direct visualization of P2X7R protein, via confocal microscopy at 20X magnification, although claiming the absence of expression in neurons, could not resolve the synaptic expression (36). Demonstrative pictures (confocal microscope, 60X magnification), taken on the same P2X7R-EGFP mouse line, display the presence of P2X7R “punctated” background signal, fairly resemblant of synaptic protein immunostaining (31, Figure 2). Such P2X7R “puncta” signals can be possibly characterized only by superresolution microscopy studies.

Many neuroscience studies regarding P2X7R have focused on microglial cells, considering the abundant expression, alongside the established immune-related functions (149). So far, it seems that microglia is one major cell type targeted by purinergic signaling, inside the CNS (109). Microglia, *in vivo*, constitutively express P2X7R (150), and keep its functional expression *ex vivo* as well (151). The expression level is dependent on the microglia phenotypic shift, but was also found affected by minor differences between similar pathological contexts (109, 152).

1.4.2. P2X7R immunological functions as targets to silence inflammation.

During the 70s, while Geoffrey Burnstock was defining adenine compounds as neurotransmitter-like molecules (66, 67, 68), the first article reported the release of histamine driven by ATP, in immune cells (153).

Identification of the innate immunological response pathways, revealed that P2X7R plays a crucial pro-inflammatory role, as the second stimulus of a two-hit model (154). The first hit, previously referred to as priming, consists of signaling by damage-associated molecular patterns (DAMPs) or pathogen-associated molecular patterns (PAMPs). This

wide spectrum of molecules activates the pattern recognition receptors (PRRs), including the Toll-like receptor (TLR) family (152). The TLR activation “warns the surroundings” about the presence of a pathogen, by inducing ATP release in the extracellular space (115, 155). Concurrently, the priming cascade activates the transcription factor NF- κ B pathway (156). Nuclear translocation of NF- κ B promotes the transcriptions of several genes, many responsible for inflammation and part of a P2X7R concerted strategy, like pro-IL-1 β and proteins of the inflammasome complex components. The second hit is the extracellular gradient of hundreds micromolar ATP, typical of acutely inflamed tissue, which activates P2X7R channels. The P2X7R current generates a K⁺ efflux, which in turn leads to several interleukin and chemokine release (157, 158), the assembly of the complex inflammasome and its proteolytic cascade, performing pro-caspases cleavage (159, 160). Activated caspase-1 rapidly processes pro-interleukins to their mature form, allowing their release, but if not promptly neutralized eventually initiates cytotoxic events (107, 158). Moreover, the P2X7R stimulation promotes the production of toxic free radicals (161). Molecular structural and functional studies found interactions between the long P2X7R intracellular C-terminal tail and twenty proteins involved in immunological functions (96). The P2X7R persistent activation, leading to non-desensitizing depolarization currents and “macropores” (78), has been considered essential for the cleavage and secretion of cytokines (162). Yet, P2X7R cytolytic death leaves behind a damaged and inflammogenic environment, giving a dichotomous meaning to its activation’s type (163).

1.4.3. Microglia and the brain immunity

Microglia is the principal immune-competent cell type resident in the CNS, guiding immunological responses, and maintaining the physiological condition. Microglial cells are sensitive to the smallest changes in the chemical environment. Within diverse pathological conditions, such as apoptosis, trauma, inflammation and infection, microglia undergo a phenotypic pro-inflammatory shift, the so-called activated state (109). The behavior of microglia results from the confluence of the internal cellular state, and a multitude of different signaling systems, operating in synergy or competition (164). The purinergic signaling system is one of microglia's principal determinants (165, 166).

1.4.3.1. Microglia and extracellular ATP

ATP is kept at low nanomolar levels in the parenchyma of the brain (54). Microglia is the principal CNS cell type involved in extracellular ATP degradation. On the microglial surface, ATP gets rapidly metabolised by the ectonucleotidase CD39 (or NTPDase1) to ADP and AMP (167). Microglia migration in response to pathological stimuli is impaired in CD39-depleted animals (168). The catalysis of ATP, operated by CD39, is pivotal for the ADP-driven chemotaxis, and the resulting microglial displacement. Indeed, the mechanism pulling the microglial branches towards gradients of increasing ATP concentrations, depends on the P2Y12R activation, sensitive to sub-micromolar ADP gradients ($EC_{50} \approx 0.01 \mu\text{M}$, 72, 165, 166, 168). The ectonucleotidase CD73 completes the cycle, by converting AMP to adenosine. In physiological conditions, ectonucleotidases prevent the activation of microglial P2XRs, a factor correlated, for example, with lower phagocytic profile (169). It has also been suggested that adenosine helps to maintain the ramified physiological morphology (170).

ATP is a complex neuro- and glio-transmitter. Small gradients of ATP occur spontaneously, generated within the normal brain homeostasis (55). Fluctuations of nanomolar ATP gradients are reflections of the brain neurological activity, behaving as a tonic signal. In a pathological scenario that involves ATP leakage (57, 58), local surges diffuse freely, building a gradient, and contemporarily being catalysed into a spectrum of active ligands. The impact of extracellular ATP on microglial range significantly, from chemotaxis to death signaling (150). Therefore we summarize the most important purinergic receptors functionally expressed by microglia.

1.4.3.2. Microglia express different purinergic receptors

The expression profile of microglial P2Rs is well-established, and only minor changes along the postnatal cortical development (171), or depending on sex and age (172), are documented. Electrophysiological studies in mice showed that male microglia have a slightly depolarized membrane's voltage, respect to female microglia, and are more sensitive to ATP-evoked P2X currents. This evidence correlates with the higher expression measured in male microglia, regarding P2Y12R, P2X4R, and P2X7R (47).

In-vitro microglia, stimulated with extracellular ATP, display two antagonizing currents: an early P2XR depolarizing current, and a delayed K^+ hyperpolarizing current, leaned on P2YR-dependent transactivation of K^+ channels. Following both P2XR and P2YR activation, a characteristic increase in the intracellular Ca^{2+} concentration is observed

(173). It is worth mentioning that microglia are extremely delicate, and every experimental condition introduces important perturbations on these cells, building up unavoidable artifacts (174, 175). It was only recently possible to estimate the membrane potential of ramified mouse microglia in a reliable manner. It appears remarkably depolarized, around -35/-40 mV *in vivo*, mainly driven by K⁺ channel expression (176). Nowadays, a resting potential of at least -40 mV, is becoming the mandatory requirement for studies of microglia physiology (47, 177, 178). Microglia specific mechanisms and P2YR-mediated modulation of electrophysiological activity are better understood than the P2XR-related one. On the other hand, P2XRs have been extensively investigated in relation with broader immunological functions, in several disease models. (109).

1.4.3.3. Ramified microglia is characterized by P2Y12R expression

The metabotropic P2Y6R, P2Y12R, and P2Y13R are abundantly and stably expressed by ramified microglia, within homeostasis.

The microglial P2Y6R expression mediates the extracellular UDP-mediated microglial phagocytic activity (179). Thanks to this mechanism, microglia perform the cleaning of the whole brain volume, eliminating all types of debris (180). The mammalian ramified microglia in physiological conditions is defined by abundance of P2Y12R and P2Y13R (109,181, 182). While P2Y13R has been mostly neglected by researchers till very recently, the P2Y12R has been extensively characterized. P2Y12R is commonly adopted as a microglial molecular marker. Also in the current study, monoclonal antibodies against P2Y12R were employed to precisely resolve microglial morphology (31, 183). The P2Y12R expression lowers along the shift towards a pro-inflammatory phenotype, possibly labelling sites of infections and neuroinflammation (166). The CD-39-generated extracellular ADP activates P2Y12R at low μ M concentrations, and triggers branch chemo-attraction (184). Notably, not a uniform large ATP increase, but the appearance of micro gradients, has been proven indispensable to this mechanism (185). P2Y12R activity mediates the directional extension of microglial branches toward the source of the purines (186, 187). It was recently confirmed that, the P2Y12R specific activation, is sufficient and necessary for such ATP chemotaxis *ex vivo* (178). Instead, the morphology and surveillance activity of microglia, the spontaneous continuous extension and retraction of its branches, appeared to depend on the membrane potential (177, 178). P2Y12R governs local membrane potential, via downstream regulation of TWIK-related

Halothane-Inhibited K^+ 1 channel hyperpolarizing current (178). The P2Y12R intracellular cascade competes with other metabotropic receptors, to balance the levels of local cyclic AMP, which ultimately determines the behavior of each microglial branch (83, 188). Microglial ATP-chemotaxis is an immediate response to pathological signs. If a neuron starts leaking ATP, it will rapidly get surrounded and contacted by several microglial branches (189). Therefore, P2Y12R is critical in the early response to viral infections. The receptors formed clusters on the microglial membrane that is in contact with the neuronal surface, and microglia appeared able to discriminate, isolate and dismantle the infected neurons (190). Eventually, an authoritative recent work identified the presence of a novel microstructure, a transient microglia-neuronal soma putative synapse. Authors suggested that from the neuronal membrane, purine-filled exocytotic vesicles release ATP, which diffuses at the interface limited by P2Y12R-enriched microglial surface (183). The role of these synapses was hypothesized to be neuroprotective (189, 191), yet more research is needed to elucidate this exciting phenomenon. In summary, when microglia are in physiological conditions, P2YRs are fundamental in damage-sensing chemotaxis, phagocytosis and surveillance.

1.4.4. The P2X7R and microglia: roles and hypothesis

The P2X receptors mainly expressed by microglia are the P2X4R and P2X7R. P2X4R is sensitive to nano- to micromolar ATP concentration, and desensitizes in seconds. For a recent review about P2X4R and microglia, see Suurväli et al., 2017 (192).

The P2X7R, sensitive to pathological concentrations of ATP, should remain silent in physiological conditions (72). This peculiar pharmacological range, made P2X7R the most studied microglial purinergic component (109). As mentioned, P2X7R are constitutively expressed by microglia (150, 151), but its levels vary between different studies, even considering different models of the same disease (193, 185). Considering the ionotropic nature of the receptor, its obvious role should be linked to membrane potential. Yet, little is known about the electrophysiological response evoked by microglial P2X7R (173, 194). Due to the difficulties in isolating these cationic currents, mainly for the lack of P2X7R specific agonists, the evaluation of the role of P2X7R mostly took place in complex systems, and sustained by the study of available loss-of-function genetic models.

One of the first treatments found to induce a consistent effect on central P2X7R is the injection, local or systemic, of bacterial lipopolysaccharide (LPS), which is an agonist of the TLR4, and has been considered a standard for P2X7R microglial studies (157, 195). LPS-driven microglial TLR4 stimulation induces the transcription of pro-inflammatory mediators, P2X7R upregulation, and ATP-dependent P2X7R autocrine stimulation (118). The activation of P2X7R leads to the release of cytokines, interleukines, nitric oxide (NO) and reactive oxygen species (ROS), and cell proliferation (195, 152). Sustained activation of this proinflammatory cascade activates a phenotypic shift, characterized by amoeboid cellular morphology that was originally described in macrophages as M1 phase (196). A considerable effort was invested in searching for molecular markers and switches able to tag or trigger the microglial phenotypic shifts, also including the P2X7R (197, 198). Nowadays, the concept of a microglial spectrum of phenotypes is preferred to the classical M1 (proinflammation) versus the M2 (resolution) microglial shift, since these are considered the spectrum's extremes which are rarely found in absolute forms (199).

The P2X7R-dependent release of chemokines and cytokines depends on the transactivation of proteolytic caspases (200). The activation of microglial P2X7R, both *in vivo* and *in vitro*, was found to trigger the assembly of the NLRP3 inflammasome complex, the master-regulator of caspase transactivation (150, 201). However, inflammogenic functions of central P2X7R were also reported in non-microglial cells, as the case of spinal ROS production, dependent on the neuronal P2X7R activation (202). The P2X7R induced Ca^{2+} -influx was also shown to trigger microglial membrane blebbing and microvesicle secretion (203), even though a recent investigation questioned this role (204). As for the formation of aqueous macropores following persistent P2X7R activation (78), different *in vitro* studies argued for cytotoxicity to increase viability, supporting opposite conclusions (197, 205, 206). Microglial P2X7R is also considered a promising PET target for the detection of microglial activation, and therefore neuroinflammation (142, 207).

As aforementioned, several P2X7R antagonists are thought to block preferentially the macropore formation (78), leaving intact the cationic current and its modulatory role for phagocytosis (208). The effects of antagonists on buffering the microglial proinflammatory shift in models of inflammatory diseases (163), epilepsy (209), and neuropsychiatric conditions (210) have been recently reviewed. On the other hand, there

are also reports suggesting P2X7R-activity dependent neuroprotection (151). The specific mechanisms following microglial P2X7R activation or inhibition have been extensively speculated, yet, direct measurements on microglia are challenging (211), and little evidence is currently available.

1.4.4.1. The P2X7R and microglia *in vivo*

Microglia have two unique features among brain cells. First it is a radar, scanning the extracellular environment for any clues of damage (164). Second, it is the repairer. Microglia respond to environmental changes by morphological adaptation, in the timescale of seconds to minutes (175, 177, 178, 188, 190). Such sharp sensitivity introduces significant morphology-related artifacts, even with procedures like *in vivo* anesthesia and fixation (175). In the current study, the protocol for transcardial fixation involved phosphate buffer saline (PBS, see methods) and 4% paraformaldehyde perfusion, being reported to be the most reliable for observations upon microglial shape (175).

When the pathological events include brain injuries, it is typically followed by a surge of extracellular ATP, from damaged cells, and probably amplified by astrocytic release (212). The ATP and UTP, released during early stages of apoptosis, act as a “find-me” and a “eat-me” signals, respectively (165, 179, 180). Sustained mM ATP gradients eventually induce the pro-inflammatory shift of microglia. Pathological events that do not perturb tissue integrity and cellular death, like the effects of psychoactive drugs such as PCP, likely introduce small nM/ μ M fluctuations of extracellular ATP concentrations, primarily driven by neuronal activity (54, 55). PCP acts as a non-competitive NMDA-R antagonist, inducing both direct inhibition and indirect disinhibition of neuronal activity in different circuits. Yet, PCP hardly provokes any significant damage to the brain tissue (9, 10, 11, 37-40). Peaks of neuronal activity, such as the PCP-driven hyperactivity of murine medial prefrontal cortex (mPFC, 10, 31), are predicted to result in low μ M ATP levels (54, 55), questioning the possibility of ligand-driven activation of P2X7R.

Nonetheless, it could be speculated that very small, confined, and poorly perfused extracellular compartments, alongside dysfunctions of the ATP degradation chain, may transiently be subject to high local ATP concentration. However, P2X7R-related activities, at any developmental stage previous to experiments (in our study, 2-3 months young-adult mice), could have triggered a cascade of adjustments, eventually producing

systemic differences between genetic models. One last, yet legitimate, hypothesis points to the possibility of P2X7R functions, which are independent from ATP binding. We acknowledge that, with the available resources, the current study was not designed to verify possible P2X7R ATP-independent activation.

1.4.4.2. The P2X7R and microglia *ex vivo*

In the last period of the PhD training, I got the opportunity to directly assay the P2X7R cellular expression and function using two genetically modified mouse lines.

The reporter mouse line P2rx7^{tg/+} (36), allowed to verify the coexpression of P2X7R-EGFP and microglial markers in prefrontal slices. The pictures indicated abundant, but not exclusive, receptor's expression in microglial cells (Figure 2). Although coming from observations on overexpressing transgenic animals, the P2X7R expression by prefrontal microglia seems reasonably evident.

Furthermore, under the supervision of Professor Tønnesen, I got introduced to the 2-photon microscopy technology. This allowed me to directly assay the P2X7R activity in relation with microglial dynamics, in few preliminary experiments, using heterozygous animals from a popular mouse line with green fluorescent microglia (213, Figures 18-22). Starting from electrophysiology acute-slice preparation, the protocol was optimized for thick-slice 2-photon imaging (see methods). Predictably, *ex vivo* slice preparation represents a dramatic input for microglial cells, which undergo a dramatic change (176), for a great part still uncovered. After the sacrifice, the cut further annihilates the spontaneous neuronal activity, and fills the parenchyma with intracellular substances and cellular debris. Nonetheless, during the first 4/5 hours after the cut, at 100 μm depth from the cut surface, the inner tissue is considered minimally perturbed, and the related data are considered valid to study microglia physiology (176, 177, 178). Additionally, genetic labeling of specific cell types also introduces biases and developmental adjustments. In the model employed in the current study, an EGFP sequence substitutes the native fractalkine receptor protein (CX3CR1) (213, Figures 18-22). Since the CX3CR1 signaling is fundamental for the development and viability of microglia, heterozygous mice CX3CR1^{+/-}EGFP^{+/-} are typically employed, also considering they display a rather normal phenotype (213). Finally, as long as two-photon-related phototoxicity is an

unavoidable artifact, we carefully settled the laser according to already published works (177, 178).

EGFP-P2X7R expression in mPFC

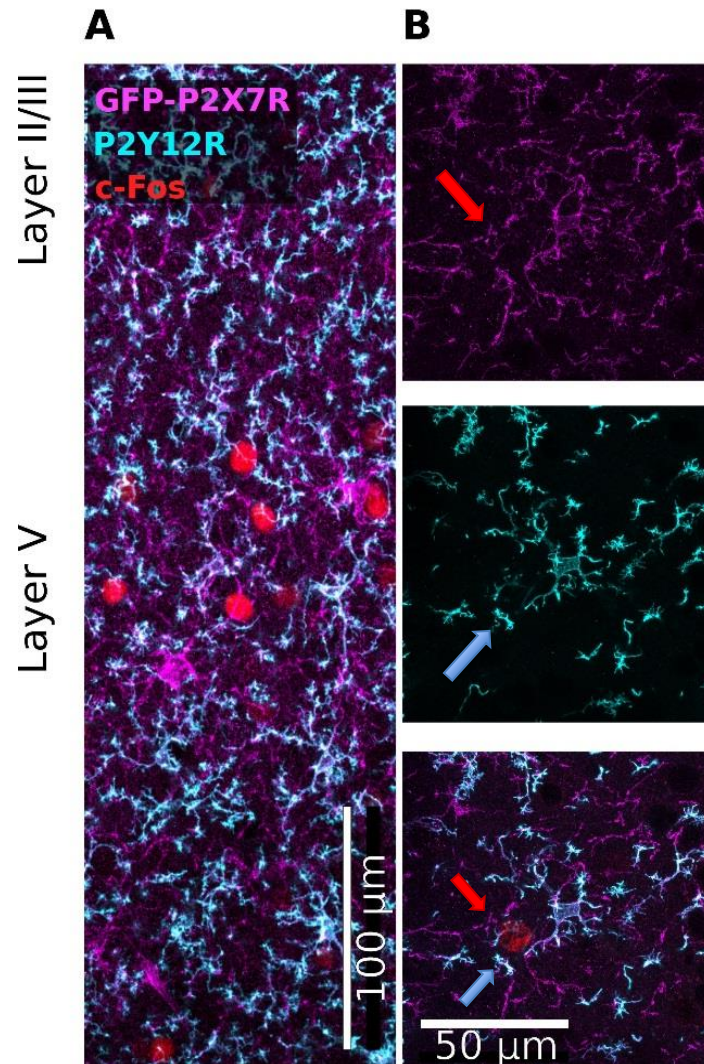


Figure 2. Expression of the fusion protein P2X7R-EGFP, localized with anti-GFP antibodies (Magenta). **A)** The prelimbic cortical layers (II to V) have been immunostained for the microglial marker P2Y12R, here cyan, and the c-Fos neuronal activity marker, here red. It is possible to see the typical band of PCP-activated neurons at layer V. Microglial fine network is equally distributed along the layer images. The P2X7R have a higher background punctated distribution, with localized clusters of expressions along the P2Y12R branches, but also clearly marking some of other cellular types, larger than microglia and negative for P2X12R expression. **B)** The higher magnification (60X oil immersion) shows how P2X7R-EGFP branches signal surrounds PCP-activated neuronal

soma with P2X₁₂R positive microglial branches (blue) but also along P2Y₁₂R negative cell parts (red).

In this subset of experiments were addressed biological questions regarding the possible influence of P2X₇R on the microglial morphology and dynamics. I collected and compared movies of fluorescent ramified microglia in ACSF control condition and alongside pharmacological applications. Treatments consisted of acute bath application with 3mM Mg-ATP and with 10 μ M of P2X₇R antagonist blue brilliant G (BBG).

As mentioned, several antagonists against P2X₇R act through a common site (90), interestingly though, it was recently reported a distinct site for the P2X₇R-BBG antagonism (214). Microglia movies were processed in order to be quantifiable (Figures 18-22).

1.5. Modeling schizophrenia: the effects of phencyclidine (PCP)

The following section aims to provide a link between our knowledge of P2X₇R and the animal models used to study schizophrenia, two topics seemingly unrelated. Following sections will overview the pathology of schizophrenia, and introduce the PCP animal model. Revisions of the preclinical studies about purinergic signaling in models for psychosis, and of the clinical investigation about schizophrenia as an inflammatory disorder, will eventually provide a link between the two topics.

1.5.1. The pathology of schizophrenia

Psychiatric diseases are characterized by several mental and behavioral patterns, which cause poor coping of ordinary life and suffering. Dysfunctional thoughts, perceptions, emotions, behavior and social interactions are common features of psychiatric diseases. Schizophrenia is one of the most emblematic psychiatric disorders, characterized by a typical young-adulthood onset, and defined by abnormalities in thought and cognition, with an estimated prevalence of 0.5% to 1% (215). Schizophrenia is typically diagnosed upon repeated psychotic episodes, commonly accompanied by antecedent decline of social and cognitive abilities (216). The most prominent neurological feature, detectable only in advanced phases of the disease, is the tissue deterioration of key brain areas, such as the PFC (217). The majority of schizophrenic patients develop comorbidities, which, when added to the typical self-neglect symptoms and suicidal thoughts, shorten the patient's average life expectancy (218). Schizophrenia, all considered, represents a

remarkable economical and social burden (219). While the etiology and pathophysiology of schizophrenia is far from being completely understood, few mechanisms are thought to be shared among a spectrum of different psychiatric conditions (220, 221). It is suggested that mental disorders result from the combinations of individual genetic/epigenetic susceptibility and environmental factors, typically traumatic experiences. Particularly meaningful are aspects regarding parenting, events surrounding pregnancy and birth, childhood traumas, brain injuries, social stress and juvenile drug consumption (216).

Traditionally, physicians categorize the symptoms of schizophrenia into positive and negative symptoms. Positive symptoms include hallucinations, delusions, disorganized thoughts and disordered movement, typically displayed during acute phases, called psychotic episodes. The negative symptoms include emotional blunting, reduced pleasure sensation, social withdrawal or cognitive deficits, and represent the most deteriorating and concealed aspects of schizophrenia (222). The need to evaluate novel drugs, specifically intended to treat cognitive deficits, produced a third “cognitive” category of symptoms. The cognitive symptoms are listed as deficits in working memory, verbal learning and memory, visual learning and memory, verbal comprehension, attention, processing speed, problem solving, and social cognition (223).

The diagnosis for schizophrenia is based exclusively on psychiatric testing, therefore the observation of the patient's behavior and the evaluation of reported experiences. The absence of any biomedical measurement depicts the difficulties in crediting relevant rodent models for schizophrenia. Intensive research into the pathophysiology of schizophrenia elucidated first the pivotal role of hyperfunctioning mesocorticolimbic dopaminergic system, leading to positive symptoms, and second the involvement of hypofunctioning cortical NMDA-R-glutamatergic transmission, inducing both symptoms categories (10, 224, 225). These hypotheses are based on observations that, both dopaminergic agonists and NMDA-R antagonists, induce acute psychotic-like episodes in healthy volunteers, and reproduce severe psychosis in schizophrenic patients with typical sub-effective doses (226, 227). Even though the outcome of both amphetamine- and PCP- (or ketamine) abuse can be described with similar terms, these are two completely different drugs affecting distinct brain circuits.

1.5.2. Schizophrenia and PCP

PCP commonly produces hallucinations, delusions, and disorganized speech, thereby mimicking several positive symptoms (228). Molecular studies related to schizophrenia corroborated a basal dysregulation of the glutamatergic system in specific areas of the brain (229). Moreover, a behavioral and cognitive downfall, similar to negative and cognitive symptoms, regularly escalates with the repetitive use of the substance (222, 229). The employed murine pharmacological PCP-model for schizophrenia aims to mimic the schizophrenia psychotic episodes via systemic delivery of sub-anesthetic doses. Treatments vary, from a single to series of daily administrations during late adolescence (60-90 days-old mice), when schizophrenia is typically diagnosed, and prior to closing of the developmental window of the frontal brain regions (222, 227).

1.5.2.1. Schizophrenia and PCP: historical overview

Phencyclidine (PCP) was the first drug of its class to be synthesized, the chemical backbone for all arylcyclohexylamine dissociative anesthetics. When the anesthetic and analgesic properties of PCP were first tested in humans, its psychotomimetic effects were immediately recognized. During recovery from sedation, acute post-anesthetic effect termed “emergence delirium”, consisting of various degrees of agitation, disorientation, delusions and hallucinations, was regularly reported (230, 231, 232). Such evidence precluded PCP from any clinical application, while it was gaining an alarming popularity in the psychoactive substances markets. To prevent its widespread use, in the late 60s the FDA banned PCP, while approving another patent, a safer arylcyclohexylamine anesthetic called ketamine (232). It would be later revealed that ketamine acts on the same NMDA-R-site as PCP, but with much lower affinity, and is still considered clinically valuable (8, 9, 233). PCP and a few analogues have been illegally synthesized and distributed in the streets of the USA, initially as drugs of deception, and subsequently as proper recreational psychedelic drugs (232). During the 70s an intense political campaign hammered against the growing epidemic of illicit substances, and PCP was pictured as the most dangerous and addictive of all. During this time, the causal relationship between chronic PCP intake and irreversible psychosis, presenting symptoms resembling those of schizophrenia, was documented (232). In 1983, the identification of the “PCP-receptor” as the glutamatergic excitatory NMDA-R initiated the pharmacological characterization of PCP-like drugs in rodents. Shortly after, rodent PCP models became standard methods to study schizophrenia, and superseded

former models based on amphetamines. Besides mimicking acute psychotic episodes, PCP chronic administration induced long-lasting negative- and cognitive-like symptoms (234). The consistency of arylcyclohexylamines treatments in generating such effects is a cornerstone of the glutamatergic hypothesis of schizophrenia (225), which postulates that the etiology of schizophrenia involves NMDA-R hypofunctionality (10). From primary NMDA-R loss-of-function would develop further consequential dysfunctions, like the dopaminergic neurochemical imbalance (235). Brain regions reportedly linked with schizophrenia-like symptoms are the limbic system, the sensory and frontal cortices and the monoaminergic mesencephalic nuclei. Yet, it was unclear whether acute psychosis would leave any noticeable molecular footprint (37, 38, 39, 40). In the early 90s, preclinical studies using NMDA-R antagonists such as PCP, ketamine and MK-801, as acute antiepileptic drugs, revealed an unequivocal neurotoxic effect in the retrosplenial and cingulate cortices of rodents (236). Even though this toxicological evidence was never confirmed in primates, it prevented further research of arylcyclohexylamines as therapeutic tools, for at least another couple of decades (232). Eventually, during the last 25 years, PCP gained popularity as a rodent model for schizophrenia, often adopted to test the efficacy of already approved as well as novel antipsychotic medications (Figure 1, 237, 238).

1.5.2.2. PCP: from pharmacology to the models for schizophrenia

The discovery of PCP pharmacology identified highly specific potent non-competitive antagonism for the NMDA-R, thus presenting an ideal model for schizophrenia (8, 9). The topical administration of PCP on the brain, whether on slices (239, 240) or via local delivery to freely moving rats (241), promptly suppresses the neuronal multi-synaptic activity.

The glutamate NMDA-R is an ionotropic, tetrameric channel of the excitatory synapses, assembled by seven possible subunits, copiously expressed by neurons, but also reported in non-neuronal cells (242). It gets classically activated by two concurrent stimuli: the endogenous glutamate and glycine ligand-binding dependent agonism, and the membrane potential's depolarization, required for removing the intracellular Mg^{2+} ion, which blocks the ion channel. Subunits from the NR1 and NR2 families present the glycine- and glutamate-binding sites, respectively (243). In addition, an atypical NR3-containing NMDA-R, with modified ionic sensitivity was recently described (244). The removal of

Mg²⁺ ions requires the activation of neighbouring depolarizing currents, like the glutamate α -Amino-3-Hydroxy-5-Methyl-4-Isloxazole Propionic Acid receptors (AMPA), a basic mechanism to filter stimuli based on their amplitudes. NMDA-R currents rapidly increase the synaptic Ca²⁺ concentration, the cornerstone for synaptic plasticity, and strongly linked with cognitive functions like memory acquisition. Moreover, sustained or repetitive stimulation of NMDA-R is responsible for excitotoxicity, a form of neurotoxicity triggered by excessive intracellular Ca²⁺ (242). The arylcyclohexylamines behave as use-dependent NMDA-R channel blockers, therefore blocking the ionotropic pore only in the open-channel configuration (245, 246). Upon this observation, it seemed appealing to apply PCP in pathologies characterized by an important component of excitotoxicity, like epilepsy and ischemia. In the late 80s, novel PCP-like drugs were designed and synthesized with the aim of introducing a new generation of antiepileptics (247, 248). The designed arylcyclohexylamines derivatives targeted the glutamate-binding NR2 family subunits (249); however, the persistent inhibition of the channel, besides suppressing neuronal activity, was found to also promote apoptosis *in vitro* (239, 240, 250). Upon systemic PCP administration, electrophysiological and molecular anatomical studies found a PCP-induced acute increase in neuronal activity, in several cortical and subcortical areas (252, 253, 254, 255). This electrical activity accompanies the acute prototypical psychotomimetic effect (251), in rodents similarly to humans (10, 37, 40, 230, 231). The analogy between the drug effects and the symptoms of schizophrenia supports translational validity of PCP schizophrenia rodent models (Figure 1). Thirty minutes after intravenous (*i.v.*) and intraperitoneal (*i.p.*) injections (5 mg/kg) to rats, PCP concentrations were recorded 3- and 10-time-fold in the brain versus the serum, respectively (256). The PCP lipophilic molecules cross the blood-brain barrier with extraordinary efficiency, and are stored dose-dependently inside adipose tissues (257). The more a drug is lipophilic the slower it will be excreted (258). These aspects are interesting when considering that the water-soluble, fast washout, amphetamines-based schizophrenia models can not provide conspicuous negative- and cognitive-like symptoms, while deficits from chronic PCP were documented days and weeks after its last administration (225, 232, 254). Previously to NMDA-R (8,9), other PCP pharmacological targets, although with lower affinity, were already recognized (259). The most appealing appeared the inhibition of

dopamine-reuptake transporters at 0.5-1 μ M PCP concentration (260). Systemic PCP increases the dopaminergic tone, especially in the mesolimbic system and frontal areas, which is the essential effect of amphetamines and cocaine (252, 260). Such evidence could have well explained not only the psychotomimetic effects, but also the addictive potential of PCP. Rats trained to self-administer *i.v.* drugs spontaneously develop addiction to PCP, although to a lower degree, when compared to classic stimulants or opioids (252). The relationship between PCP and the dopaminergic system will be further discussed in section 5.3.1.

The PCP-induced increase of dopaminergic tone and of neuronal activity reportedly requires the systemic delivery of the drug (240, 260). The dichotomy of the systemic versus topical pharmacological effects will be further elaborated in sections 5.3.2.3. and 5.3.2.4.

The PCP-induced acute behavioral psychotomimetic effects undergo desensitization in mice with prolonged treatment, parallel to the decline of the dopaminergic activation and the basal dopaminergic tone in rats (38, 254, 257). After 7-14 days of systemic daily PCP injections (10 mg/kg), once exhausted the acute hyperlocomotion phase, mice present a spectrum of symptoms that mimic the negative and cognitive symptomatology (42, 251, 254). The search for the underlying mechanisms, following the acute and subchronic PCP treatments, generated contradictory evidence, with more than one hypothesis (227, 235, 261).

1.5.3. Proposed models for the neurological substrate of schizophrenia

From the 60s PCP was considered a drug of psychiatric interest (10, 37, 38, 39, 40, 230). Yet, the predominant target of PCP was unidentified till 1983, while prior published data suggested a central dopaminergic role (37; 38, 229). Amphetamines, with their long-time established dopaminergic pharmacology, have been the first drug-of-choice for modeling psychiatric conditions (225, 227, 260). Following the description of PCP as an NMDA-R antagonist, sprouted the idea of potential clinical valuability for PCP-counteracting and glutamatergic potentiating agents (10). Up to my knowledge, the first general explanation for the PCP mechanism consisted of the reduction of NMDA-R activity at synapses, involving different large regions of the brain, including the cortical sensory- and frontal-areas (10). The strongest translational feature of schizophrenia models employing PCP settles in the generation of long-term negative- and cognitive-like symptoms, measurable

in animal models by standardized behavioral paradigms (42, 235, 254). The strongest theoretical points of PCP-models consist the abundant and ubiquitous expression of its target (10), a main difference compared to amphetamines. The widespread synaptic distribution of NMDA-R allows PCP to directly manipulate the activity of distant brain areas (225).

In the last 30 years, it has been consistently demonstrated that a few subtle neurological dysfunctions are ingrained in families with a history of schizophrenia (262, 263). These traits are called biotypes, and can be precisely localized into restricted brain areas. Biotypes of the primary auditory cortex, venue of auditory hallucinations, gained interest, considering that these are the most common hallucinations in schizophrenia. For example, the echoic memory is a kind of auditory working memory that gives us the ability to store and compare temporally consequent sounds, therefore discerning different pitch. Individuals with familial history of schizophrenia typically display a higher threshold for echoic memory (264). Such deficits in perception are estimated to underlie more complex disabilities, like the inability to recognize social expressions, the difference between a happy or a sad voice (265, 266). Another biotype concerns mismatch negativity, a similar discriminatory function between a series of different sounds (267, 268). An early electrophysiological study of the auditory cortex, in monkeys, showed that the local administration of PCP, on the surface of the primary auditory cortex, mimicked the mismatch negativity deficits found in schizophrenic patients (269). The mismatch negativity deficits were later successfully replicated with the systemic injection of ketamine (270). Although experiments performed in primates (269) were never reproduced, the fact that PCP exerts a direct pharmacological modulation of cortical neurons, while amphetamines only affect neurons from small subcortical nuclei, provides evidence that arylcyclohexylamines are the superior pharmacological model of schizophrenia.

The latest update from the authors of the original formulation of glutamatergic hypothesis claims that PCP penetrates superficial cortical layers, inhibiting in a function-dependent fashion the NMDA-R currents of pyramidal neuron's apical dendrites (261). But, despite its development and supporting evidence, this idea has been challenged, and at least partially dismissed, by preclinical works on animal models which proposed alternative mechanisms (235). These different, and not mutually exclusive, theories on PCP

schizophrenia models can be categorized into monoaminergic mechanisms (237, 238, 252), cortical inhibitory interneurons mechanisms (235), primary thalamic versus prefrontal disinhibition mechanisms (271), among other, even more specific, hypothesis (272, 273). In conclusion, the current recommendation suggests considering these models as the summation of small effects, which synergistically converge into the prototypical phenotype.

1.5.3.1. Dopamine in the PCP model: positive and cognitive symptoms

Because intimately related to both psychosis and addiction, the midbrain dopaminergic systems were among the first to be investigated with respect to PCP (37, 274). The dopaminergic systems are composed by nuclei of dopaminergic neurons, with somata occupying confined spaces of the mesencephalon, and long projections, extensively distributed, especially in the frontal brain (225). The nigro-striatal pathway is composed by neurons of the substantia nigra (or A9), that principally innervate the basal ganglia. The A9 output is pivotal to motor functions, and gets disrupted in Parkinson's disease. The other midbrain dopaminergic pathways originate in the ventral tegmental area (VTA), or A10. Part of the VTA corticolimbic axons project to the nucleus accumbens, a small subcortical nucleus undertaking the control of motivation, reward and addictions. The larger part of VTA neurons compose the cortico mesolimbic pathway, which projects to the frontal cortex and the limbic system, and is critical for cognitive and emotional processing (275, 276, 277).

Administration of PCP induces an acute frontal dopaminergic release, which originates from the arylcyclohexylamines-dependent increase of the general firing rate of VTA neurons; a highly possible mechanism explaining the addictive effect of these substances (252). The increase in VTA activity correlated with the specific potency of the NMDA-R antagonism. PCP also blocks dopamine reuptake, which typically lowers the VTA activity, and this effect of the drug can be observed once the dosage reaches *i.v.* cumulative dose of 1 mg/kg. (252). As mentioned earlier briefly, the acute PCP-related frontal hyperdopaminergia undergoes fast tolerance, decreasing after only three consecutive daily treatments, in rats (257). In the mice VTA, subchronic (7-10 days) PCP treatments reduce both basal dopamine release and the expression of tyrosine hydroxylase (TH), hallmark of dopaminergic deterioration (254). Moreover, it sensitized the rat frontal cortex and striatum to dopamine agonists, like amphetamines, amplifying their dopamine-

release effect. Several studies correlated the PCP hyper locomotor activity, likened to the positive symptoms of schizophrenia, with the acute increase in prefrontal dopamine concentration (38, 257, 274). Increasing the levels of extracellular glycine, endogenous agonist of the NMDA-R, partly counteracted the subchronic PCP-induced amphetamine sensitization, supposedly by buffering the PCP antagonism (278). Another intriguing study, on VTA neurons, reported two opposite effects of PCP. Acute PCP application induced the expected inhibition of excitatory inputs. Anyway, a strong enhancement of glutamatergic currents was recoded when the neurons came from PCP-chronically treated rats (272). A recent *ex vivo* study of the nucleus accumbens found significant decrease in dopamine basal release with repeated NMDA applications; however, low-dose subchronic PCP administration did not alter dopamine release dynamic (279).

Therefore, systemic PCP definitively influences the dopaminergic signaling. Yet, the pharmacological evidence, within the range of doses which elicit psychotomimetic effects, exclude the possibility of a direct effect on non-NMDA-Rs (227; 233, 260). Sub-anesthetic treatments, adopted for schizophrenia models, keep the PCP levels in the brain way lower than those required for monoamines transporter inhibition (260).

As previously mentioned, the dopaminergic output, especially the mesocorticolimbic pathway, regulates the frontal dopamine concentration, which is crucial for higher brain functions. It is generally accepted that the dopamine level in the PFC has an inverted “U” relationship with cognitive performance (276, 277). The further it fluctuates from the optimal level, independently whether under- or over-concentrated, the poorer the functional outcome, a common observation in schizophrenia clinical research (277).

1.5.3.2. The glutamatergic hypothesis: search for the PCP target

PCP affects a fundamental and diffused biochemical equilibrium, displays paradoxical effects whether local or systemic administration is applied, and prolonged treatment elicits irreversible negative- and cognitive-like symptoms (225, 232, 241, 254, 271, 273). While the general hypothesis of PCP silencing cortical apical dendrites may account for biotypes of schizophrenia (262-270), alternative theoretical models are required to explain the effect of PCP in specific brain areas. The current work focused on the PFC, more precisely the mPFC of the mouse. The next section will justify the choice for this brain area, and explain some anatomical features.

1.5.3.2.1. PCP and the rodents cognitive functions: the medial PFC

The rodent mPFC of the brain coordinates functions like cognitive process, regulation of emotion, motivation, and sociability. Local lesions in mPFC, and the consequent impairments of the associated functions, are found in essentially every neurological and psychiatric model with components of cognitive dysfunctions (280). It is thought that the mPFC of rodents, at least partly, corresponds to the dorsolateral prefrontal cortex (dlPFC) of the brain of human and non-human primates (281). Both areas collect information from large cortical and subcortical areas, and integrate the updated information to output structures (280).

Working memory, an important function of mPFC, is defined as the temporary storage and computation of sensory stimuli no longer existing (282) and to compare it to presently ongoing stimuli, to maintain only those considered relevant, and to integrate them with newly coming stimuli. This allows the individual to continuously update and adapt their thoughts and behaviors as required. Similar to echoic memory, working memory is frequently damaged in schizophrenic patients, and is often responsible for the poor outcome of schizophrenic patients (262-270, 283). Most importantly, working memory deficits in schizophrenia are resistant to any currently available treatment (2, 3, 284, 285, 286).

In rodents, both the mPFC-related working and episodic memory get consistently disrupted following repetitive PCP treatments (254, 42, 285, 286). A recently published study showed a correlation between the subchronic PCP-induced memory deficits and abnormalities in the rodent mPFC activity (286). The rodent mPFC is also one of the affected areas following systemic PCP delivery to undergo pronounced local enhancement of neuronal activity; which, similarly to the dopaminergic activation (252), also correspond to the behavioral expression of positive-like symptoms (241, 255, 273, 287). Considering its involvement in both the acute and subchronic PCP effects, and its connection with the behavioral expression of the symptoms, our study focused on the mPFC over other potentially affected brain areas (31).

1.5.3.2.2. Prefrontal cortex: anatomical overview

The PFC occupies approximately 29%, 17% and 8.5% of the total cortex, in humans, chimpanzees and lemurs, respectively (288, 289). As early as the 1960s, the involvement of the PFC was postulated in neurological symptoms involving the disruption of higher

integrative functions (290). The mammalian neocortex typically develops six distinct cytological layers, where the first “molecular layer” lays on the external brain surface, and the sixth “multiform layer” borders the subcortical white matter (Figure 3). The rodent mPFC lacks the fourth granular layer, which defines it as an agranular cortex, a characteristic partly shared by the primate dlPFC (291). This anatomical analogy, combined with the functional ones, reinforce the hypothesis regarding the similarity between human and mice brain areas to model schizophrenia (292).

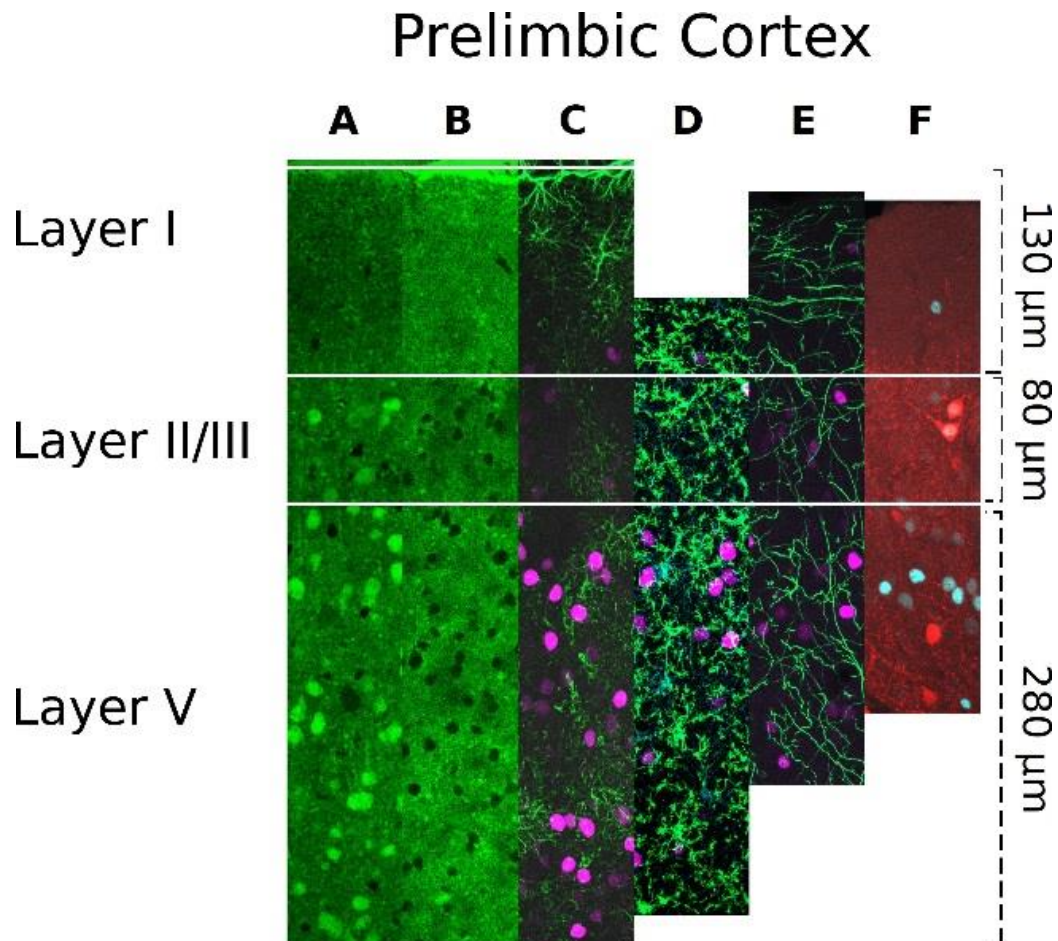


Figure 3. Imaging of the C57Bl/6 prelimbic cortical layers. **A)** and **B)** are images of an electrophysiology acute slice, at 15 and 30 μm depth from the cut surface. The slice was perfused *ex vivo*, using ACSF mixed with calcein fluorophore at 50 μM , and imaged with 2-photon microscope setup. The neuronal cell bodies are mainly dead (permeabilized to calcein) on the surface (**A**), and more healthy, with non permeabilized cell body, deeper in the tissue (**B**). **C)** Examples of wild type acute PCP-induced c-Fos activation (magenta) and astrocytic marker (GFAP, green), of **D)** P2X7R-EGFP mouse cortex with the microglial marker (P2Y12R, green) and anti-GFP (P2X7R signal, cyan), and **E)** in P2rx7⁻

⁺ mPFC with tyrosine hydroxylase positive fibers. In **F**), wild type acute PCP effect is imaged, with c-Fos in cyan and parvalbumin in red.

Within the five cellular layers of the rodent mPFC (**293**), the layer I is scarcely populated by cell bodies, and is occupied by dendrites from neurons originating from deeper layers, as well as nerve terminals from other areas (**294**). The layers II/III and V/VI are densely populated by the somata of pyramidal neurons (**295**). Excluding the multipolar neurons of the layer VI at least 10 types of cortical pyramidal excitatory neurons can be identified along the mPFC layers (**296**), each with characteristic microanatomical location, size, and dendritic ramification. Yet, all communicate with long-distance targets (**297**).

In rodents, pyramidal neurons contribute to 80-90% of the total cortical neurons. The remaining 10-20% is represented by inhibitory GABAergic interneurons (**280**). Well-known molecular markers, along with distinct electrophysiological properties, can be used to discriminate between different types of inhibitory interneurons. The perisomatic fast-spiking parvalbumin (PV) expressing interneurons, distinguished by the expression of PV high-affinity calcium-binding protein, account for over 40% of the whole interneuron population. PV interneuron activity is critical to coordinate high frequency (theta) oscillations, participating in higher cognitive functions, thus particularly appealing for clinical psychiatry (**298, 299**). Other interneuron populations can be characterized distinct marker gene expression, such as the dendritic targeting somatostatin interneurons, thought to modulate inputs of pyramidal neurons (**300**), the vasoactive intestinal polypeptide expressing-interneurons or the cholecystokinin expressing- interneurons (**298, 280**).

Along the rodent mPFC, dorso-ventral differences in the laminar organization and neuronal connectivity divide the cortex into three neuroanatomical subregions, namely the agranular cingulate cortex (ACC), the prelimbic cortex (PL), and infralimbic cortex (IL), from dorsal to ventral mPFC (**301**). The inputs to the mPFC circuits are predominantly received by the superficial layer II/III, and relayed to the cortical layers V and VI. The principal output of the mPFC circuit is the projections from the large pyramidal neurons of layer V (**280, 288, 302**). Most importantly, inputs to the PL and IL cortices come from the mediodorsal nuclei of the thalamus (mdTh), basolateral amygdala, ventral hippocampus, and the contralateral mPFC (**280, 288, 302**). The mdTh

thalamocortical projections are topologically distributed, targeting pyramidal and GABAergic interneurons, and mediate processes of perception and sensation. It is postulated that proper communication between these two regions is essential in the generation of consciousness (303, 304, 305). The rodent mPFC collects inputs from the lateral portion of the mdTh, a nucleus relaying the activity of subcortical areas (288). A special class of innervating fibers derives from wide-distribution systems, namely dopaminergic, serotonergic, noradrenergic and cholinergic nuclei (288). The levels of these neurotransmitters exert complex influential modulations of the overall mPFC and brain activity (276, 277, 288, 306). For example, the release of acetyl-choline in the mPFC, from fibers originating in the basal forebrain, is necessary for successful performance in attentional and cognitive tasks (307). Following a common cortical feature, PFC sends back fibers to all the structures it receives input from (288, 302).

The decreased volume or thickness of the PFC is one of the most recurrently observed pathological sign in advanced stages of schizophrenia, and also in related animal models, thought to derive from synaptic loss (308). A second hallmark feature is the decreased GABAergic signaling, derived from the reduced density of PV or somatostatin interneurons (235, 309).

1.5.3.2.3. PCP and the cortical parvalbumin (PV) interneurons

The most accredited explanation for the paradoxical mPFC hyperactivating effect, induced by systemic PCP (241, 255, 273, 287) is probably the preferential inhibition of GABAergic interneurons, particularly the PV subtype (235, 309, 310). In the rodent cortex two main types of PV interneurons can be distinguished: the chandelier cells, inhibiting pyramidal outputs, via cartridges of synapses imprinted on the axon initial segment, and the basket cells, operating axo-somatic inhibition. Therefore, the general PV interneurons population can facilitate both feedforward and feedback inhibition (311). In particular, the feed-forward inhibition accounts for synchronizing high-frequency brain activity oscillations, which were found to be dysregulated, when cognition and information processing deficits were present (312, 313). Optogenetic experiments found that the PV interneurons' fast-spiking activity is necessary and sufficient for the generation and maintenance of gamma oscillations (~25–100 Hz, 314). Diseases involving cognitive impairments, including schizophrenia and autism spectrum disorders (ASD), display significant alterations of PV-dependent oscillations (315, 316). A study

on NMDA-R genetic deletion found altered PV interneurons excitability, leading to a selective deficit in working memory (317). In analogy with human pathology, the rodent mPFC in experimental models of cognitive-like symptoms showed reduced expression of PV and GAD67, a GABA-synthesizing enzyme (235, 318, 319), alongside other neuronal channels (320).

Disruption of the mPFC GABAergic network is often considered at the core of cognitive and cognitive-like symptoms. Yet, the specific deviation in the healthy cascade of events both in schizophrenia and in PCP models is still unclear. Apparently, the maturation of the PV interneurons is of particular interest. The maintenance of a specialized extracellular matrix, the perineuronal net (PNN, 321), defines the critical period for network plasticity during the postnatal development (322), by stabilizing the synapses (323, 324) and protecting against oxidative stress (325). Abnormalities in PNN were related to schizophrenia and schizophrenia models (326), and a gene expression profile typical of immature PV interneurons was identified in different psychiatric conditions (327). Psychiatric disorders such as ASD and schizophrenia are generally considered neuro-developmental disorders (220, 221). A very heterogeneous range of independent developmental faults is thought to trigger developmental consequences, finally converging in the disruption of PV circuits, and related cognitive performances. Preclinical research produced a variety of reliable environmental and genetic manipulations, aimed to model schizophrenia symptoms. A large meta-analysis showed that the majority of rodent schizophrenia models converge on an elevated oxidative stress in PV interneurons, which correlated with PNN damage in the dorsal mPFC (319).

Perinatal treatments with PCP generate schizophrenia models that display behavioral and neuropathological abnormalities, including PV interneuron dysfunction (250, 328). It is possible that minimal invasive treatment of newborns, such as with drugs like PCP, may represent a sort of developmental trauma, potentially leading to adulthood deficits (235). Yet, the most employed schizophrenia PCP-models aim to mimic late adolescence schizophrenic episodes (2-3 months of age in mice, 222, 235). A renowned hypothesis argues that PCP could block preferentially the NMDA-Rs of cortical GABAergic interneurons, with evidence pointing toward the PV population. The resulting decrease in inhibition, in turn, would lead to desynchronized neuronal activity, thus introducing areas with increased local firing rate, and related psychotic-like behaviors (329). As expected,

the lowered activity of PV interneurons was shown to lead to uncontrolled increase of local firing (235), while the functional connectivity between distal brain areas fades following PCP administration (330). Hypotheses explaining such PCP selectivity range from different composition to specific subunit affinity (331, 332). Moreover, the PV interneurons display a fast-spiking profile, presenting enhanced probabilities for the use-dependent PCP, to block NMDA-Rs in open configuration.

To map precisely which areas display an acute increase of neuronal activity, an established method is immunohistochemistry against the activity-dependent expression of c-Fos. Following systemic PCP administration, the c-Fos staining is found increased in several brain areas, including the mPFC glutamatergic neuronal nuclei (333), while another work demonstrated that there were no identified signs of preferential inhibition or activation of PV interneurons in the mPFC (255). The subchronic PCP treatment consists of a complex cumulative effect which persists the drug withdrawal. The mimicry of schizophrenia negative and cognitive symptoms (37, 254, 334) is often accompanied by the deterioration of cortical interneurons, especially PV expression (309, 319, 335), and possibly related to mPFC network abnormalities (253, 336).

1.5.3.2.4. PCP effects on mPFC: connectivity hypothesis

Similar to the PFC, the thalamic circuit abnormalities have also been linked with the emergence of psychotic symptoms (337). While perisomatic PV interneurons control the pyramidal output (288, 297), monoamine neurotransmitters dramatically modulate mPFC activity, where their receptors are abundantly expressed (288, 338, 339). Typical and atypical antipsychotics, which show high affinity for monoamine receptors (namely D2R and, e.g. clozapine, serotonergic 5-HT_{2A/2C}, 5-HT_{1A} receptors and α -adrenoceptors, respectively), have been speculated to primarily target the PFC (253).

Systemic PCP administration in anesthetized rats modulates the mPFC pyramidal activity via activation of midbrain efferent fibers. As a result, a longitudinal band of c-Fos positive neuronal nuclei appears between the mPFC layers III to VI (340). This laminar mPFC portion receives the majority of thalamocortical excitatory inputs from the centromedial and mdTh (341), an area which also gets hyperactivated by systemic PCP treatment (271), since PCP increased the firing rate by approximately 50% of pyramidal neurons, while decreasing the activity by 30% in both the mPFC and the mdTh (333). To understand the relationship between mdTh and PCP pharmacology (342, 343), Kiss and colleagues found

that the arylcyclohexylamines-induced disruption of slow cortical oscillations was mimicked by local application of lidocaine on the mdTh (344). Moreover, topical application of muscimol, a GABA_A receptor agonist, on the dorsal thalamus, interfered with the behavioral hyperactivity induced by PCP-like drugs in rats (345). Interestingly, local delivery of PCP to the ventral hippocampus reportedly induces mPFC hyperactivity (241, 273). On the other hand, the direct influence of the hippocampal formation was later disproven (271). Apparently, only systemic PCP administration evokes glutamate and monoamine level increase in the PFC area, another possible explanation to the mPFC hyperactivity (346).

The reciprocal corticothalamic connections suggest two possible mechanisms for the acute PCP effect: (1) the preferential blocking of NMDA-R inputs onto GABAergic neurons of the PFC, termed top-down mechanism, or (2) of subcortical structures, like the basal ganglia or the reticular nucleus of the thalamus (Rt), termed bottom-up mechanism. The latter mechanism can potentially disinhibit the thalamocortical excitatory afferents, driving the mPFC hyperactivation (271). The relay neurons of the thalamus receive both direct monosynaptic corticothalamic excitatory inputs, and disynaptic, Rt-mediated, feed-forward inhibitory inputs (347). The Rt is composed of GABAergic neurons, which filter signals running between the thalamus and its connected structures, and receive 70% of excitatory synapses from corticothalamic fibres (348). Theoretically, regarding a pure top-down scenario, the mPFC-driven excitation should trigger the activity of both the mdTh and the Rt neurons; however, the latter could not be validated by experimental evidence (271). On the other hand, activity induced by PCP in mPFC can be consistently reproduced and is unlikely to be driven exclusively by thalamocortical signaling (271).

Electro-encephalogram (EEG) recordings have been extensively employed in the research of markers, endophenotypes or prognostic indicators for schizophrenia (349). The EEG recordings are based on the rhythmic activity of the neuronal network, defined as oscillations. Oscillations are classified by the frequency range, important to codify various types of information, and coordinating different networks in the temporal plane. The fast γ oscillations (30-80 Hz) are involved in sensory and cognitive processes, and impaired in schizophrenia (350). The slow δ oscillations (1–4 Hz) are typically associated with deep sleep and relaxation, and depend strongly upon thalamocortical activity (351).

The EEG performed during acute ketamine treatment in healthy subjects (226) showed the augmentation of γ oscillations (40–85 Hz) alongside the reduction of δ components. Interestingly, the inhibition of low frequency oscillations can be induced also by employing LSD-like hallucinogenic drugs, which principally disrupt the serotonergic neurotransmission, but was found to strongly affect also the mPFC activity (227, 352). Lysergic-acid derivative drugs, which uphold validity as pharmacological models for some schizophrenia symptoms, are 5-HT_{2A} receptor agonists (353), a receptor typically antagonized by atypical antipsychotics (354). The fact that both PCP and LSD-like drugs disrupt slow oscillations may suggest a similar neurological substrate. Recent evidence, eventually, indicates the possibility that PCP positive-like symptoms could be mediated by the preferential acute modulation of PV interneurons, while the long-lasting disruption of gamma oscillatory activity would depend on PCP indiscriminated NMDA-R antagonism (350).

To study the involvement of thalamocortical projections would be of great interest; however, in the current work, we focused mainly on the involvement of the mPFC, since performing the complex *in vivo* experiments required to precisely address this question was outside of our ability to execute.

1.6. Schizophrenia and P2X7R: the neuroinflammatory hypothesis

The PCP models for schizophrenia in young adult mice can be divided to:

- Acute single PCP systemic administration. Produces a transient neurochemical imbalance, associated with molecular and cellular disturbances, profoundly altering the whole physiological brain activity, and producing positive-like behaviors.
- Repetitive PCP treatments. The progression of psychotomimetic experiences, accompanied by the daily withdrawal experiences, accumulates specific PCP-dependent damages. Each PCP “punch” reinforces a plastic adaptation of brain circuitry. The resulting behavior presents long-lasting abnormalities, similar to negative and cognitive symptoms.

These following sections will introduce a concept very interesting for studies related to brain immunological functions, the neuroinflammatory phenomenon in schizophrenia (355): the presence of a latent and mild neuroinflammatory phenomenon accompanying the progression of the schizophrenia pathology has been proposed (356).

Immune responses present during parturition have been described as a risk factor for schizophrenia. Simulations of viral infection during pregnancy are among the validated preclinical models for schizophrenia and autism in rodents (220, 221). Other schizophrenia-related direct indications of neuroinflammation are the high levels of pro-inflammatory markers inside and outside the CNS, and the numerous infectious agents identified by epidemiological study as risk factors (357).

Diffusion magnetic resonance imaging (MRI) techniques are powerful tools to gain insight into living human schizophrenic brains. White matter abnormalities (358), signs of axonal degeneration, likely due to alterations of the myelin sheath (359), and, more recently, active neuroinflammation, were successfully identified (360). Free-water MRI can recognize even small increase in the amount of extracellular fluid in the parenchyma deriving from inflammatory processes (361). Experiments performed on first episode schizophrenic patients showed an increased volume of extracellular fluid in both white and gray matter, concurrently with a low, or absent, axonal degeneration, suggesting that neuroinflammation may precede later white matter deterioration (360).

Recently, research focus has shifted towards exploring the influence of “neuroinflammation and glial cells” in neurodegenerative diseases; however, limited data are available to link neuroinflammation and schizophrenia. A recent meta-analysis revealed the presence of activated microglia near damaged oligodendrocytes and swollen and vacuolated astrocytes in schizophrenic brains (362). Another study found that schizophrenic brains contain an increased number of microglia, although the expression of surface proteins is altered in these cells (363). Hampering the shift of microglia towards proinflammatory phenotype via pharmacological intervention was found to be beneficial in rodent schizophrenia models (364). The acute PCP-induced lesion of neurons in the rodent retrosplenial cortex can be visualized by the delayed appearance of activated microglia, overlapping to the damaged cortical layer (232, 236). Apparently, PCP administration induces neuroinflammation in certain brain regions; however, no microglial activation could be identified in rodent mPFC, even after subchronic treatment with very high doses (365). It is worth mentioning that endogenous ATP signalling is thought to modulate behavioral responses in schizophrenia-like symptoms (366).

In conclusion, while apparently the mPFC in experimental models of schizophrenia present limited evidence on the existence of a neuroinflammatory environment,

confirming the influence of P2X7R loss-of-function on anti-inflammatory processes may provide potential benefits.

1.6.1. P2X7 Receptor: the immunological bridge to psychiatric disorders

In the last decades, P2X7R emerged to be broadly involved in a variety of CNS pathologies (22), including psychiatric disorders (210). The first observation suggesting the involvement of P2X7R in the phenotypes of psychotic episodes came from a behavioral study on a broad spectrum of stressors (physical restraint, amphetamine and lipopolysaccharide treatments) in P2X7R^{-/-} mice (25), published by our laboratory. Csölle and colleagues, besides describing anti-depression phenotype in P2X7R^{-/-} animals (367), revealed a resistance against acute amphetamine hyperactivity. The proposed hypothesis regards a central-P2X7R mechanism that may reinforce the activation of the stress hypothalamus-pituitary-adrenal axis (25). About stress-induced depression models, it was noticed previously that P2X7R loss-of-function retains some benefits, without affecting the basic- and anxiety-related behaviors (368). After extensive research on the role of P2X7R in mood disorders, it has been recently hypothesized that ATP released by astrocytes and activated microglial P2X7R, leads to neuroinflammation, which can potentially govern the inflammatory aspect of the disease (212).

The loss of P2X7R attenuated psychotomimetic effects following d-amphetamine administration independently of transient mechanisms that are not linked with neuroinflammation. As mentioned, amphetamines are currently employed to model mania and schizophrenia-like psychotic episodes (227). Experiments studying amphetamines and P2X7R loss-of-function, repeatedly resulted in a weakened amphetamine-induced hyperactivity (369, 370, 371). The most recent work correlated the lack of amphetamine responsiveness with measurements of proinflammatory and excitotoxic mediators. Repeated treatments with amphetamine induced the increase of proinflammatory IL-1 β , TNF- α , and TBARS levels in specific brain areas; these changes were absent after P2X7R blockade (372). A study of the striatum in rodents receiving methamphetamine revealed increased P2X7R and decreased TH expression. The upregulation of P2X7R, alongside other methamphetamine effects, were also reproduced *in vitro* with embryonic stem cell-derived microglia (373). Another treatment with the substituted methamphetamine 3,4-methylenedioxymethamphetamine (MDMA or ecstasy) produced some disruption along the blood-brain barrier (BBB). Authors found

that BBB lesions could be due to early cellular damage induced by P2X7R-mediated enhancement of metalloprotease activity (374, 375).

P2X7R loss-of-function in mania, similar to depression, could in theory restrict the slow progression of neuroinflammation (372, 212). However, it is difficult to provide a theoretical explanation on the actual mechanisms: how the lack of functional P2X7R, principally expressed by glial cells, and silent under physiological conditions, could diminish amphetamine-induced acute flooding of dopamine in the frontal brain? Reportedly, ATP concentration is under the threshold necessary for P2X7R activation during drug-induced psychiatric events (366). Most likely, the local nucleotide concentration far exceeds what can be measured from plasma or whole tissue samples, and evidently can activate P2X7R during drug-induced psychiatric events.

1.6.2 Purinergic Receptors in animal models for schizophrenia

Ideas and theories about how the purinergic signaling system could be implicated in schizophrenia pathophysiology, have been first formulated decades ago (376).

For example, it is known that network oscillation activity raises significantly the extracellular ATP concentration in the brain (377). The CNS cell type that releases ATP could originate from astrocytes, which *in vitro* displayed activity-dependent exocytosis of both glutamate and ATP (378), and *in vivo* are responsible for the glutamate uptake, therefore modulating extrasynaptic glutamatergic signaling (379).

Adenosine receptors A1 and A2A have attracted particular attention for schizophrenia research, due to their fast signaling and numerous modulatory functions. A1R and A2AR control the synaptic plasticity and the release of glutamate and dopamine (380). The A1R activation inhibits glutamate release and reduces NMDA-R current, while A2AR agonists trigger the release of glutamate in striatal and cortical regions (381, 382). Moreover, postsynaptic A2AR activation leads to potentiation of NMDA-R currents, therefore controlling the basic synaptic plasticity (383). Presynaptic A1R inhibition, on the other side, reinforces the dopamine release (384). The activation of dopamine D2R leads to a reduced glutamate release by the formation of A2A/D2 or even A1/A2A receptor heteromers, which further complicates the scenario. For example, in the striatal region, heteromers A2A/D2 exert antagonistic interactions, meaning that adenosine/A2AR interaction lowers the D2R affinity for dopamine (224). Clinical trials demonstrated that drugs enhancing adenosine bioavailability can bring significant improvement in

controlling positive symptoms, but only when co-administered with antipsychotics (385, 386). Reduced striatal A2AR transcription, translation and increased methylation in the gene's coding region were found in the 50% of schizophrenic patients (387). Mice deficient for the A2AR showed schizophrenia-like phenotype, fitting in the standards of validity as a pathological model, presenting typical anatomical and behavioral alterations (388). Adenosine effects are not restricted to neurons: mice lacking the astrocytic expression of A2AR also developed certain psychomotor and memory impairments (389). Eventually, diminished activity of ectonucleotidases and consequently the reduced levels of extracellular adenosine, were also described in samples obtained from striatum of post-mortem schizophrenic patients (390). All the data considered, reduction in adenosine concentration might explain at least some of the pathological mechanisms in schizophrenia (391).

The P2Y1R, an unusual purinergic receptor protagonist of a few studies in the fields of cognition and psychiatric disorders, was found functionally expressed at spines and dendrites of pyramidal neurons and PV interneurons in the layer V of rat mPFC. Interestingly, no sign of the P2Y1R expression was found on TH-positive fibers (392). In the layer V neurons, activation of P2Y1 receptors by ATP/ADP lead to the inhibition of long-term depression (393), a pivotal form of synaptic plasticity. More recently a P2Y1R-dependent role on the activity of mPFC pyramidal cells was confirmed (394).

P2Y1R was also pinpointed by a study on chronic amphetamine treatments. The behavioral sensitization, developed with the repeated administration of psychostimulants, is thought to have a purinergic component (391). Intracerebroventricular pre-treatment with a general purinergic antagonist, prior to chronic amphetamine treatment, successfully prevented the development of behavioral sensitization, although finding an amphetamine-dependent upregulation of P2Y1R on glial striatal cells (395). In this case, it was proposed that the activation of P2Y1R, by endogenous ATP, could represent an intermediary step in the sensitization process to amphetamine (366). Whether neuronal or glial, P2Y1R seems implicated in the context of schizophrenia. Nonetheless, the ATP gradients for P2Y1R activation are, again, far from those required for the P2X7R.

A phenomenon closer to our subject of interest, is the observation that ATP induces the release of dopamine from nerve terminals in the striatum and nucleus accumbens. Reactive Blue-2, a P2Y receptor antagonist, largely inhibited this ATP-stimulated

dopamine release. This experiment provides indirect evidence that P2 receptors possibly participate in dopamine levels modulation (396).

Finally, pharmacological studies on antipsychotic drugs showed that haloperidol, chlorpromazine and fluspirilene attenuate the ATP-evoked responses mediated by P2X receptors, and without blocking the action of dopamine D2 receptors (367). More recently, it was found that the tricyclic antipsychotics prochlorperazine and trifluoperazine are negative allosteric modulators of the human P2X7R (397). In 2016 it was published, by our laboratory, that P2X7R genetic deletion or pharmacological blockade alleviates the acute psychotomimetic effects of PCP at low doses of 2 and 5 mg/kg (30). These changes were accompanied by alterations of the expression of schizophrenia-related genes in the PFC (30). However, it is unclear how changes in the activity of P2X7R lead to expression adjustments and behavioral alterations.

In the current study, we aimed to investigate the role of P2X7R in rodent schizophrenia models, based on acute and subchronic PCP delivery, in animals lacking or overexpressing the P2X7R; and to identify the underlying mechanisms involved. Initially we investigated the existence of a chronic smoldering proinflammatory state in the PFC, developing alongside the PCP subchronic treatment, since neuroinflammation might be a fitting pathway in which P2X7R could be involved and may contribute to. However, we found limited evidence which suggested neuroinflammation in the PFC during the experimental model of schizophrenia. Following, we studied the mPFC in the acute PCP model for positive symptoms, from which the majority of the current work was built. We then extended our previous observations to a P2rx7 subchronic PCP model, which reproduced cognitive deficits related to the working memory. Moreover, we tested the heterozygous animals overexpressing P2X7R-EGFP (36) to acute treatment with a regular and a low dosage of PCP, which better depicts an array of negative symptoms (330).

2. Aims

Schizophrenia is a complex psychiatric condition of which etiology, neurological substrate and pathological decline are still largely uncovered. Available treatments, although bearing risks of important side effects, can manage positive symptoms, but lack

efficacy for symptoms regarding cognitive dysfunctions. Preclinical studies implying PCP systemic administrations in rodents offer the possibility to observe, in healthy wild-type individuals, quantifiable behaviors related to the whole schizophrenia spectrum symptomatology.

P2X7Rs are protein channels abundantly expressed in the brain, mainly silent and considered to participate principally in pathological contexts. Empirical evidence demonstrated that loss-of-function of P2X7R exerts protective effects in several neurological disease models (22, 30). Yet, the P2X7R mode of action and molecular mechanisms, in models of psychosis, remain unclear and indirect evidence points to different directions.

Considering the complexity of the PCP pharmacology, were chosen as biological model two lines of P2X7R genetically modified mice, rather than treatments with P2X7R agonist and antagonists. The P2rx7^{-/-} strain expresses a loss-of-function truncated receptor, and the P2rx7^{tg/+} strain overexpresses a functional eGFP-fused P2X7R. The initial experiments were based on the examination of animal behavior. Indeed, like for the human diagnosis of schizophrenia, the validity of schizophrenia models is built over identifying the behavioral expression of symptoms. Once validated the model, the study followed a progressive training in different techniques along the PhD period. Beyond substantiating or dismissing potential benefits behind the P2X7R loss-of-function in positive- and cognitive-like PCP-induced symptoms, the project pursued the characterization of possible mechanisms where P2X7R could impact on the medial prefrontal cortex of the mouse.

Thus, our specific aims in this study were the following:

- Establishing in the laboratory a pharmacological mouse model of positive and cognitive symptoms of schizophrenia by employing acute and subchronic delivery of PCP.
- Identify possible differences regarding PCP-related behaviors between the P2rx7 genetically modified strains, and investigate the possible correlation with molecular and neurological measurements in the mouse mPFC.
- Investigate the possibility of involvement of neuroinflammatory phenomena in the PCP model in relation to P2X7R expression in the mouse mPFC.

- Examine the role of local P2X7R functional expression in native conditions at the level of the mouse mPFC.

3. Materials and methods

3.1. Animals

The behavior, histology, microscopy, cytokine quantification, and tritium-enriched dopamine ($[^3\text{H}]\text{-DA}$) release experiments were conducted in accordance with the principles and procedures described in the National Institutes of Health Guide for the Care and Use of Laboratory Animals and approved by the local Animal Care Committee of the Institute of Experimental Medicine (Budapest, Hungary, ref. No. PEI/001/778–6/2015). The electrophysiology and 2-photon experiments were approved and performed according to National and European regulations (RD1201/2005; 86/609/CEE) following the guidelines of the International Council for the Laboratory Animal Science at the University of the Basque Country UPV/EHU (CEEA 290/2015).

60-90 days old adult male mice, drug and test naïve, from wild-type ($\text{P2rx7}^{+/+}$), P2X7R knock-out $\text{P2rx7}^{-/-}$ and overexpressing $\text{P2rx7}^{\text{tg}/+}$ C57Bl/6 strains were housed 12/24 hours light and temperature-controlled room, with food and water *ad libitum*.

Homozygous $\text{P2rx7}^{+/+}$ mice were bred on C57Bl/6J background. The $\text{P2rx7}^{-/-}$ mice were kindly supplied by Christopher Gabel from Pfizer, Inc. (Groton CT, USA) or purchased (for electrophysiology experiments, Charles River, **35**). $\text{P2rx7}^{-/-}$ offsprings were cross-bred with $\text{P2rx7}^{+/+}$ mice, and heterozygotes offsprings were used as breeding stock for the F1 generation. Genotypes from the tails of $\text{P2rx7}^{+/+}$ and $\text{P2rx7}^{-/-}$ animals were confirmed by PCR analysis. The overexpressing P2X7R-EGFP C57Bl/6J mouse (line 17 in C57Bl/6N) was obtained from Annette Nicke (**36**) and bred heterozygously, thus offsprings $\text{P2rx7}^{\text{tg}/+}$ were tested. Male mice were raised in a group-cage until tested.

The fluorescent microglia mice $\text{CX3CR1}^{-/+}\text{EGFP}^{+/-}$ (**213**, Figures **18-20**), kindly provided by Maria Domercq, were employed for *ex vivo* microglia study. 3 female littermates (60, 61, 62 days-old) provided data of figures **18** and **19**, and seven 52-57 days-old $\text{CX3CR1}^{-/+}\text{EGFP}^{+/-}$ females and males were used for training and preliminary data of figure **20**.

3.2. Treatments

All treated animals were handled and habituated to the behavioral unit at least 24 hours before treatments. Injections and behavior tests were performed in separate rooms. Acute

treatment consisted of a single *i.p.* injection (volume 10ml/kg) of vehicle (0.9% NaCl sterile) or PCP at 10 mg/kg and 2 mg/kg dosages, referred as “PCP” and “low-dose PCP” respectively (PCP-HCl, Sigma-Aldrich Kft, Budapest, Hungary) freshly dissolved in vehicle. 180 minutes after the acute treatment, 10 animals P2rx7^{-/-} and P2rx7^{+/+}, and 12 animals P2rx7^{tg/+} and P2rx7^{+/+} were deeply anesthetized (Nembutal 100 mg/kg, Sigma-Aldrich Kft, Budapest, in vehicle at 10 mL/kg) and fixed by transcardial perfusion (Figure **6D**, **12A**). For the low-dose PCP experiment, 18 P2rx7^{-/-} and 18 P2X7R-EGFP2rx7^{tg/+} animals were habituated to the experimental room (30 mins.), received the injection and waited in the home-cage for 45 mins. Then, animals were tested in pairs (same genotype and treatment) in a circular open-field (10 mins., Figure **11A**). Subsequently, they were deeply anesthetized and transcardially perfused.

Subchronic treatment consisted of daily vehicle or 10 mg/kg PCP injections for 7 consecutive days (**42**). Cohorts of single-caged: 26 P2rx7^{+/+} and 30 P2rx7^{-/-} animals followed 7-days withdrawal period before sacrifice (**31**, 4.10, Figure **13**); 18 P2rx7^{+/+} and 26 P2rx7^{-/-} animals followed 14-days withdrawal period (4.12, Figure **15**); 10 P2rx7^{+/+} animals followed a 5-days withdrawal period (4.13, Figure **16**), 10 P2rx7^{+/+} and 10 P2rx7^{-/-} animals followed 4-days of withdrawal (4-14, Figure **17**), and a cohort of group-caged 28 P2rx7^{+/+} and 20 P2rx7^{-/-} followed 7-days withdrawal period (4.11, Figure **14**). Independent treatments were conducted with a maximum of 8 animals per genotype. The animals were perfused or decapitated after deep anesthesia.

3.3. Real-time qPCR

To measure the expression of P2X7R in the PFC, 5 wild-type and knock-out mice were sacrificed. The PFCs, cut at bregma \approx 1.20, were snap-frozen in liquid nitrogen and kept at -80°C. Total RNA isolation was performed using TRI Reagent® (Sigma-Aldrich, St. Louis, MO, USA) according to the manufacturer’s protocol. RNA concentrations were measured using Nanodrop 2000c Spectrophotometer (Thermo Fisher Scientific, Wilmington, DE, USA). The RNA integrity was verified by electrophoretic separation on 1% agarose gel. Reverse transcription from 1 μ g RNA into cDNA was performed using High-Capacity cDNA Archive Kit (Applied Biosystem, Foster City, CA, USA) according to the manufacturer’s protocol. Based on the previously published primer sequences (**128**), the following 3 regions of P2X7R were measured by Real-time quantitative PCR

(RT-qPCR): an extracellular region (1), an intracellular region (2), and an absent region in the knock-out mice (3, disrupted).

Primer sequences used to amplify the disrupted region was 5'-TGCATCACCACTCCAAGCTCTTCCAT-3' (forward primer) and 5'-CACCAGCAAGGGATCCTGGTAAAGC-3' (reverse primer); to amplify the extracellular part 5'-GCACGAATTATGGCACCGTC-3' (forward primer) and 5'-ACACCTGCCAGTCTGGATTCCT-3' (reverse primer); and to amplify the intracellular part 5'-AGGATCCGGAAGGAGTT-3' (forward primer) and 5'-TAGGGATACTTGAAGCCACT-3' (reverse primer) was used. The housekeeping gene, GAPDH, was used for normalization to account for intra-well variability (5'-TTCACCACCATGGAGAGGGC-3' (forward primer) and 5'-GGCATGGACTGTGGTCATGA-3' (reverse primer)).

The RT-qPCR reactions were performed using SensiFast SYBR Green No-Rox kit (Bioline Reagents Ltd., London, UK) according to the manufacturer's protocol in 10 μ l total volume. The RT-qPCR products of the P2X7R were visualized by electrophoretic separation on 1% agarose gel (data not shown).

3.4. Behavioral studies

3.4.1. Acute treatments

P2rx7^{+/+}, P2rx7^{-/-} and P2rx7^{tg/+} 71-81 days-old mice housed in individual cages at least 3 days before treatments. In P2rx7^{+/+} vs. P2rx7^{-/-} experiment, 5 received PCP and 4 vehicle, while in the P2rx7^{+/+} vs. P2rx7^{tg/+} experiment 9 PCP and 3 vehicle. Mice in their cages were habituated to the experimental room at dim (\approx 50 lux, P2rx7^{-/-}) or normal (\approx 250 lux, P2rx7^{tg/+}) light for 1 hour before experiments. Animals were individually transported to the treatment room, injected, and returned to the experimental within maximum 3 mins. in a clean home-cage (test arena). In P2rx7^{-/-} experiments, arenas were placed on an infrared backlight platform (IR, 850 nm) under a ceiling camera with an IR filter (Basler aca1300-60gc GigE camera equipped with Computar H3Z4512 CS-IR 4.5-12.5 mm F1.2 lens; filter Heliopan 35.5 RG850). This IR system generated high-contrast movies, depleted of reflected light artifacts, common with plexiglass. In P2rx7^{tg/+} experiments were performed under normal light. The animals were recorded for 90 mins. after the injections, then placed back to their home-cages for an additional 90 mins. before anesthesia, and fixation via perfusion. Experiments were independently repeated 2 times.

For the low-dose PCP study, P2rx7^{+/+} and P2rx7^{tg/+} animals were separated in individual cages the day before the experiment. 8 and 6 P2rx7^{+/+} and P2rx7^{tg/+} animals were treated with vehicles, and 10 and 12 with low-dose PCP, respectively. Habituation to the experimental room (30 mins.) and injections in treatment room were conducted in pairs. 45 mins. later mice were subjected to a circular open-field and social withdrawal tests (Figure 11) at normal light for 10 mins. (30). The scored behavioral variables were distance traveled, social interaction, ataxia, and stationary stereotyped behavior. The first two parameters were scored with a computer-based event recorder (Solomon, by <https://solomon.andraspeter.com>). Social investigations were defined as sniffing and contacting the partner's body with the nose. Stereotyped behavior and ataxia were manually scored, according to previously described protocols (398, 399). The experiment was independently repeated three times.

3.4.2. Subchronic Treatment

60-90 days-old P2rx7^{+/+} and P2rx7^{-/-} male mice were housed in individual cages and randomly assigned to PCP or vehicle subchronic treatment. On the 3rd day of treatment, 90 mins. after the injection, 4 randomly selected animals per group were placed one by one into a glass cylinder (10 cm diameter) and recorded for 5 mins. at normal light. The locomotor tests were repeated on the day after the 4th injection (24 hours washout).

After 3 days of treatment washout (72 hours from the last injection), the animals were tested in a y-maze (custom-built: arm length 30 cm; width 7 cm; walls height 20 cm; angle 120° equal) for 10 mins. at normal light and recorded. Animals that did not reach 20 alternations were excluded. Successful alternations were considered when an animal visited the three different arms consecutively, with the central body point passing the 20% of the arm length. Repeated passages from the center of the maze to the same arm were considered the same single-arm exploration (Figure 13), or as same arm entries (repeating visit in the same arm, passing the 20% arm-length, to the center, and back to the same arm passing the 20% arm-length, Figure 14).

Open-field tests of 10 mins. (Figure 13D) and 15 mins. (Figure 15) were performed in arena measuring 33 cm per 45 cm per 18cm. The novel object recognition (NOR) test was performed before the first (pre-treatment control), and 24 hours after the last subchronic injection, at normal light conditions, in a novel home-cage. Familiar-objects exploration: 10 mins.; inter-trial interval: 10 mins.; NOR test: 3 mins. The 10 drug-naïve P2rx7^{+/+}

animals, single-caged for 3 days in the behavioral unit before the first NOR (Figure 16A). Behavior was quantified and analyzed offline using Noldus EthoVision XT[®], object exploration as time spent sniffing/touching the objects.

3.5. Histology

3.5.1. Acute treatment

To study the neuronal activity during the psychotomimetic effect of PCP *in vivo* (40 mins. after acute injection), animals were sacrificed after reaching the peak of c-Fos protein expression (90 mins., 286, 400). Therefore, 180 mins. after the treatment, each animal received pentobarbital anesthesia. After 10-20 mins., the animals were transcardially perfused, rinsed for 3 mins. with saline (flow rate 5 ml/min) and followed by 15 mins. perfusion with 4% paraformaldehyde (PFA, Merck-Sigma) in 0.1 M phosphate buffer (PB, Na₂HPO₄·2H₂O; NaH₂PO₄, Merck-Sigma) solution. To compare c-Fos stainings, the time schedule was strictly respected. Brains were removed and post-fixed in 4% PFA at 4 °C overnight. The following day, the collected brains were extensively washed in PB. The prefrontal cortices were coronally sliced (40 µm thickness, Vibratome Leica VT 1200 Wetzlar, Germany) and rinsed in PB before staining protocols. Coronal slices of the PFC (bregma +1.70 - +2.10) were selected for immunohistochemistry.

3.5.2. c-Fos DAB

Two free-floating slices from 3 saline- and 4 PCP-treated animals per genotype (P2rx7^{+/+} and P2rx7^{-/-}) were incubated for 10 mins. in 3% H₂O₂ in PB, then rinsed in PB (3 times for 10 mins.). The pre-made blocking buffer (ImmPRESS UNIVERSAL REAGENT, Vector laboratories, MP-7500) was supplemented with 0.5% Triton X-100 (Tx, Merck-Sigma), and 7.5% of normal donkey serum (NDS, Jackson Immunoresearch, Europe LTD). After 1 hour of blocking, slices were incubated with the primary rabbit anti-c-FOS antibody (1:1000, Santa Cruz Biotechnology sc-52, Dallas, US) in PB containing 0.05% sodium azide (Merck-Sigma) for 24 hours at room temperature (RT) and 72 hours at 4 °C. Eventually, the slices were rinsed in PB and incubated with the secondary anti-mouse/rabbit HRP-conjugated ImmPRESS UNIVERSAL REAGENT (Vector laboratories, MP-7500) for 1 h. DAB was developed using the commercially available DAB-REACTION KIT (Vector Laboratories, SK-4105) according to the manufacturer's instructions.

3.5.3. Fluorescence immunohistochemistry

A similar protocol to the above DAB staining was performed for single, double and triple fluorescence immunostainings. Free-floating slices were rinsed in PB and blocked for 1 hour (10% NDS; 0.5% Tx in PB). Antibody against murine c-Fos (1:1000, 226.004 Synaptic System, Göttingen, Germany) was dissolved in PB-0.05% sodium azide, 0.1% NDS, and 0.2% Tx. Slices were incubated with the c-Fos primary solution for 1 day at RT and 2 days at 4 °C. For c-Fos double- and triple-immunostainings, additional primary antibodies were added on the 3rd day of anti-c-Fos incubation, against murine proteins: Parvalbumin (PV, 1:500, PVG-213, Swant, Marly, Switzerland), P2Y12R (1:400, AS-55043, AnaSpec, San Jos, California), NeuN (1:400, MAB377, Merck Millipore, Darmstadt, Germany), tyrosine hydroxylase (TH, 1:400, EP1532Y, Abcam, Cambridge, UK) and GFP (P2rx7^{tg/+}, 1:500, GFP-1020, Aves Labs). Similarly, non c-Fos immunostainings underwent 2 hours blocking (5% NDS; 0.2-0,3 % Tx in PB) at RT, and primary antibody (dissolved in blocking solution) overnight incubation at 4 °C. Staining against P2Y12R and GFP for demonstrative localization of P2X7R in mPFC microglia, and against Iba-1 (1:400, 019-19741 FUJIFILM Wako Pure Chemicals U.S.A Corporation) and GFAP (1:4000, ab4674, Abcam) for unpublished analyses (**Figure 17**). Eventually, the slices were rinsed with PB and incubated for 1-2 hours at RT with the corresponding secondary antibodies (1:500, 706-605-148 Alexa Fluor 647 Donkey anti-guinea pig for c-Fos; 715-585-150 Alexa Fluor 594 Donkey anti-mouse for NeuN; 711-605-152 Alexa Fluor 647 Donkey anti-rabbit for TH and Iba-1; 705-585-003 Alexa Fluor 594 Donkey anti-goat for PV; 711-545-152 Alexa Fluor 488 Donkey anti-rabbit for P2Y12R, Jackson ImmunoResearch, Europe LTD; A-11039 Alexa Fluor 488 Goat anti-chicken for GFP; ThermoFisher; ab150169 Alexa Fluor 488 Goat anti-chicken for GFAP; Abcam).

After DAB-revelation or secondary incubation, slices were rinsed in PB (3 for 20 mins.) and mounted with ProLong™ Gold Antifade Mountant (P36934, Thermo Scientific).

3.6. Confocal microscopy

Microscopy was carried out at the Nikon Microscopy Center in the Institute of Experimental Medicine at the Hungarian Academy of Science. Pictures were taken with a confocal Nikon C2 microscope (20X-water and 60X-oil immersion objectives). Bright field c-Fos DAB pictures were taken with a color camera (DS-Fi3), 11 steps per z-step= 2.5 µm. Fluorescent pictures, 11-20 steps per z-step=0,5-1 µm (acute: c-Fos, c-Fos/PV;

c-Fos/TH; c-Fos/P2Y12R/NeuN; P2Y12R/GFP; subchronic: c-Fos/PV/NeuN; P2Y12R/GFAP); 30-38 steps z-steps 1 μm (acute c-Fos/P2Y12R); single-plane large pictures (subchronic Iba-1). Images were analyzed using the software FIJI ImageJ, through which all standardized processing and quantifications were obtained (401). Automated c-Fos nuclear counting in mPFC regions-of-interest; layers width: I= 120-140 μm ; II/III= 80 μm ; V= 320-350 μm ; VI> 280 μm (Figure 3A right). The c-Fos mean gray values were measured over the counted masks with FIJI ImageJ. The 2D/3D Sholl analyses was performed using the FIJI ImageJ application (402).

3.7 [³H]-Dopamine release experiment

The [³H]-DA release experiments were conducted using a previously published method (27, 30). 2-3-months-old male mice (32 P2rx7^{+/+}, 11 P2rx7^{-/-} and 4 in P2rx7^{tg/+}) were anesthetized under light CO₂ inhalation, decapitated, and the brain was rapidly removed. The PFC was dissected in ice-cold Krebs' solution saturated with 95% O₂ and 5% CO₂ and chopped in coronal 400 μm -thick slices (McIlwain tissue chopper). Acute slices were incubated for 45 mins. at 37 °C in 1 mL Krebs solution with 5 $\mu\text{Ci/mL}$ [³H]-DA (specific activity 60 Ci/mmol; ARC, Saint Louis, MO, USA), bubbled with 95% O₂ and 5% CO₂. Once loaded with [³H]-DA, the slices were sealed in chambers and continuously perfused with 95% O₂, and 5% CO₂-saturated modified Krebs solution, 37 °C (flow rate: 0.7 mL/min). After 90 mins. to wash excessive [³H]-DA, perfusate samples were collected over 3 min periods and assayed for tritium content. At the 20th minute of perfusate collection, the slices were exposed for 3 mins. to 20 μM veratridine (Sigma Chemical Co., St. Louis, MO, USA) perfusion. The radioactivity of the samples was measured using a Packard 1900 TriCarb liquid scintillation spectrometer and an Ultima Gold Scintillation cocktail. The release of tritium was expressed as a percentage of the total amount of radioactivity (released and inside the tissue), normalized over the tissue weight, therefore defined as fractional release. The PFC [³H]-DA uptake was determined by the sum of radioactivity released plus the tissue remaining content, after the experiment, expressed in Bq/g. Basal [³H]-DA outflow was calculated as the fractional release measured in two consecutive 3 mins. samples under drug-free conditions. The veratridine-induced [³H]-DA efflux was calculated as the net release in response to the veratridine stimulation, by subtracting the release before the stimulation from the values measured after stimulation.

3.8 Electrophysiology

8 P2rx7^{+/+} and 6 P2rx7^{-/-} male mice 59 to 75 days-old were anesthetized with isoflurane (IsoVetR 469860, Braun) and decapitated. The brain was rapidly extracted and immersed in ice-cold N-methyl D-glucamine based cutting solution (NMDG 92 mM, NaHCO₃ 30 mM, NaH₂PO₄ 1.25 mM, HEPES 20 mM, glucose 25 mM, Na-ascorbate 5 mM, Na-pyruvate 3 mM, Thiourea 2 mM, KCl 2.5 mM, MgSO₄ 10 mM, CaCl₂ 0.5 mM; all from Merck-Sigma; pH 7.3) for 2 min, before being embedded in 2% low temperature melting agarose gel (Merck-Sigma) and sliced in ice-cold NMDG-based solution with a Compressstome (300 μm thickness, VF-300-0F Precisionary). Coronal PFC slices (bregma +1.70- +2.50) recovered for 30 mins. in an NMDG-based cutting solution bubbled with 95% O₂ and 5% CO₂ at 37 °C. Slices were transferred for an additional hour in artificial cerebrospinal fluid (ACSF, 300/306 mOsm, pH 7.3, NaCl 119 mM, KCl, 2.5 mM, MgCl₂ 1.6 mM NaHCO₃ 26 mM, NaH₂PO₄ 1 mM, HEPES 5 mM, D-glucose 10 mM, CaCl₂ 2.5 mM; Merck-Sigma) at RT. Patch-clamp experiments of neurons in the PL mPFC cortical layer V were guided by IR differential interference contrast video microscopy (CleverExlore, MCI Neuroscience). A pipette solution containing K-gluconate 125 mM, KCl 5 mM, HEPES 10 mM, EGTA 1 mM, 4 mM Na₂GTP, 0.3 mM, NaP-creatine 10 mM, ascorbic acid 3 mM (280-295 mOsm, pH 7.3; all from Merck-Sigma) was used, yielding a tip resistance of 4–5 MΩ. Recordings were obtained 200 s after whole patch-clamp configuration (steady-state condition). The resting membrane potential (V_m) was recorded in current-clamp mode at 0 pA for 10s. Current/Voltage (I/V) relationship and action potential firing were obtained with 0.4 s square pulse current step injections, from -100 pA to +280 pA at 20 pA increments (I_{step}, 1 per second). 100 ms before each I_{step}, a 1 ms current pulse of -75 pA was injected, to normalize the V_m after depolarization. The membrane potential at 0 pA, before and after I_{step}, were taken from the average voltage of the 30 ms before I_{step} (V_m_{pre}) and of the last 0.1 s after 0.3 s from I_{step} (V_m_{post}). Injection of 0 to 500 pA ramp current over 1 s was used to calculate the rheobase, the current amount required to elicit the first action potential. All currents and voltages were registered and controlled using a HEKA EPC10 amplifier. Data were analyzed using the Fitmaster software (HEKA electronic).

3.9 Two-photon microscopy imaging of fluorescent microglia *ex vivo*

Differences respect to the aforementioned electrophysiological acute-slices preparation were the thickness (450 μm) and less recovery time in ACSF (control) or 10 μM BBG in ACSF. From the sacrifice, no more than 4 hours passed before the movies were obtained (176). Slices in an electrophysiology chamber under a 2-photon microscope (Femto-2D, Femtomics, Hungary) were continuously perfused with 37°C bubbled ACSF, 10 μM BBG in ACSF, 3 mM MgATP in ACSF and both BBG and ATP in ACSF. Quantified movies were collected at a minimal tissue depth of 70 μm . Acknowledging that phototoxicity is unavoidable, we set the laser with already published parameters (176, 177, 178).

3.10. Two-photon fluorescent microglia movie analysis

In figure 18B is underlined one main issue of 2-photon movies: the three-dimensional (3D) drift. While imaging a defined volume, often the slice slowly shifts inside the recording chamber, depending on the perfusion current and laser-induced heating. When the cells move along a 3D vector over time, a semi-automated alignment (3D registration, FIJI ImageJ, Figure 18B, center) can be applied. The maximum projections of registered movies (Figure 18B, left) are easily quantifiable. Calculation of relative microglia-occupied area (cell volume) and surveillance (microglial newly-occupied area, calculated as the progressive maximal projection with z-axis as time) were obtained with FIJI ImageJ functions, and normalized over the movie first time-frame considered.

For the quantification of the field-of-view rates of microglial expansion and retraction, the values were calculated as the image portion resulting from the signal subtraction:

$$\begin{aligned} \text{for retraction (red)} &= \text{time-frame}_n - \text{time-frame}_{n+1} \\ \text{for expansion (cyan)} &= \text{time-frame}_n - \text{time-frame}_{n-1} \end{aligned}$$

Calculation of the net expansion per time-frame was obtained from the difference between red and cyan:

$$\text{net expansion} = \text{red}_n + (- \text{cyan}_n)$$

The net expansion calculation is depleted from slow xy-plane drifts, and considers only actual changes in signal morphology (Figure 19). Eventually, the average of net expansion over a number of time-frames can be useful to see which cellular behavior happens over a longer period. The frame rate of BBG experiments was 2 mins. and the duration 42-44 mins, while in ATP experiments was 1 minute frame rate for 21-22 mins.

3.11. Cytokine quantification

Cytokine quantification from the PFC of subchronically treated animals was performed as described in our previous paper (29). Briefly, after 7-days PCP or vehicle withdrawal period, brain samples were collected after light CO₂ anesthesia. Tissue was homogenized and centrifuged, as previously published (403), and supernatants were collected to measure the levels of the inflammatory mediators IL-1 α , IL-1 β , IL-6, IL-10, TNF- α , and CXCL1 (KC) using BD Cytometric Bead Array Flex Sets (BD Biosciences). Measurements were performed on a BD FACSVerser flow cytometer, and data were analyzed using FCAP Array v. 5 (Soft Flow). Cytokine concentrations in the brain tissue were normalized to total protein levels measured by photometry using a BCA Protein Assay Kit (Thermo Fisher Scientific, Pierce). Absorbance was measured at 560 nm using a Victor 3V 1420 Multilabel Counter (PerkinElmer). Cytokine levels are expressed as picograms per milliliter.

3.12. Statistics

Statistical analyses were performed using STATISTICA version 64 (StatSoft. Inc., Tulsa, OK, USA) and Graph Prism version 5 (GraphPad Software, San Diego, CA, USA). The RT-qPCR data was analyzed using the $-\Delta\Delta C_t$ ($2^{-\Delta\Delta C_t}$) calculation method, for comparison was used unpaired nonparametric Mann-Whitney test. Differences between two groups were analyzed using the Student's *t*-test. Between multiple groups, one-way analysis of variance (ANOVA) followed by a *post-hoc* Kruskal–Wallis or Dunn's comparison test, or two-way ANOVA followed by Bonferroni's *post hoc* test, or Mann-Whitney *U*-test were used, as appropriate for multiple comparisons. Specific tests are reported in captions of the figures. All data are expressed as a mean \pm standard error of the mean (SEM). Symbols for *p*-values: * vs. first column/group; # vs. second column/group; \$ vs. third column/group. Values of *p*-values: * <0.05 , ** <0.01 , *** <0.005 , **** <0.001 . A *p*-value lower than 0.05 was considered statistically significant.

4. Results

4.1. P2rx7 receptor expression in C57Bl/6 Prefrontal cortex

To confirm the validity of the applied knock-out model, RT-qPCR experiments were performed to detect P2rx7 gene transcripts (Figure 4A). The RNA was extracted from the whole frontal area (Figure 4B). The RT-qPCR measurement confirmed that the disrupted sequence was markedly reduced in P2rx7^{-/-} mice compared to P2rx7^{+/+} mice. No differences were detected in extra- and intracellular sequence levels between genotypes (Figure 4C). The visualization of RT-qPCR products by electrophoretic separation (data not shown) confirmed that the 90 bp band, corresponding to the truncated sequence of Pfizer P2rx7^{-/-} mice, appeared only in the P2rx7^{+/+}.

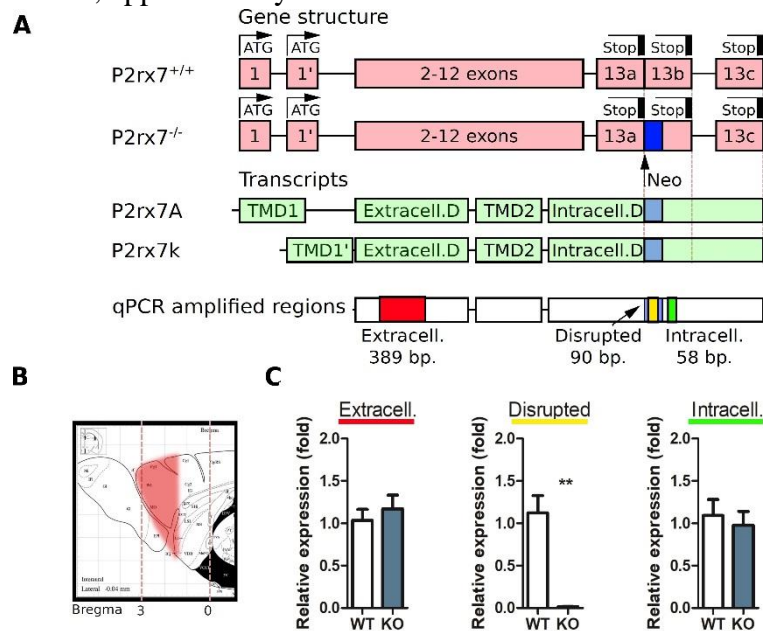


Figure 4. P2rx7 expression analysis in the PFC with RT qPCR. **A)** Schematic representation of the P2rx7 gene in P2rx7^{+/+} and P2rx7^{-/-} mouse lines, the principal splicing variants found in C57Bl/6 line, and the amplified regions in the RT-qPCR. **B)** Schematic representation of the PFC analyzed. (404, sagittal). **C)** P2X7R expression analysis in P2rx7^{+/+} and P2rx7^{-/-} mice in PFC by RT qPCR. Relative expressions calculated as fold changes normalized to GAPDH. The figure shows the mean \pm SEM (N=5, both groups). Statistics: unpaired Student's *t*-test, *p*-value ** < 0.01 (C). Collaboration with Pàl Tod (31).

4.2 Acute PCP treatment-induced hyperactivity was alleviated in P2rx7^{-/-} mice

To evaluate the involvement of P2X7R in PCP-induced hyperlocomotor activity, an open-field auto-tracking experiment was performed using a novel cage as arenas. P2rx7^{+/+} and P2rx7^{-/-} mice were treated with vehicle and 10 mg/kg PCP *i.p.*, and placed immediately in the arena. After PCP injection, every subject increased the locomotion and persisted in stereotypic behaviors, such as head weaving and rotational movement. Hyperlocomotion and frequency of rotations peaked between 40 and 80 mins. after PCP delivery (Figures 5B, 5C). The effect of PCP was significantly more pronounced in P2rx7^{+/+} animals, in terms of stereotypy, and P2rx7^{+/+} hyperlocomotory behavior lasted longer (Figure 5C).

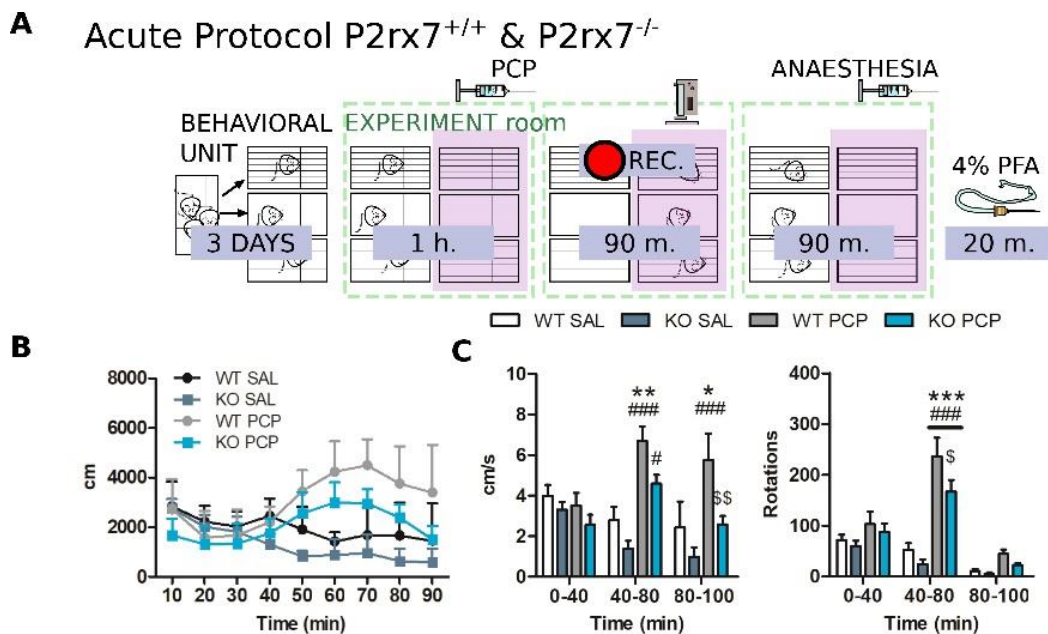


Figure 5. P2rx7^{-/-} mice are less sensitive to the psychotomimetic effects of acute PCP. **A**) Schematic representation of the behavioral protocol of acute treatment. The pink panel represents the IR backlight, and the pink rectangle in front of the camera the IR filter. **B**) Distance traveled by animals after the injection. **C**) Mean velocity (left) and numbers of rotations (right) averaged in 40 mins. time blocks, plus the remaining recorded time. The psychotomimetic effect of PCP was evident 40 mins. after injection. N=4 (SAL), N=5 (KO PCP), and N=6 (WT PCP). The figure shows mean \pm SEM. Statistics: two-way ANOVA followed by Bonferroni's *posthoc* test, *p*-value * < 0.05; ** < 0.01; *** < 0.005 vs. WT SAL; *p*-value # < 0.05; ### < 0.005 vs. KO SAL; *p*-value \$ < 0.05, \$\$ < 0.01 vs. WT PCP (C).

4.3 P2rx7^{-/-} layer-specific neuronal activation in the mPFC is lower

As mentioned in the introduction, acute systemic PCP induces hyperactivity of the mPFC circuit. To follow this effect, neuronal activation was monitored using c-Fos immunohistochemistry in combination with the behavioral protocol (Figure 5A). The c-Fos proto-oncogene is a transcription factor of which the expression directly correlates with single-cell neuronal activity. In other words, c-Fos is a molecular marker for recently active neurons (405). Since c-Fos is typically detected 60-180 mins. after the behavior of interest, all animals followed a strict time scheduled protocol (Figure 5A). Along the mPFC of PCP-treated animals, appeared the aforementioned band of c-Fos immunopositive neuronal somata (c-Fos⁺), primarily at the level of layer V (Figure 6A, 340). Quantification of c-Fos⁺ revealed a ventrodorsal gradient of active neuron concentration. This robust PCP-driven engagement of the IL and PL areas was not present in saline-treated animals (Figure 6B). The decreased PCP-related behavior in P2rx7^{-/-} mice (Figure 5C) was associated with a lower concentration of PCP-induced c-Fos⁺ in the layer II/III of ventral mPFC (Figure 6B). Considering that the nuclear level of the c-Fos protein proportional to neuronal activity (406), a deeper study of areas of interest for PCP effect is possible. To limit technical biases, two different anti-c-Fos antibodies with different protocols were used (Figures 6A, 6C). The histogram representing the distribution of c-Fos⁺ average intensity signal showed a subtle difference between the tested genotypes (Figure 6D). Pragmatic discrimination between activated (c-Fos⁺) and strongly activated (here referred as c-Fos⁺⁺) neurons enabled to set the dimension and intensity thresholds (200 μm^2 area and 400 mean gray value intensity, ImageJ standardized units), respectively. A significant decrease in the concentration of c-Fos⁺⁺ neurons was detected in the layer V of IL and PL areas in P2rx7^{-/-} mice (Figure 6E). Considering the current results, the psychotomimetic effects of 10 mg PCP, behavioral and mPFC layer-specific neuronal activation, seem partially buffered by the genetic deletion of P2rx7^{-/-}.

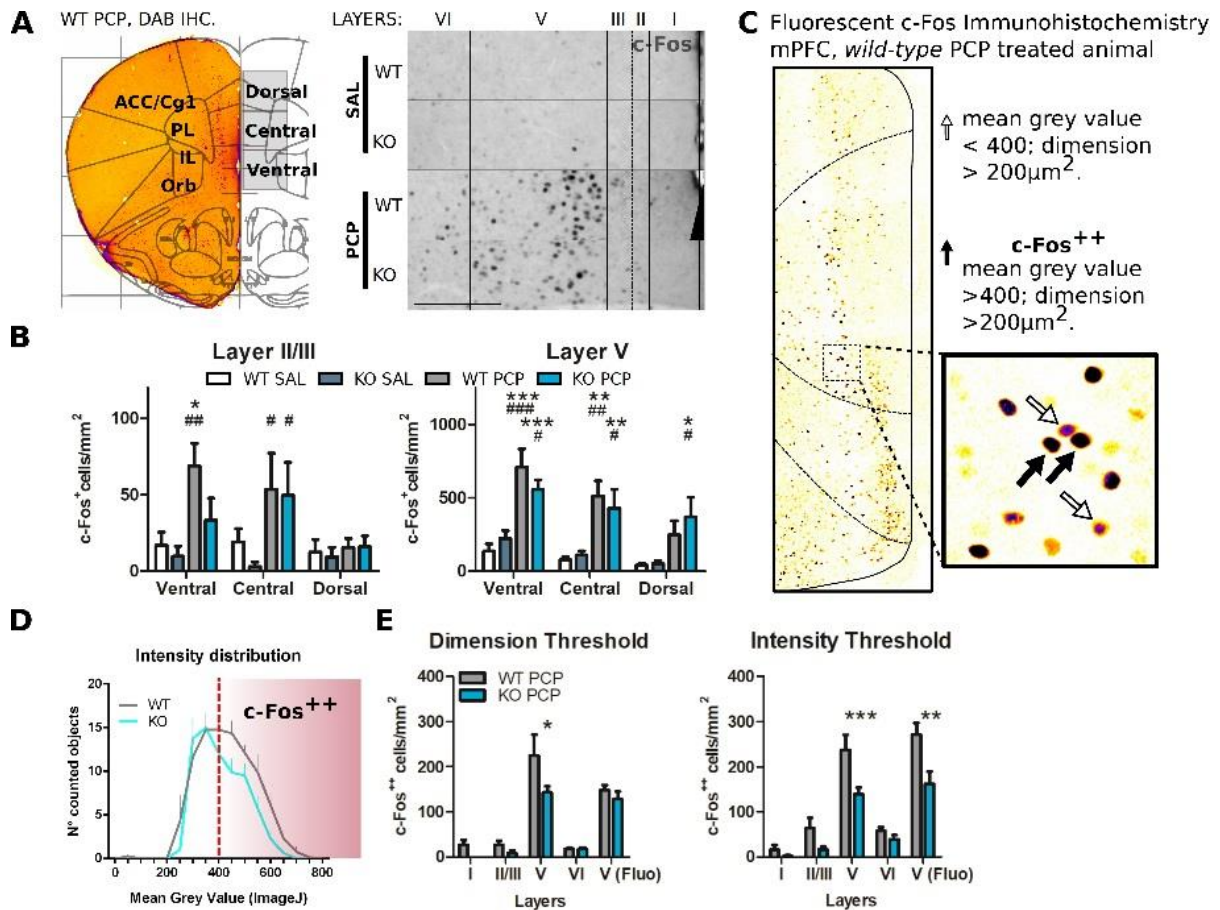


Figure 6. The reduced PCP behavioral outcome in $P2rx7^{-/-}$ correlates with lower PCP-driven hyperactivation of mPFC neurons. **A)** Representative c-Fos/DAB immunostaining of a coronal PFC from a $P2rx7^{+/+}$ PCP treated mouse (404, bregma +2.00). In the left hemisphere are represented the quantified areas (left). Representative immunostaining used for automated c-Fos nuclei count. Layer width, from midline: I= 120-140 μm ; II/III= 80 μm ; V= 320-350 μm ; VI= minimum 280 μm . Scale bar: 200 μm (right). **B)** Quantification of c-Fos⁺ in layers II/III and V of the medial PFC. **C)** Representative picture of coronal PFC immunofluorescent staining (WT PCP) with a different c-Fos antibody. In the insert, white arrows indicate c-Fos⁺ activated nuclei (mean gray value < 400, dimension > 200 μm^2) while the black arrows indicate strongly immunostained c-Fos⁺⁺ nuclei (mean gray value > 400; dimension > 200 μm^2 . Insert 165 μm^2 . **D)** Averaged histogram of the mean grey value for the automatically detected c-Fos positive nuclei in layer V PCP-treated PL and IL areas (ventral and central mPFC pictures). The red dashed line represents the c-Fos⁺⁺ intensity threshold (400 units of mean gray value, FIJI ImageJ). **E)** Quantification of PL and IL content of strongly activated c-Fos⁺⁺ nuclei, by dimension (left) and intensity (right) threshold. Automatic counting with FIJI ImageJ of each mPFC layer for DAB immunostaining, and in the isolated layer V for fluorescent

immunostaining. N=3 (Sal), N=4 (PCP). Shown is mean \pm SEM. Statistics: two-way ANOVA followed by Bonferroni's *posthoc* test, p -value * < 0.05; ** < 0.01; *** < 0.005 vs. WT SAL; p -value # < 0.05; ## < 0.01; ### < 0.005 vs. KO SAL (B); p -value * < 0.05; *** < 0.005 vs. WT PCP (E).

4.4 P2X7R deficiency does not affect PCP-related changes in PV interneurons

PV interneurons are proposed determinant to both the PCP and schizophrenia underlying mechanisms (see section 5.3.2.3.). Double immunohistochemistry for c-Fos and PV neuronal markers were performed in the mPFC of acute PCP-treated $P2rx7^{+/+}$ and $P2rx7^{-/-}$ mice. Images were manually quantified by an investigator blinded to the experimental conditions (Figure 7A). Nonetheless, no difference was found between the tested genotypes, nor the total number of PV positive interneurons (Figure 7B), nor the percentage of the PV-immunopositive cells activated by the systemic PCP effect at the level of the layers II/III and V (Figure 7C). We therefore excluded a substantial involvement of cortical PV interneurons in the differential PCP-effect on the tested genotypes.

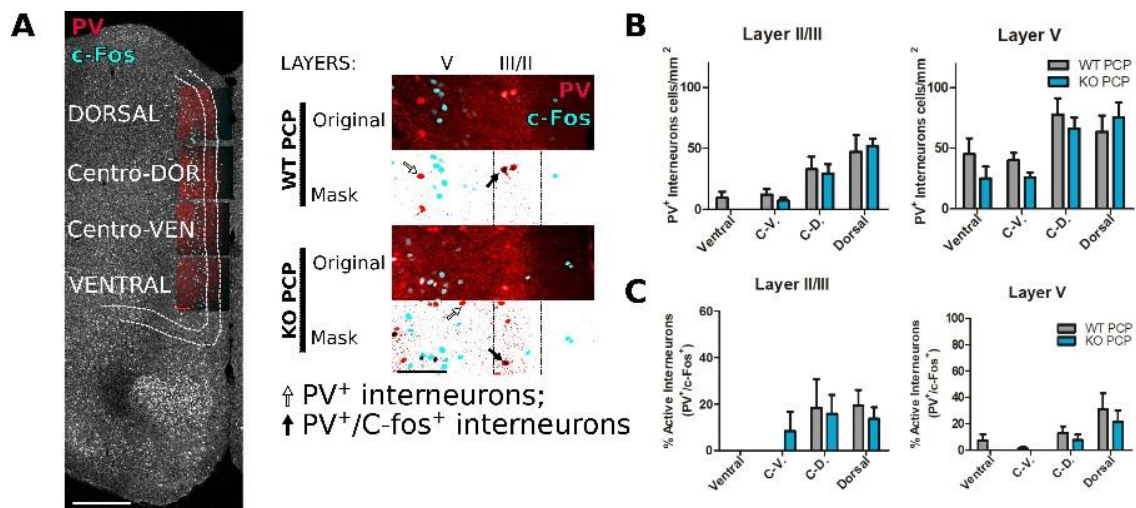


Figure 7. PV interneurons display unaltered density and levels of activity in PCP-treated mPFC of $P2rx7^{-/-}$ and $P2rx7^{+/+}$ animals. **A)** Double immunostaining of c-Fos and PV. Reconstructed mPFC from a $P2rx7^{+/+}$ PCP mouse. Scale bar, 500 μ m (left). Representative images of dorsal mPFC double immunostaining (right). Are shown the original stacks maximal projections (up) and masks of threshold images (down) to facilitate the manual interneurons counting (PV⁺: black arrow; double PV⁺ and c-Fos⁺ white arrow) Scale bar 100 μ m. **B)** Results of manual counting of PV⁺ interneurons

concentrations in mPFC of PCP-treated animals. C) Results of the manual counting of double-positive PV⁺ and c-Fos⁺ interneurons expressed as the percentage of the counted PV⁺ interneurons. Layers II/III = 80 μ m; V = 320-350 μ m. N=4 (WT PCP), N=3 (KO PCP). Shown is mean \pm SEM. Statistics: two-way ANOVA followed by Bonferroni's *posthoc* test, no significant differences, *p*-value>0.05.

4.5 The PFC and dopamine release from the striatum

We moved our focus on the dopaminergic influence. No significant genotype-related anatomical differences were observed in a pilot experiment, by quantifying mPFC double immunostaining for c-Fos and TH, a dopamine- and noradrenaline-synthesizing enzyme expressed in axon terminals (Figure 8A). Beyond confirming a significant PCP-induced increase of c-Fos expression in P2rx7^{+/+} mPFC layer V (200/220 μ m from the midline, Figure 8B, upper panel), no change in TH-fiber density was identified (Figure 8B, lower panel and 8C). We next studied the properties of the release from PFC dopaminergic fibers. [³H]-DA-loaded acute *ex vivo* slices of PFC provide an opportunity to clarify the involvement of P2rx7 expression on treatment-naïve dopaminergic efferents. The strong Na⁺ channel-mediated [³H]-DA release, pharmacologically induced by 3- mins. 20 μ M veratridine perfusion on the wt slices (407 Figure 8D) did not differ between controls and P2rx7^{-/-} or P2rx7^{tg/+} animals. The current data confirm our previous finding (30), that PFC of P2rx7^{-/-} animals display lower basal dopamine release (Figure 8E, left panel). On the other hand, the uptake of dopamine found in P2rx7^{tg/+} PFC was lower when compared to the corresponding wild-type controls (Figure 8F, right panel).

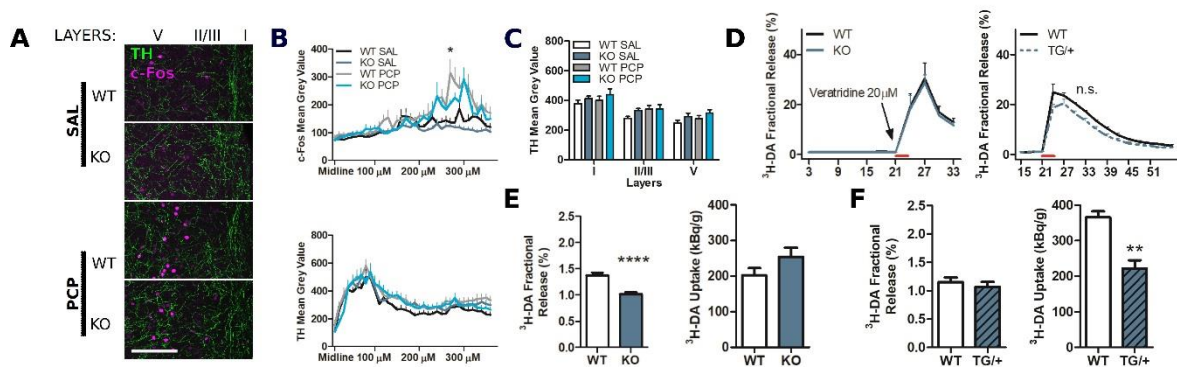


Figure 8. The PFC of P2rx7^{-/-} displays lower dopamine release, while P2rx7 overexpression leads to lower dopamine uptake, compared to wild-type PFC. A) Example of P2rx7^{-/-} and P2rx7^{+/+} mPFC double immunostaining of c-Fos and the dopamine- and

noradrenaline-synthesizing fiber's marker TH. Z-stack maximal projections. Scale bar 100 μm . **B**) Medial-to-lateral longitudinal quantification of the c-Fos (up) and TH (down) immunoreactivity (FIJI ImageJ). **C**) Quantification of TH expression, pilot experiment. N=2; 6 pictures per animal. Shown is mean \pm SEM. Statistics: two-way ANOVA followed by Bonferroni's *posthoc* test. B(up) * p -value < 0.05 ; WT PCP vs. KO PCP, 270-280 μm depth from midline. **D**) Graph displays stimulated fractional release from PFC slices induced by 20 μM veratridine perfusion. N=28 (WT); N=11 (KO), left; N=4 (WT); N=4 (TG/+), right. Shown is mean \pm SEM. Statistics: two-way ANOVA followed by Bonferroni's *posthoc* test. Scoring: no significant differences, p -value > 0.05 . **E**) Results of the P2rx7^{-/-} [³H]-DA release experiments. N=14 (WT); N=8 (KO). **F**) Results of the P2rx7^{tg/+} [³H]-DA release experiments. The quantification suggests that the newly tested P2X7R-EGFP line displays lower PFC DA uptake respect to the wild-type PFC; N=4 (WT) N=4 (TG/+). Shown is mean \pm SEM. Statistics: unpaired Student's *t*-test with Welch corrections, p -value **** < 0.001 vs. KO (E); p -value * < 0.05 vs. TG/+ (F). In collaboration with S.E. Vizi laboratory, (31).

4.6 P2X7R gene deficiency may play a role in microglial contacts with hyperactive neuronal soma

After typical PCP-related topics, we addressed the role of the P2X7R expressed by microglial cells in the context of PCP-driven mPFC neuronal activation. P2Y12R immunohistochemistry was used to label resting, not-activated microglia (165, 166, 183), and exclusively expressed by microglia in the cortex (109, 408). Coronal slices of IL and PL cortical layer V from vehicle- and PCP-treated P2rx7^{-/-} and P2rx7^{tg/+} animals were immunohistochemically stained against P2Y12R (Figures 9A, 9C), c-Fos and P2Y12R (Figures 9G, 9I), and c-Fos, P2Y12R and NeuN (mature neuronal nuclear marker, Figure 9E). Manual counting and automated analyses of the P2Y12R immunostainings showed no differences in microglial density and general ramification, while the mean signal was lower in acute PCP-treated P2rx7^{-/-} when compared with PCP-treated P2rx7^{tg/+} mice (Figure 9B). IL and PL maximal projections of 10 μm thick stacks allowed us to perform a soma-centered 2D-Sholl analysis on non-isolated microglial cells (Figure 9C, left). This atypical Sholl analysis does not present the characteristic "crossing branches count" curve from single-cell ramifications. The microglia ramification in the cortex shapes an intricate

and homogeneous network of processes. Each cell presents a unique 3D morphology, typically extending tens of microns, rendering challenging the precise reconstruction and isolation of entire cells in an imaged volume. Therefore, the analysis in **9C**, first proposed by (31), provided a mixed Sholl-analysis profile, where instead of the typical bell-shaped curve of a single cell, the number of crossing branches increased linearly with the extension of the Sholl radius (Figure **9D**). It is reasonable to consider that the area immediately surrounding the microglial nucleus (0-20 μm radius Sholl circles, red bar Figures **9C**, **9D**), represents the ramification of a single cell. Microglial nuclei are evenly distributed in the cortex, rarely less than 20 μm apart. A larger Sholl radius (20-40 μm , green bar Figures **9C**, **9D**) covers the territory patrolled by branches from several cells, here referred to as inter-cellular territory (Figure **9C**, right panel). Adopting the graph identity function ($f(x)=x$, red-dashed line Figure **9D**) as the y Cartesian axis graph allows the better visualization of differences in the microglial ramification profiles (Figure **9D''**). The graph **9D''** illustrates that single-cell ramifications are similar between all groups (Figure **9C**; red bar). Distal from the microglial nucleus, the saline-treated $\text{P2rx7}^{-/-}$ microglial processes resulted significantly denser respect to the $\text{P2rx7}^{+/+}$ ones (Figure **9C**, left panel; green bar, **9C**, right panel; the green-colored area, **9D''**; green bar). Interestingly, this intercellular territory difference faded with acute PCP treatment (Figure **9D''**). To decipher possible relationships between neurons and microglia in acutely PCP-treated animals, mPFC slices were triple-immunostained for P2Y12R, NeuN, and c-Fos (Figure **9E**). Neuronal nuclei positive for NeuN and negative for c-Fos were considered not involved in PCP hyperactivation, here referred to as inactive neurons. Examination of microglial branches toward active nuclei was performed using the aforementioned 2D Sholl analysis (**9C**), but this time centered on active or inactive neurons of the layer V (Figure **9E**). We found that c-Fos^+ neuronal nuclei were surrounded by a higher number of microglial branches in both the genotypes, compared to the inactive neurons in the same field of view (Figure **9F**). Despite the confirmation of an activity-driven microglial chemotaxis (183, 191), this 2D Sholl analysis failed to detect any difference between $\text{P2rx7}^{-/-}$ and $\text{P2rx7}^{+/+}$ microglia (Figure **9F''**). During visualization and manual analysis of IL and PL microglia and c-Fos^+ in PCP-treated animals (Figure **9G**), we noticed that strongly activated neurons (c-Fos^{++}) in $\text{P2rx7}^{-/-}$ tissue had the tendency to be in contact with microglial cell body, though not statistically significant (Student's t-test $p=0.0967$,

Figure 9H). To obtain the precise quantification of microglial branches in the proximity of hyperactive neuronal nuclei, large z-stacks, over 30 μm thick, were analysed. A 3D Sholl analysis of P2Y12R positive branches, focused on c-Fos⁺ nuclei, was performed (Figure 9I). This eventual 3D Sholl analysis, performed over a radius of 15 μm , revealed a higher number of microglial branches recruited by c-Fos⁺ in the P2rx7^{-/-} mPFC layer V (Figure 9J).

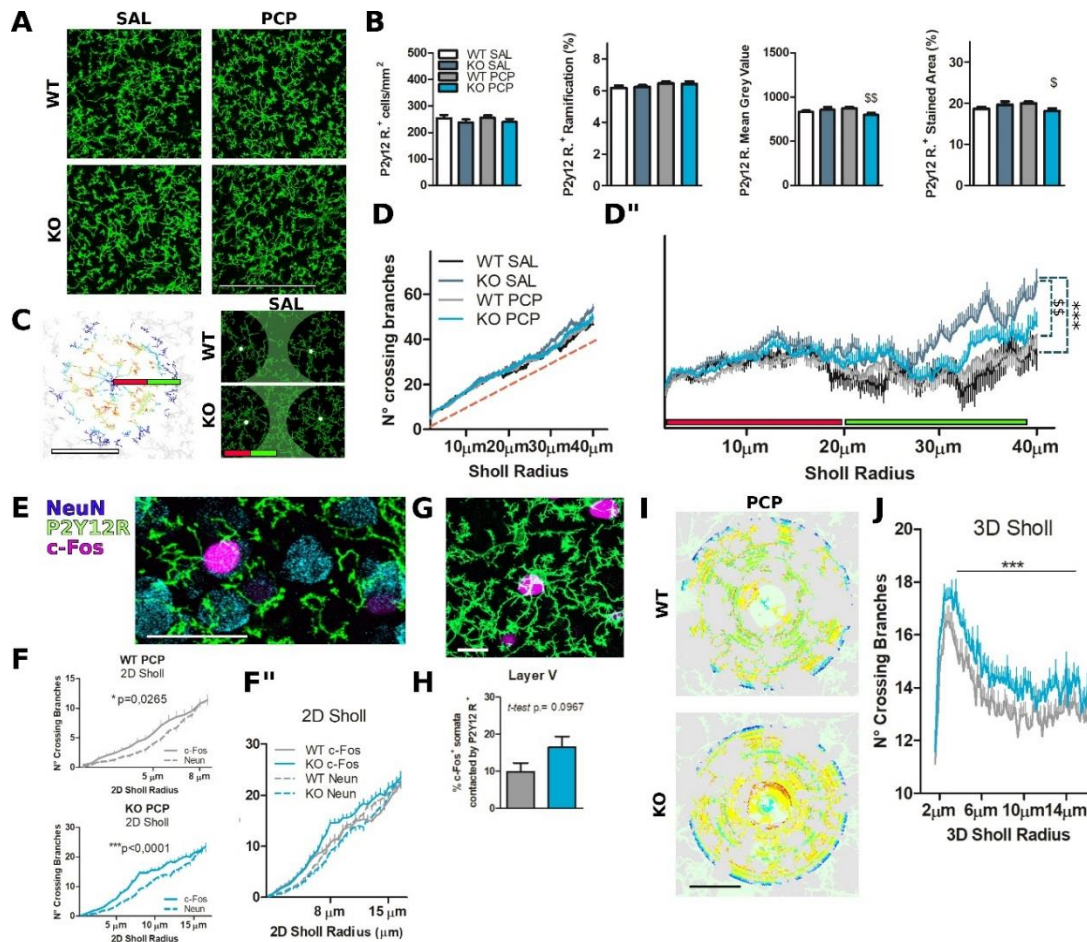


Figure 9. Microglial cells organize their processes around hyperactivated neurons, and their ramification is partly dependent on P2X7R expression. **A)** Representative images of medial PL layer V immunostaining for the microglial membrane marker P2Y12R. Scale Bar, 100 μm . **B)** Quantification of P2Y12R positive cells. Manual cell counting (left), automated quantification (FIJI ImageJ): general ramification as percentage of stained area, skeleton stacks (left center); signal intensity as mean gray value (center-right) and percentage of threshold-stained area (right). N=3 (SAL), N=4 (PCP). Shown is mean \pm SEM. Statistics: two-way ANOVA followed by Bonferroni's *posthoc* test, *p*-value $^{\$} < 0.05$; $^{\$\$} < 0.01$ vs. WT PCP. **C)** Example of 2D Sholl analysis of the mPFC layer V non-

isolated microglia (WT SAL), skeleton of stack's maximal projection (FIJI ImageJ). The first 20 μm of the Sholl radius is likely to be occupied by a single-cell harborization (green line); from 20 μm to 40 μm of Sholl radius (inter-cellular territory) are present ramifications of several cells (red line). Scale bar, 40 μm (left). Representative images of the difference in inter-cellular territory ramification from vehicle-treated P2rx7^{+/+} and P2rx7^{-/-} microglia. **D**) Quantification of the 2D Sholl analysis represented as the number of crossing branches per radius value of non-isolated microglial cells. The red dashed line is the identity function $F_{(x)}=x$. **D''**) The graph presented in D, but with the y-axis changed with $F_{(x)}=x$, for better visualization. N=3 (SAL), N=4 (PCP); 2D cell-center numbers analyzed: n=38 (WT SAL), n=48 (KO SAL), n=60 (WT PCP), n=59 (KO PCP). Shown is mean \pm SEM. Statistical analysis was performed Mann-Whitney U-test over the curves between 0-20 μm (not significant) and 20-40 μm , p -value ***<0.005 vs. WT SAL; p -value \$\$<0.01 **E**) Example of triple immunostaining of PCP-treated mPFC layer V for P2Y12R, c-Fos and neuronal nuclei (NeuN). Scale Bar 30 μm . **F**) Quantification of the 2D Sholl profiles of microglial branches surrounding PCP-activated (continuous line) or inactive (dashed line) neuronal nuclei. Wild-type PCP-treated animals, in PL and IL layer V areas, displayed preferential microglial contact in the 8 μm radius mins. The preferential microglial contact towards activated neurons is significant, in terms of the radius (15 μm) in P2rx7^{-/-} animals. N=4; 2D cell-center numbers analyzed: n=52 (WT NeuN), n=51 (KO NeuN), n=34 (WT c-Fos), n=36 (KO c-Fos). Shown is mean \pm SEM. Statistics: two-way ANOVA followed by Bonferroni's *posthoc* test, exact p -values are displayed on graphs, *: c-Fos vs NeuN. **F''**) Values presented in F grouped in a single chart. In the 8 μm Sholl radius: 2-way ANOVA followed by Bonferroni's *posthoc* test. Between genotypes no significant differences, p -values >0.05. **G**) Example of mPFC layer V double immunostaining representing microglia soma in contact with an activated c-Fos⁺ neuronal nucleus. Scale bar 15 μm . **H**) Quantification of the manually counted cell-body contacts between the microglia and activated neurons, as a percentage of counted c-Fos⁺ nuclei. N=4. Shown is mean \pm SEM. Statistics: unpaired Student's *t*-test, exact p -value on the graph, not significant. **I**) Example of c-Fos⁺ nuclei centered 3D Sholl analysis of P2Y12R⁺ microglial cell membrane, in the mPFC layer V from PCP-reacted P2rx7^{+/+} and P2rx7^{-/-} mice. Scale bar 15 μm . **J**) Results from the quantification of the 3D Sholl analysis. N=3; 3D cell-center numbers: n=52 (WT PCP); n=45 (KO PCP). Shown

is mean \pm SEM. Statistics: Mann-Whitney U-test, p -value *** <0.005 KO PCP vs WT PCP.

4.7 Intrinsic properties of P2rx7^{-/-} mPFC layer V pyramidal neurons

After data regarding the PCP-induced hyperactivity, we decided to collect direct evidence from mPFC layer V pyramidal cells. Acute slices and patch-clamp electrophysiology of untreated animals allowed us to investigate whether congenital/developmental intrinsic hypoexcitability of neurons in P2rx7^{-/-} animals may be involved (Figure 10A). To lower the developmental-derived variability, only neurons from mice older than 59 days were recorded. Recordings of thirteen neurons from 8 P2rx7^{+/+} animals and twenty-one neurons from 6 P2rx7^{-/-} animals were analyzed. No differences were found between P2rx7^{+/+} and P2rx7^{-/-} neurons in series resistance ($35.7 \pm 3.2 \text{ M}\Omega$ P2rx7^{+/+}; $33.4 \pm 2.4 \text{ M}\Omega$ P2rx7^{-/-}) and membrane resistance ($375.6 \pm 38.7 \text{ M}\Omega$; $433.5 \pm 56 \text{ M}\Omega$). Similarly, no difference was observed in average V_m, recorded at 0 pA current-clamp (Figure 10B). Taken as measures of intrinsic excitability, rheobase and IV relationships were recorded in current-clamp mode, using ramp and step protocols, respectively. No difference in these values was detected between P2rx7^{-/-} and P2rx7^{+/+} control animals (Figure 10C, 10D). Anyway, following action potential-induced depolarization, P2rx7^{-/-} PFC neurons displayed faster repolarization of the membrane potential than P2rx7^{+/+} neurons (red segment Figures 10A, 10E). Moreover, during depolarizing current injections, P2rx7^{+/+} neurons fired a higher number of action potentials with respect to P2rx7^{-/-} neurons at the same current pulse, suggesting a difference in spike accommodation (Figure 10F). These data suggest that pyramidal neurons from young adult C57Bl/6J animals in mPFC layer V of P2rx7^{-/-} and P2rx7^{+/+} have similar input-related response characteristics, and a similar current amount is required to reach the action potential threshold (rheobase). We found that P2rx7^{+/+} neurons in mPFC layer V respond more robustly to membrane depolarization than P2rx7^{-/-}. Wild-type neurons fired a higher number of action potentials, therefore presenting a shorter refractory period, and a longer-lasting membrane depolarization after action potential firing. This is consistent with our previous results, indicating that P2rx7^{-/-} neurons could be less responsive to strong driven activation.

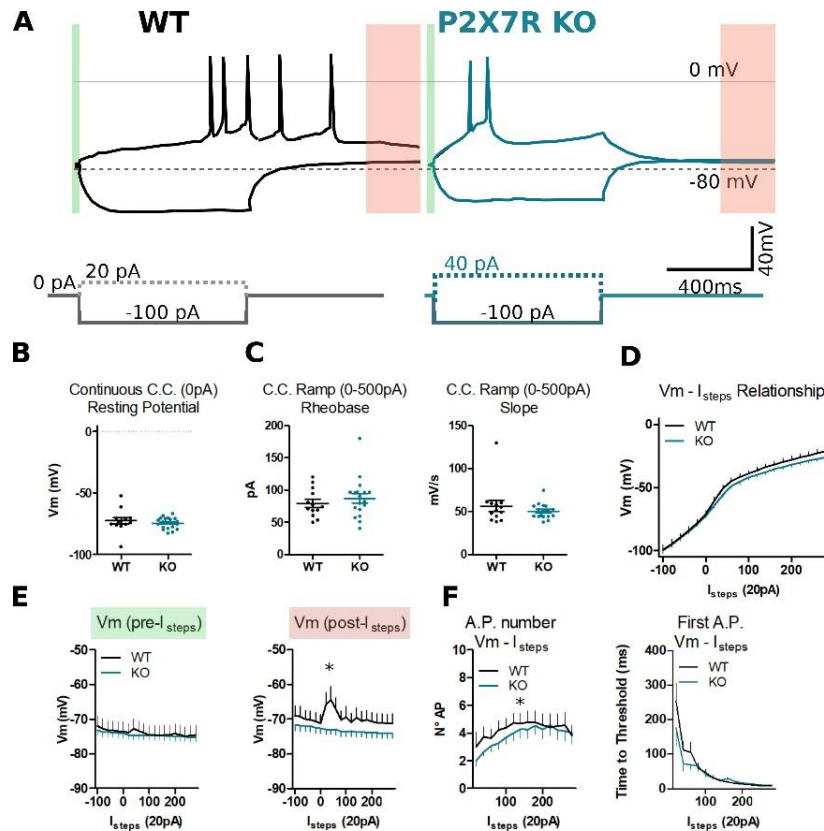


Figure 10. P2rx7^{-/-} mPFC layer V neurons display faster re-polarization after firing action potentials, with respect to P2rx7^{+/+} neurons. **A)** Example of whole-cell patch-clamp traces from P2rx7^{+/+} and P2rx7^{-/-} mPFC layer V pyramidal neurons during current step injection (I_{step}) protocol. Recordings of 400 ms hyperpolarizing step (-100 pA), and the first step triggering action potential firing ($+20$ pA for P2rx7^{+/+}, left; 40 pA for P2rx7^{-/-}, right). **B)** Average V_m in current-clamp configuration. Holding current at 0 pA for 10 s. **C)** Analysis of the ramp current injection (0 - 500 pA) over 1 s. Column analysis (B, C), each point represents an individual neuron. $N=8$ P2rx7^{+/+} (13 neurons); $N=6$ P2rx7^{-/-} (21 neurons). Shown is mean \pm SEM. Statistics: unpaired Student's *t*-test. Scoring: no significant differences, p -value >0.05 . **D)** Current clamp step protocol (I_{step}) I/V relationship. I_{step} minimum of -100 pA, I_{step} maximum of $+280$ pA, I_{step} size of 20 pA, I_{step} time of 400 ms, and sweep frequency of 1 Hz. Averages \pm SEM voltage over 400 ms I_{step} . **E)** Membrane voltage before and after I_{step} in the current clamp at 0 mV. Average voltage over 30 ms before I_{step} (A green, $V_{m\text{pre}}$, left), and over 100 ms (A red, 300 - 400 ms after I_{step} , $V_{m\text{post}}$, right). **F)** Action potentials count during the 400 ms I_{step} (left), and plot of the time to the threshold of the first action potential. $N=8$ P2rx7^{+/+} (12 neurons); $N=6$

P2rx7^{-/-} (19 neurons). Shown is mean \pm SEM. Statistics: Mann-Whitney U-test, *p*-values * < 0.05 KO vs WT. In collaboration with Jan Tønnesen (31).

4.8 P2X7R-EGFP overexpressing reporter mice displayed higher sensitivity to acute low-dose PCP treatment

Our work on P2rx7^{-/-} and P2rx7^{+/+} suggests that P2X7R deficiency ameliorates the acute PCP-induced hyperactivity, both in terms of behavior and mPFC circuit. The diminished activation of P2rx7^{-/-} layer V neurons possibly relate to lower basal dopamine release, increased microglia-hyperactive neuron interaction, and faster neuronal repolarization after action potential firing. To corroborate findings in knock-out animals, it is pivotal to test an alternative model, possibly ruling out collateral artifacts, such as developmental abnormalities. Therefore, we began to study a recently developed mouse model, the heterozygous C57Bl/6J mouse line overexpressing the P2X7R-EGFP protein (36), here referred to as P2rx7^{tg/+}. To assess susceptibility to acute PCP, P2rx7^{tg/+} and P2rx7^{+/+} mice were subjected to a low-dose PCP treatment (2 mg/kg *i.p.*), followed by a modified protocol of the open-field and social withdrawal tests, previously validated for PCP studies. Their behavior was recorded over a 10 min trial period (45 min after the PCP or vehicle, Figure 11A) and analyzed by a person blinded to the experiment conditions, as previously described (30). Basal levels of locomotion, social behavior, stereotypical behavior, and ataxia were not different between saline-treated animals. The low-dose PCP treatment affected several behavioral parameters (Figure 11B). In P2rx7^{+/+}, acute PCP treatment strongly diminished the social interaction, and promoted stereotypical behavior (Figure 11B, left-center panel and right-center panel). However, low-dose PCP did not significantly alter the locomotion of P2rx7^{+/+} animals, and failed to trigger ataxia (Figure 11B, left and right panels). In contrast, the low-dose PCP effect involved all tested behavioral parameters in P2rx7^{tg/+} mice, which exhibited hyperlocomotion and features related to ataxia already appearing in few individuals (Figure 11B, left and right panels). To visualize, and thus confirm, the P2X7R protein expression in the mPFC, we have performed immunostaining against P2X7R-EGFP and the microglial marker P2Y12R, using the P2rx7^{tg/+} reporter mice. Figure 11C shows the overall P2X7R expression pattern, by immunostaining against the EGFP part of the chimeric protein, and the microglial membrane. The receptor appears abundant on microglia, yet we observed

EGFP positive /P2Y12R negative cellular fibers, and puncta as well, implying that P2X7R is also expressed by other neural cell types (Figure 2, 11C).

A Acute (low dose) Protocol P2rx7^{+/+} & P2rx7^{tg/+}

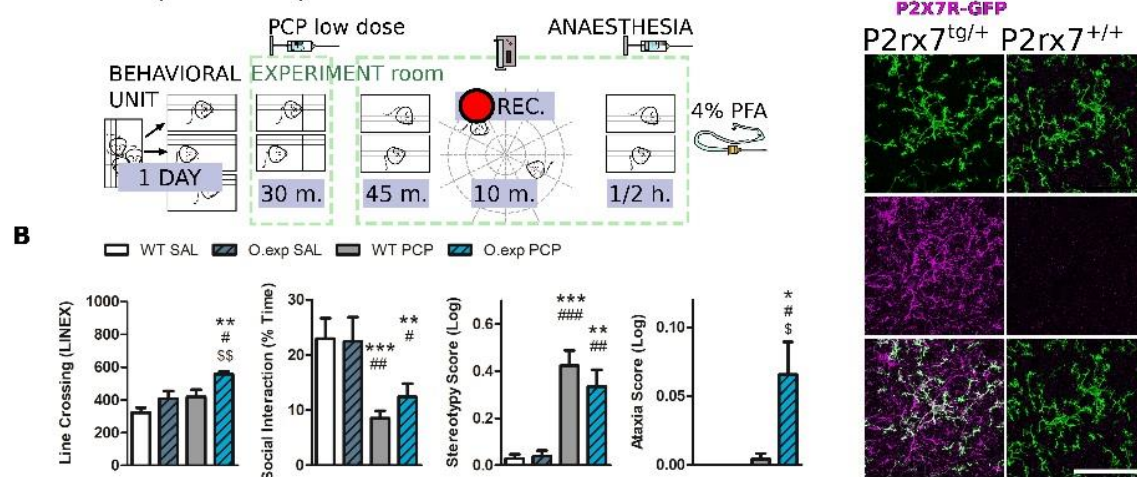


Figure 11. P2rx7^{tg/+} mice are more susceptible to the acute low-dose of phencyclidine (PCP) psychotomimetic effect. **A)** Schematic representation of the behavioral protocol for acute PCP treatment (2 mg/kg *i.p.*). **B)** Quantification of different aspects of the PCP-induced behavior in the coupled open-field test. Locomotor activity (left), time spent performing social behavior (left-center), and scores for stereotypical behavior (center right) and ataxia (right) were quantified and analyzed. N=10 (WT SAL), N=12 (O.exp SAL), N=6 (WT PCP), N=12 (O.exp PCP). Shown is mean \pm SEM. Statistics: one-way ANOVA followed by Dunn's comparison *posthoc* test (left and left-center); and Kruskal-Wallis test (center-right and right), *p*-value * < 0.05; ** < 0.01; *** < 0.005 vs. WT SAL; *p*-value # < 0.05; ## < 0.01; ### < 0.005 vs. TG/+ SAL (O.exp Sal); *p*-value \$ < 0.05; \$\$ < 0.01 vs. WT PCP. **C)** Example of the P2rx7^{tg/+} layer V medial PFC double immunostaining for P2Y12R (green) and GFP, labeling the P2X7R-GFP protein (violet). Scale bar 50 μ m. Collaboration with Paula Mut-Arbona (31).

4.9 Acute PCP treatment-induced hyperactivity and layer-specific neuronal activation in the mPFC was exacerbated in P2rx7^{tg/+} mice

To corroborate the data coming from P2rx7^{-/-} experiments, the acute PCP experiment was repeated (with the difference of normal light condition), testing the P2rx7^{tg/+} mouse line (Figure 12A). PCP increased locomotion and elicited stereotypic behavior in all treated animals. Hyperlocomotion and rotational stereotypic behavior peaked between 30 and 70 mins. after injection (Figures 12B, 12C). The effect of PCP in P2rx7^{tg/+} animals was

strongly pronounced in terms of stereotypy, respect to the $P2rx7^{+/+}$ mice (Figure 12C). Fluorescent c-Fos immunostaining of treated animals showed the typical band of c-Fos immuno-positive neuronal somata, corresponding to the layer V of the IL and PL areas, analysed at two different bregma (Figure 12D). A similar c-Fos analysis to the one performed previously in $P2rx7^{-/-}$ was carried out on 5 μm thick stacks maximal projections images, focusing on the layer V of the IL and PL areas of PCP-treated mice. The exacerbated stereotypy of $P2rx7^{tg/+}$ mice was found accompanied by a higher concentration of strongly activated ($c\text{-Fos}^{++}$) positive nuclei, specific to bregma +1.70, in the IL and PL region of the Layer V (Figure 12E). In this case, the dimension and intensity thresholds to count $c\text{-Fos}^{++}$ neurons were set at 100 μm^2 and 1100 mean gray value (ImageJ standardized units), respectively, according to the visual comparison with previous $P2rx7^{-/-}$ analysis. The overexpression of P2X7R seems to carry the opposite effect of genetic deficiency of $P2rx7^{-/-}$ mice, presenting exacerbated PCP-driven psychotomimetic effects and increased layer-specific neuronal activation in the mPFC.

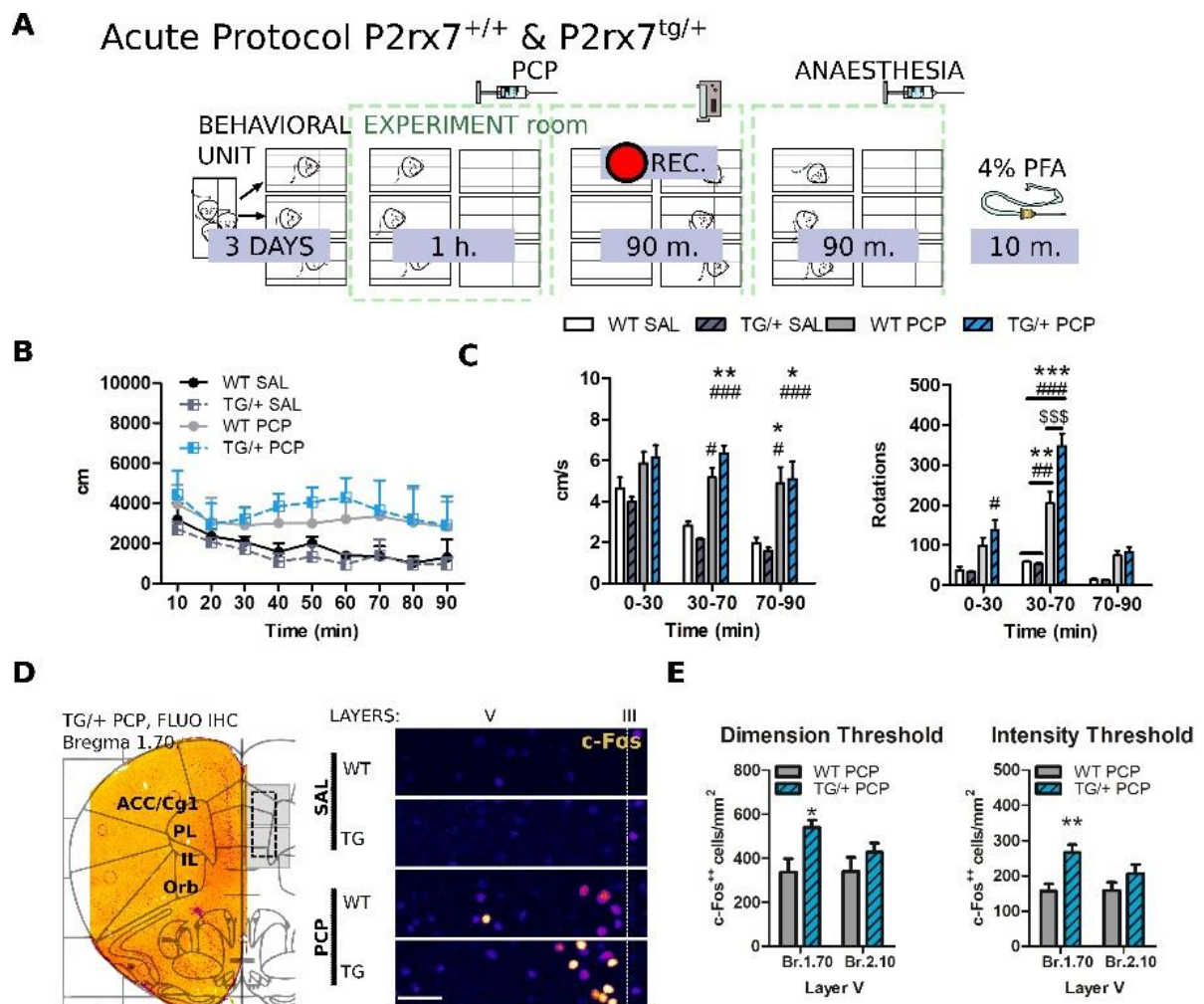


Figure 12: P2rx7^{tg/+} mice display exacerbated acute PCP psychotomimetic effect, correlated with a higher PCP-driven hyperactivation of mPFC neurons. **A)** Schematic representation of the behavioral protocol for acute treatment. **B)** Distance moved by the animals after the injection, in 10 mins. time bins. **C)** Average velocity (left) and numbers of circle rotations (right) averaged for the first 30 and second 40 mins., plus the remaining recorded time. N=3 (SAL), N=9 (TG/+ PCP), and N=9 (WT PCP). Graph shows mean \pm SEM. Statistics: two-way ANOVA followed by Bonferroni's *posthoc* test, *p*-value * <0.05 ; ** <0.01 ; *** <0.005 vs. WT SAL; *p*-value # <0.05 ; ## <0.01 ; ### <0.005 vs. TG/+ SAL; *p*-value \$\$\$ <0.005 vs. WT PCP. **D)** Representative c-Fos fluorescent immunostaining of a coronal PFC from a P2rx7^{tg/+} PCP treated mouse (**404**, bregma +2.00). The left hemisphere represents the field of view of quantified pictures. Scale bar: 1mm (left). Representative images of immunostaining from the 5 μ m projected images used for automated c-Fos nuclei counting. Layer V width range V= 280-350 μ m. Scale bar: 50 μ m (right). **E)** Quantification of PL and IL content of c-Fos⁺⁺, by dimension (left) and intensity (right) threshold. Automatic counting with FIJI ImageJ in the isolated layer V for fluorescent immunostaining. Graph shows mean \pm SEM. Statistics: unpaired Student's *t*-test, *p*-value * < 0.05 ; ** < 0.01 vs. WT PCP. Collaboration with Paula Mut-Arbona and Andras Iring (**31**).

4.10 Subchronic PCP did not induce detectable prefrontal neuroinflammation, and failed to induce working memory deficits in P2X7R deficient animals

Eventually, we decided to evaluate the possible impact of cognitive symptoms induced by repeated PCP administrations on single-caged P2rx7^{-/-} and wild-type animals (seven daily 10 mg/kg *i.p.* injections, **42**) with a battery of behavioral tests (Figure **13A**). Before treatments, P2rx7^{-/-} animals had a higher body mass compared to the P2rx7^{+/+} animals (**409**), which normalized after 24 hours after the first injection (Figure **13G**). After the first treatment, animals were recorded within the respective home-cages. PCP-treated animals displayed typical PCP-driven hyperactivity (Figure **13F**). In normal light conditions, the difference between PCP-treated P2rx7^{-/-} and P2rx7^{+/+} animals is not evident. To confirm whether repeated PCP injections did not induce lasting alterations in basal locomotor activity, four animals per group were tested in a confined environment, (a glass cylinder). Twenty hours after the third PCP or vehicle treatment no difference in

locomotor activity was observed (Figure **13B**). At the end of the subchronic treatments animals experienced 72 hours of withdrawal, before being tested in a y-maze. We were particularly interested in assessing the status of the working memory, a function strictly dependent on the mPFC microcircuit integrity. Working memory dysfunctions are a major symptom of schizophrenia still currently untreatable and well mimicked in PCP models (**283, 284, 285, 286, 410**). Both PCP- and vehicle-treated P2rx7^{-/-} animals covered a significantly shorter distance during the trial, yet the number of total alternations was not affected by either genotype or treatment (Figure **13C** left and center panels). P2rx7^{+/+} PCP-treated mice displayed fewer correct alternations with respect to the P2rx7^{+/+} saline- and P2rx7^{-/-} PCP-treated animals. The scores of P2rx7^{-/-} animals were unaffected by subchronic PCP, which failed to induce working memory deficits with P2X7R deficiency (Figure **13C**, right panel). After two additional days of washout, each animal was submitted to an open-field test (large arena) for 10 mins, during which the locomotor activity was not influenced by either the genotype or treatment, on the (Figure **13D**). Considering that neuroinflammatory events are accompanied by changes in cytokine concentrations, we quantified brain levels of those reportedly dependent on P2X7R-mediated mechanisms (**150 107**). The 7th day of treatment withdrawal, the retrosplenial cortex and the PFC were extracted, homogenized and quantified (Figure **13E**). While no differences were found between groups in the retrosplenial cortex, a significant constitutive increase in the fractalkine ligand (CX3CL1) level was found in the P2rx7^{-/-} PFC after both PCP and vehicle subchronic treatments. The levels of other measured cytokines were not affected, by either the treatment or genotype (Figure **13E**). The effect of subchronic PCP on the PFC level of IL-1 β was not significantly different between the two genotypes, also when expressed as percentage of the control (Figure **13E''**). The IL-1 β level was higher in the retrosplenial cortex of P2rx7^{-/-} mice with respect to the prefrontal level ($p < 0.05$, two-way ANOVA followed by Bonferroni's *post-hoc* test). No obvious stimulation of any interleukin tested takes place after subchronic PCP, and all measurements are close to the detection limit of the technique. These subchronic experiments suggest a beneficial role of P2X7R deficiency in PCP-induced working memory deficit in rodents, which is not accompanied by induction of neuroinflammatory phenomenon.

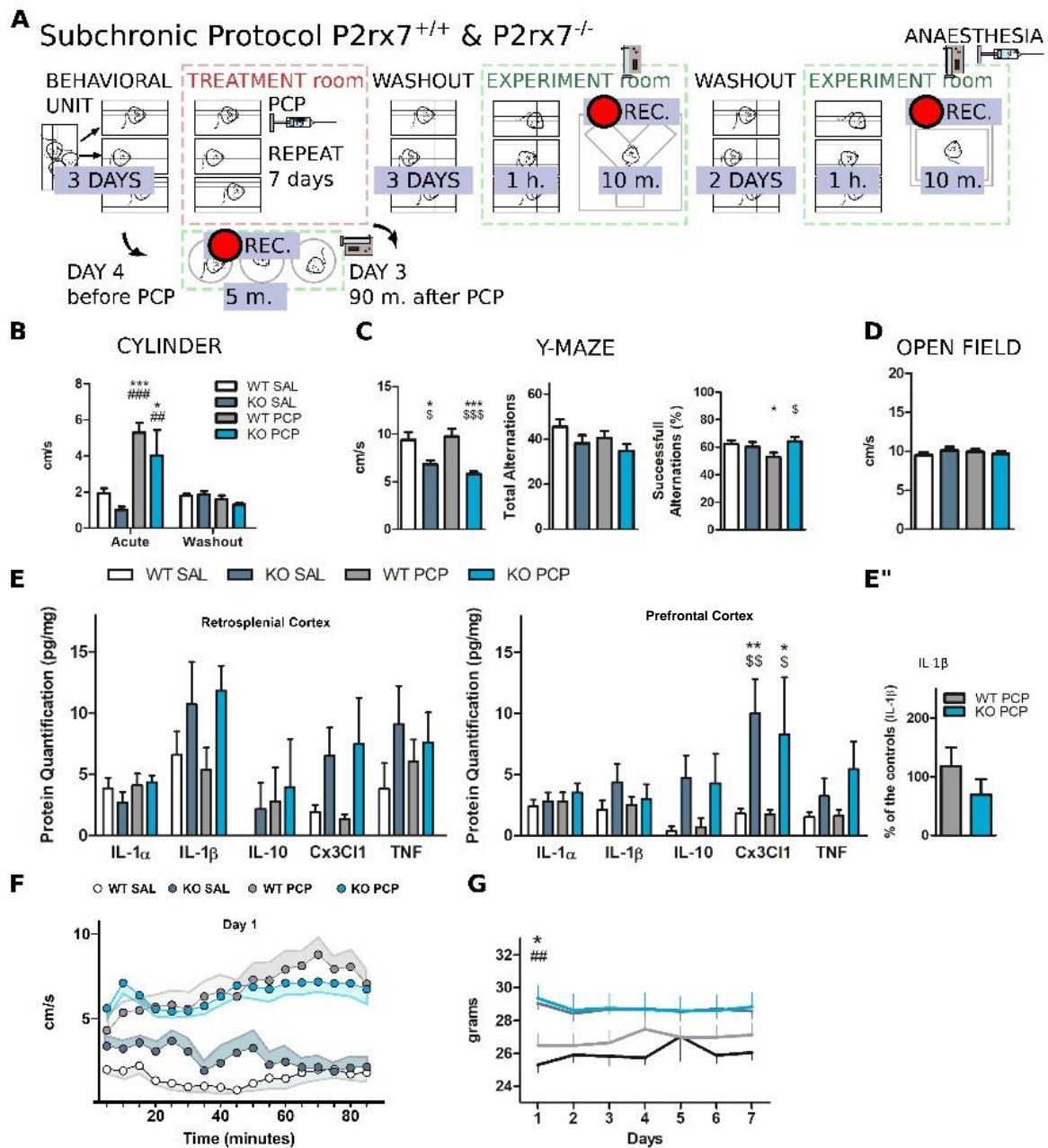


Figure 13. P2rx7^{-/-} animals showed reduced deficit in working memory after PCP subchronic treatment, and treatments did not provoke neuroinflammation. **A)** Schematic representation of the behavioral protocol for the subchronic treatment; *i.p.* injections 7 consecutive days in treatment room (red square), tests in separated experimental room (green square). **B)** Velocity in a glass cylinder during a 5-mins. test. “Acute”: test performed 90 mins. after the third PCP/saline injection; “washout”: test performed 20 hrs after the third PCP/saline injection. N=4. Graph shows mean ± SEM, two-way ANOVA followed by Bonferroni’s *posthoc* test, *p*-value * < 0.05; *** < 0.005 vs. WT SAL; *p*-value # < 0.05; ## < 0.01 vs. KO SAL. **C)** Results of the y-maze test, performed the third

day after subchronic withdrawal. Semi-automated analysis with Noldus EthoVision XT[®]. N=12 (SAL, WT PCP); N=14 (KO PCP). Mean \pm SEM, two-way ANOVA followed by Bonferroni's *posthoc* test (left, center); unpaired Student's *t*-test, (right, successful alternations), *p*-value * < 0.05; *** < 0.005 vs. WT SAL; *p*-value ^{\$} < 0.05; \$\$\$ < 0.005 vs. WT PCP. **D**) Average velocity over 10 mins. in an open-field test. N=7 (WT SAL); N=8 (WT PCP); N=11 (KO). Mean \pm SEM, two-way ANOVA followed by Bonferroni's *posthoc* test, non significant. **E**) Interleukins quantification with bead-array CBA analysis, from retrosplenial (left) and PFCs (right) of P2rx7^{-/-} and P2rx7^{+/+} vehicle or PCP subchronically treated mice. Brains extracted 14 days after the first injection. N=8. Graph shows mean \pm SEM, two-way ANOVA followed by Bonferroni's *posthoc* test, *p*-value * < 0.05; ** < 0.01 vs. WT SAL; *p*-value ^{\$} < 0.05; ^{\$\$} < 0.01 vs. WT PCP. **E'')** Level of IL-1 protein, expressed as a percentage of the control in PFC. N=8. Mean \pm SEM, unpaired Student's *t*-test **F**) Acute hyperlocomotory effect of *i.p.* saline or 10 mg/kg PCP in home-cage, normal light condition. N=8 (SAL), N=12 (PCP). Mean \pm SEM. **(G)** Animals' weight during the PCP subchronic treatment. N=8 (SAL), N=12 (PCP). Mean \pm SEM, with two-way ANOVA followed by Bonferroni's *posthoc* test, *p*-value * < 0.05 KO vs. WT SAL; ^{##} < 0.01 KO vs. WT PCP.

4.11 Single-cage housing condition is necessary to induce cognitive-like symptoms in the current PCP model

During the optimization of the behavioral paradigms, a series of PCP subchronic experiments were performed on group-caged mice, 4-5 littermates per cage since the first arrival to the behavioral unit. Since animals were randomized for treatments, the cages hosted mixed groups of salines- and PCP-treated animals. The only time these group-caged animals were separated was during the daily injections and the 90 mins. immediately after it, when animals were kept in individual cages to avoid overcrowded or stressful conditions, arising from PCP-hyperactive mice. Y-maze tests, after a 72 hours washout period, were performed and compared with single-cage cohort results (**31**, Figure **13**). The working memory deficit induced by subchronic PCP was not detected in group-caged animals, at least partly depleting this protocol of schizophrenia-model validity (Figure **14A**). Alike for single-caged, group-caged animals displayed similar numbers of total alternations between treatments and genotypes (Figure **14C**). Interestingly, the

difference in velocity found between genotypes in single-cage condition (Figure 13C, left) disappeared in group-caged experiments (Figure 14D), where all groups displayed low locomotory behavior. The same arm entries are the action of poking into an arm, in the current case passing the 20% of arm length. This analysis is not common and therefore excluded from the submitted publication (31). Single-cage animals perform higher numbers of same arm entries, respect to group-caged animals (Figure 14B). Moreover, single-cage PCP-treated $P2rx7^{+/+}$ mice repeated more same arm entries than $P2rx7^{-/-}$ animals, independently from the treatment (Figure 14B).

Y-Maze test

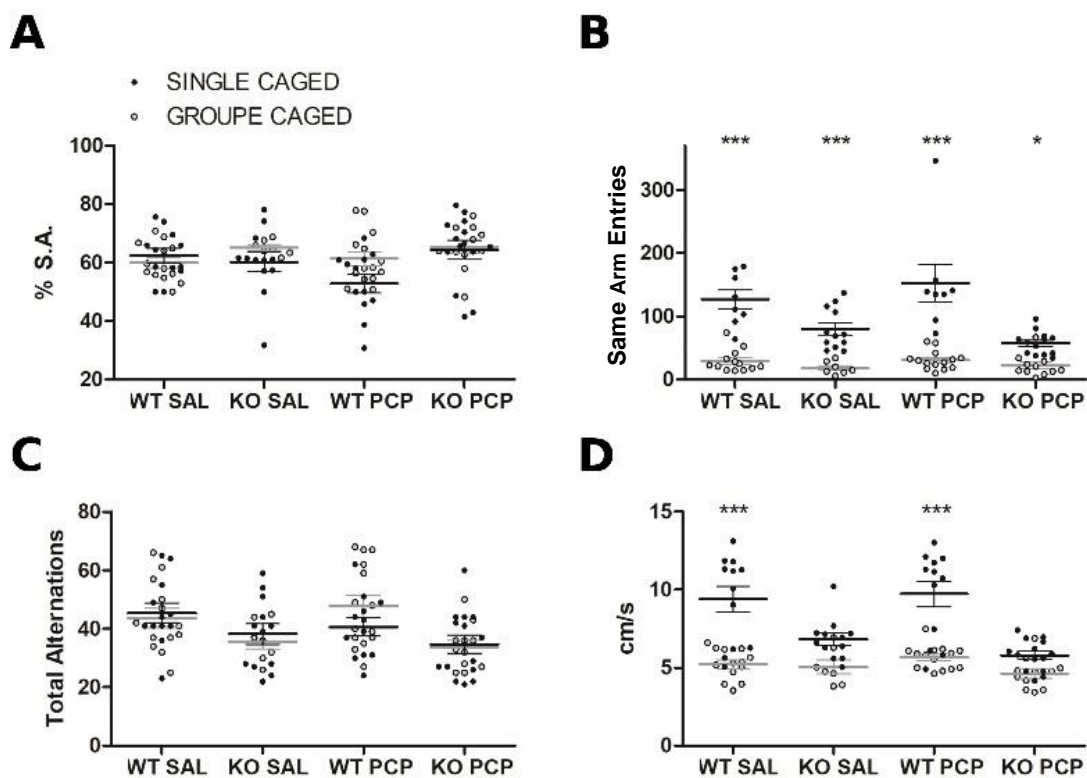


Figure 14 Different housing conditions during subchronic PCP treatment influence the outcome of y-maze behavioral experiment. **A)** 10 mins. continuous recording of subchronically treated $P2rx7^{-/-}$ and $P2rx7^{+/+}$ mice. Quantification of the percentage of spontaneous successful alternations; **B)** the same arm entries repetitions; **C)** total alternations, considering a threshold of 20 alternations to consider the test valid; **D)** auto-tracked animals' velocity. Number of animals for single-cage analysis (31, Figure 13,) in A, B and C are: N=12 (WT SAL), N=12 (KO SAL), N=12 (WT PCP), N=14 (KO PCP); in D are: N=8 (WT SAL), N=12 (KO SAL), N=8 (WT PCP), N=13 (KO PCP). Number of animals for the group-caged analysis are: N=13 (WT SAL), N=7 (KO SAL), N=14

(WT PCP), N=11 (KO PCP). Shown is mean \pm SEM, two-way ANOVA followed by Bonferroni's *post-hoc* test, *p*-value * < 0.05; *** < 0.005. Group-caged vs. single-caged; (B) intra single-cage two-way ANOVA followed by Bonferroni's *post-hoc* test, *p*-value ### < 0.005 WT SAL vs. KO PCP; WT PCP vs. KO SAL, KO PCP.

4.12 Long-lasting effects of subchronic PCP treatments

Open-field tests in large arenas (15 mins.) were performed 10 and 11 days after the last subchronic injection. Analyses were obtained through auto-tracking software (Noldus EthoVision XT[®]). The typical exploratory behavior was observed in all groups, sustained velocity and less than 50% the time spent along the borders of the arena (Figure 15A, left). The only subtle difference regarded the number of spontaneous rotations, since PCP-treated P2rx7^{-/-} mice performed less rotations than PCP-treated P2rx7^{+/+} animals (Figure 15A, bottom left). This difference was not detected in saline-treated animals, or with repetition of the test 24 hours later (Figure 15A bottom, 15B bottom). Observing the habituation effect (Figure 15B), a clear drop in activity was detected by animal's velocity (Figure 15B, up), while no changes in the time spent along the periphery of the arena were detected (Figure 15B, center). The longitudinal adjustment of velocity suggests that, at this time point, in all PCP-treated mice contextual memory mechanisms are functioning correctly.

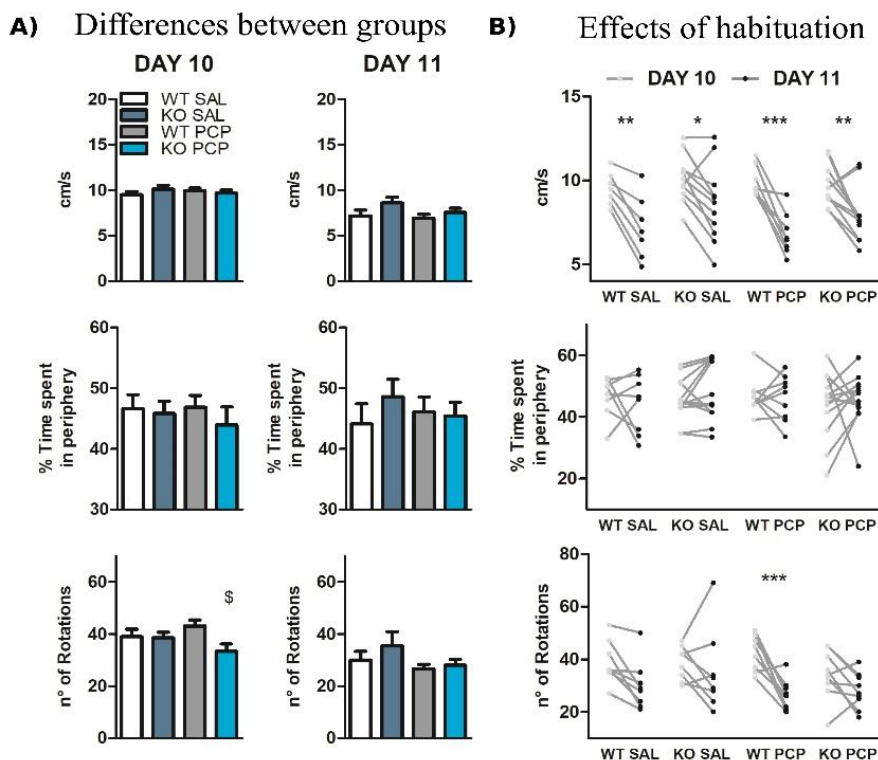


Figure 15. Open-field 10 and 11 days after last sub-chronic treatment, performed by P2rx7^{-/-} and P2rx7^{+/+} mice. Quantified with auto-tracking Noldus EthoVision XT[®]. **A)** Average velocity (up), percentage of time spent in periphery of the arenas (center), and number of spontaneous circular rotations (bottom), during the consecutive open-field 15 mins. tests, day 10 (left); day 11 (right). Number of animals, velocity, percentage and rotations, day 10, respectively: N= 7, 8, 8 (WT SAL), N= 11, 12, 8 (KO SAL), N= 8, 9, 9 (WT PCP), N= 11, 12, 10 (KO PCP); day 11: N= 8, 8, 8 (WT SAL), N= 12, 12, 8 (KO SAL), N= 9, 9, 9 (WT PCP), N= 13, 13, 9 (KO PCP). Graphs shows mean ± SEM, one-way ANOVA followed by Bonferroni's *post-hoc* test, *p*-value [§] < 0.05 vs. WT PCP. **B)** Quantified behavioral results (each animal represented by a line) along the consecutive open-field tests. The significant change in velocity, found in all groups found, is an example of habituation. Number of animals for velocity, percentage, rotations to quantify the habituation are, respectively: N=7,8,8 (WT SAL), N=11,12,8 (KO SAL), N=8,9,9 (WT PCP), N=11,13,9 (KO PCP). Mean ± SEM, two-way row-matching ANOVA followed by Bonferroni's *post-hoc* test, *p*-value * < 0.05; ** < 0.01; *** < 0.005 day 10 vs. day 11.

4.13. Immunohistochemical study of P2rx7^{+/+} mPFC after subchronic PCP treatment

In order to find a neurological substrate for the subchronic PCP effect, a pilot study on 10 P2rx7^{+/+} animals aimed to identify pathological signs in mPFC. A contextual-memory test often found in PCP studies (NOR) was longitudinally tried on this cohort before and after subchronic treatments. Drug-naïve mice performed the NOR successfully, discriminating and preferring the newly introduced object (Figure 16A). Anyway, the treatments induced lower activity and shorter exploring time. It is possible to observe a non significant tendency for successful discrimination in both saline and PCP groups (Figure 16A). After 4 additional washout days brain samples were collected. The mPFC was stained against PV (Figure 16B), and PL cortices PV interneurons manually counted (Figure 16C). Following the here employed PCP treatment, we could detect the PCP detrimental effect on PV cortical expression, reported in other studies (309, 319, 335). PV immunostainings of the mPFC presented an irregular pattern particularly challenging to measure rigorously (Figure 16B, 16D). Intensity of PV signal after subchronic PCP

was not different in the layers II-V of the mPFC PL area (Figure 16F), while it was found slightly weaker in the mPFC of $P2rx7^{-/-}$ animals after acute PCP, a difference becoming significant in the dorsal area (Figure 16E). Subchronically treated mPFC were also stained against NeuN and c-Fos (Figure 16G), the latter marking neuronal basal activity during the light-phase. The c-Fos images displayed low contrast between the background and the different nuclei (Figure 16G). A matlab automated protocol employed to count active neurons did not show any difference between PCP and saline treated animals (Figure 16H).

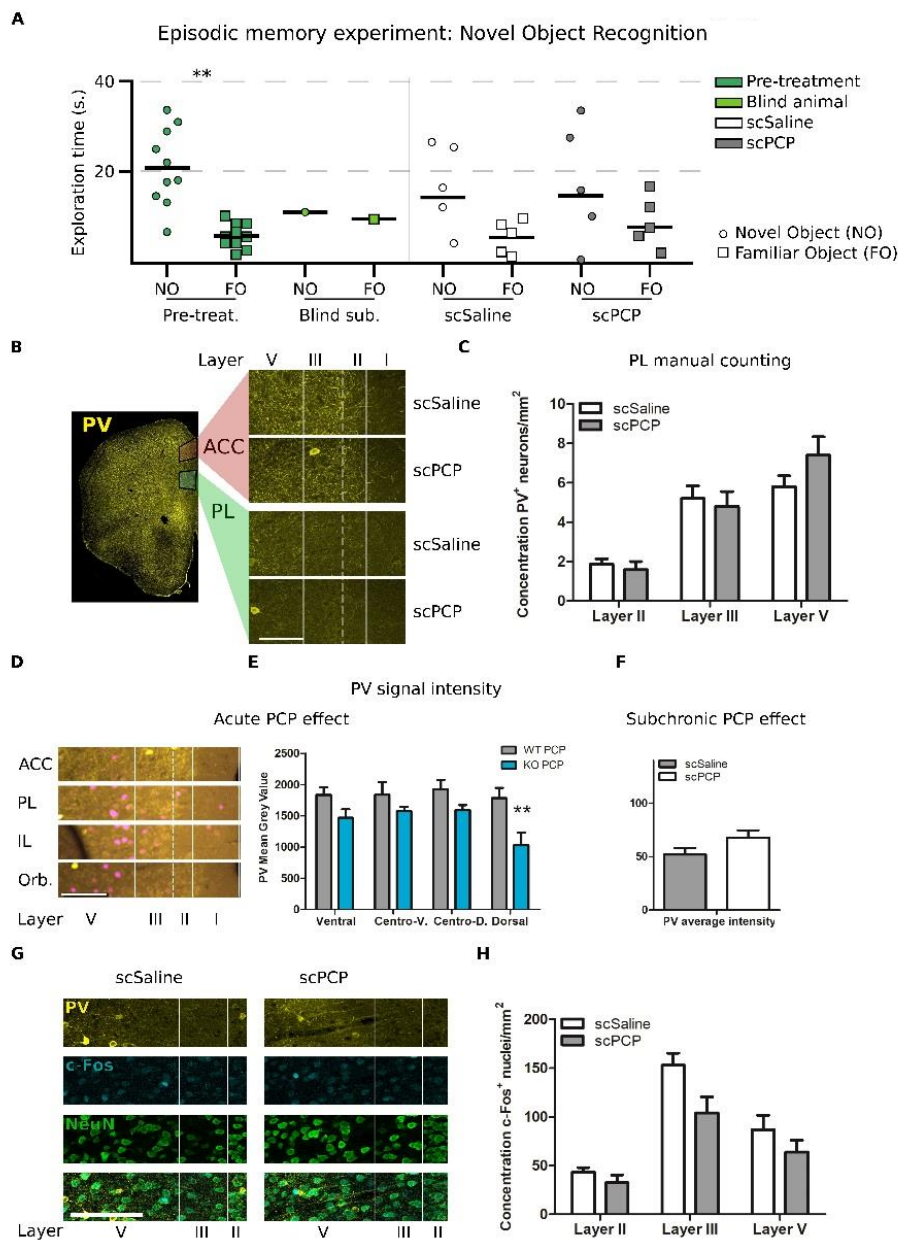


Figure 16. The applied PCP subchronic regime in $P2rx7^{+/+}$ animals did not induce specific episodic memory deficit, and did not provoke mPFC PV-depletion or c-Fos

abnormal expression. **A)** Results of the NOR episodic memory performance of 3 mins. N=10 pre-treatment; N=1 semi-blind animals; N=5 subchronic treated animals per group. Graph shows mean \pm SEM. Statistics: unpaired Student's *t-test*, *p*-value ** = 0.007. **B)** Examples of PV immunostainings: mPFC large picture (right) and inserts (5 μ m stacks maximal projections). ACC agranular cingular cortex. Scale bar 100 μ m. **C)** Results of the manual counting of PV-positive neurons in PL from saline and PCP subchronically treated P2rx7^{+/+} mice. N=4. Graph shows mean \pm SEM, two-way ANOVA followed by Bonferroni's *post-hoc* test, not significant **D)** Representative pictures of P2rx7^{+/+} mPFC immunostaining for PV and c-Fos, from the acute PCP experiment, showing the differences in the PV expression along mPFC (Orb. Orbital cortex). **E)** PV mean signal intensity from acute PCP-treated P2rx7^{+/+} and P2rx7^{-/-} animals. N=3. Graph shows mean \pm SEM, two-way ANOVA followed by Bonferroni's *post-hoc* test, *p*-value ** < 0.01 vs. WT PCP. **F)** PV mean signal intensity of mPFC (layer II-V) from subchronically treated P2rx7^{+/+}. N=5. Shown is mean \pm SEM, Statistics: unpaired Student's *t-test*, not significant **G)** Neighboring slices from subchronically treated P2rx7^{+/+} animals were additionally immunostained for NeuN. **H)** Automated quantification of c-Fos⁺ in the mPFC of subchronically treated P2rx7^{+/+} animals. N=5, Graph shows mean \pm SEM. Statistics: unpaired Student's *t-test* and one-way ANOVA followed by Bonferroni's *post-hoc* test, not significant.

4.14. Histological profile of glial cell types in subchronically treated PCP animals

Considering the role of P2X7R in neuroinflammation, glial components were selected for histological analysis of subchronically treated P2rx7^{+/+} and P2rx7^{-/-} mice. PFC of mice, sacrificed 4 days from the last subchronic treatment, were stained against the microglial markers Iba-1 (ramified phenotype, upregulated in neuroinflammation), P2Y12R (ramified, downregulated in neuroinflammation) and the astrocytic marker glial fibrillary acidic protein (GFAP, upregulated during active astrocytosis). Iba-1 stainings pictures of the whole PFC (single-focal plane) were manually divided in 3 ROI, spanning from layer I to layer VI. Microglia counts per ROIs were automatically processed (FIJI ImageJ, Figure 17A). Iba-1⁺ nuclei and signal displayed a general downregulation in the PCP-treated P2rx7^{-/-} PFC (Figure 17B, 17C). Indeed, its density of microglial nuclei resulted significantly lower respect to all other groups, in the agranular insular cortex (Figure 17A,

17B). For anti-P2Y12R immunostainings of layer II-VI in the PL cortex, fixed volume z-stacks were analyzed instead, (stack's volume $43588 \mu\text{m}^2 \times 5.46 \mu\text{m}$, Figure **17D**). Manual counting did not reveal any difference in P2Y12R-positive microglial cell density (Figure **17E**). Eventually, the GFAP staining was generally weak in the whole PFC (Figure **17F**). Even though manually counted astrocytes resulted in small differences between genotypes and treatments, such low numbers of positive cells makes statistics unreliable (Figure **17G**). On the other hand, GFAP is strongly expressed by hippocampal astrocytes (Figure **17H**).

The cognitive deficits, in PCP-models as in schizophrenia, are typically associated with abnormalities in PFC. Applying our and others models (**42**), we could not detect any histological damage induced by repeated PCP treatments.

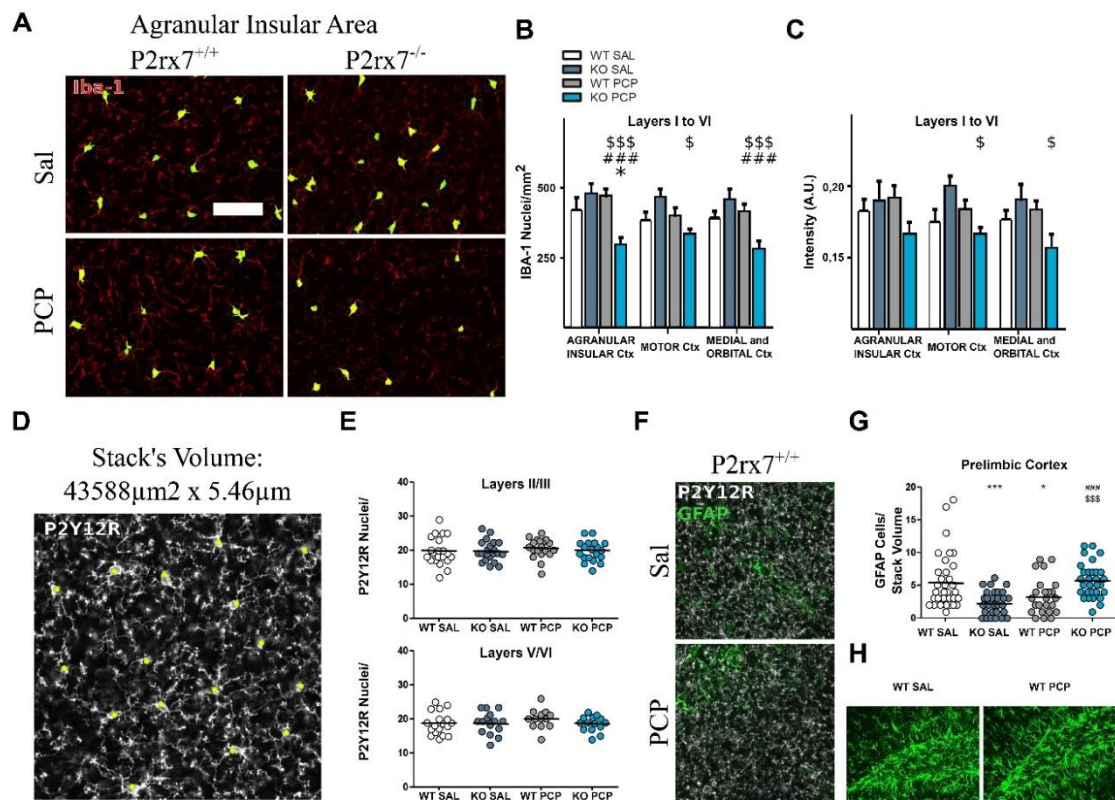


Figure 17. Effects of subchronic PCP on glial cells in the PFC of $P2rx7^{+/+}$ and $P2rx7^{-/-}$ mice. **A**) Examples Iba-1 stainings automatically quantified, Iba-1 nuclear count. Insert in ROIs: agranular insular area. Scale bar $60 \mu\text{m}$ **B**) Iba-1 positive nuclei automatic quantification results. **C**) Iba-1 average signal quantification results. $N=3-4$, minimum 3 pictures per animal. Graph shows mean \pm SEM, two-way ANOVA followed by Bonferroni's *post-hoc* test, p -value $* < 0.05$ vs. WT SAL; p -value $^{\$} < 0.01$; $^{\$ \$ \$} < 0.005$ vs.

KO SAL; p -value $^{###} < 0.005$ vs. WT PCP. **D)** Example of P2Y12R immunostaining manually counted, green dots correspond to counted nuclei. Stack's Volume $43588 \mu\text{m}^2 \times 5.46 \mu\text{m}$, displayed in the figure. **E)** Results of the P2Y12R microglia nuclei concentration, in mPFC layer II/III (up) and V/VI (down). $N=5$, 3 pictures per animal. Graph shows mean \pm SEM, two-way ANOVA followed by Bonferroni's *post-hoc* test, not significant. **F)** Examples of double immunostaining for P2Y12R and GFAP. Portions of mPFC from P2rx7 $^{+/+}$ PCP or saline subchronically treated mice. Stack's volume as in D. **G)** Results from manual counting of GFAP positive cell nuclei in the PL cortical area, from layer I to layer VI. $N=5$, 6 pictures per animal. Shown is mean \pm SEM, two-way ANOVA followed by Bonferroni's *post-hoc* test, p -value $^* < 0.05$; $^{***} < 0.005$ vs. WT SAL; p -value $^{###} < 0.005$ vs. KO SAL; p -value $^{$$$} < 0.005$ vs. WT PCP. **H)** Example of abundant astrocytic GFAP signal in the hippocampus of wild-type saline and PCP subchronically treated animals.

4.15 Effects of pharmacological manipulation of P2X7 receptor on CX3CR1 $^{+/-}$ EGFP $^{+/-}$ microglia dynamics in *ex vivo* slices, analyzed with two-photon microscopy

In conclusion of the results section, are presented preliminary results concerning P2X7R pharmacology and the microglia morphology and dynamics in acute slices. Animals heterozygous for the fractalkine receptor and an EGFP transgene (CX3CR1 $^{+/-}$ EGFP $^{+/-}$, **213**) observed via a 2-photon setup consent the visualization of fluorescent microglia more than $100 \mu\text{m}$ deep inside the slice. For the following experiments MgATP and the P2X7R antagonist BBG were kindly supplied by Dr. Ana Bernal-Chico. In Figure **18A** is summarized the protocol used to obtain fluorescent microglia movies. In Figure **18B** it is possible to see the development, from the “raw” 3D movie to the “quantifiable” 2D registered movies. This final elaboration will definitely lose some details, but it offers a compromise between agile calculation on areas, with respect to heavy calculations of rendered volumes. Experiments to assay the effects of the perfusion and the washout of $10 \mu\text{M}$ BBG on microglial dimensions and dynamics consisted of 44 mins. time-lapse recordings of fluorescent microglia in mPFC PL area. Results from the whole field of view analysis (Figures **18C**, **18D**). Results from manually isolated microglial cells (Figure **18E**). Graphs on the left represent the progression of the microglial stained area, therefore the relative total volume occupied by microglia (normalized over first time-frame).

Graphs on the right represent the so-called surveillance index (177, 178), a new volume of parenchyma which microglia is progressively occupying (normalized over first time-frame). BBG pre-application or perfusion does not exert any significant effects along the 20 mins. recordings (Figure 18C). Field of view analysis did not detect significant effects of the BBG washout, which anyway was unraveled by the isolated cell analysis (Figure 18E). After 15 mins of BBG washout, the volume occupied by individual microglial cells was significantly larger without changing the rate of surveillance.

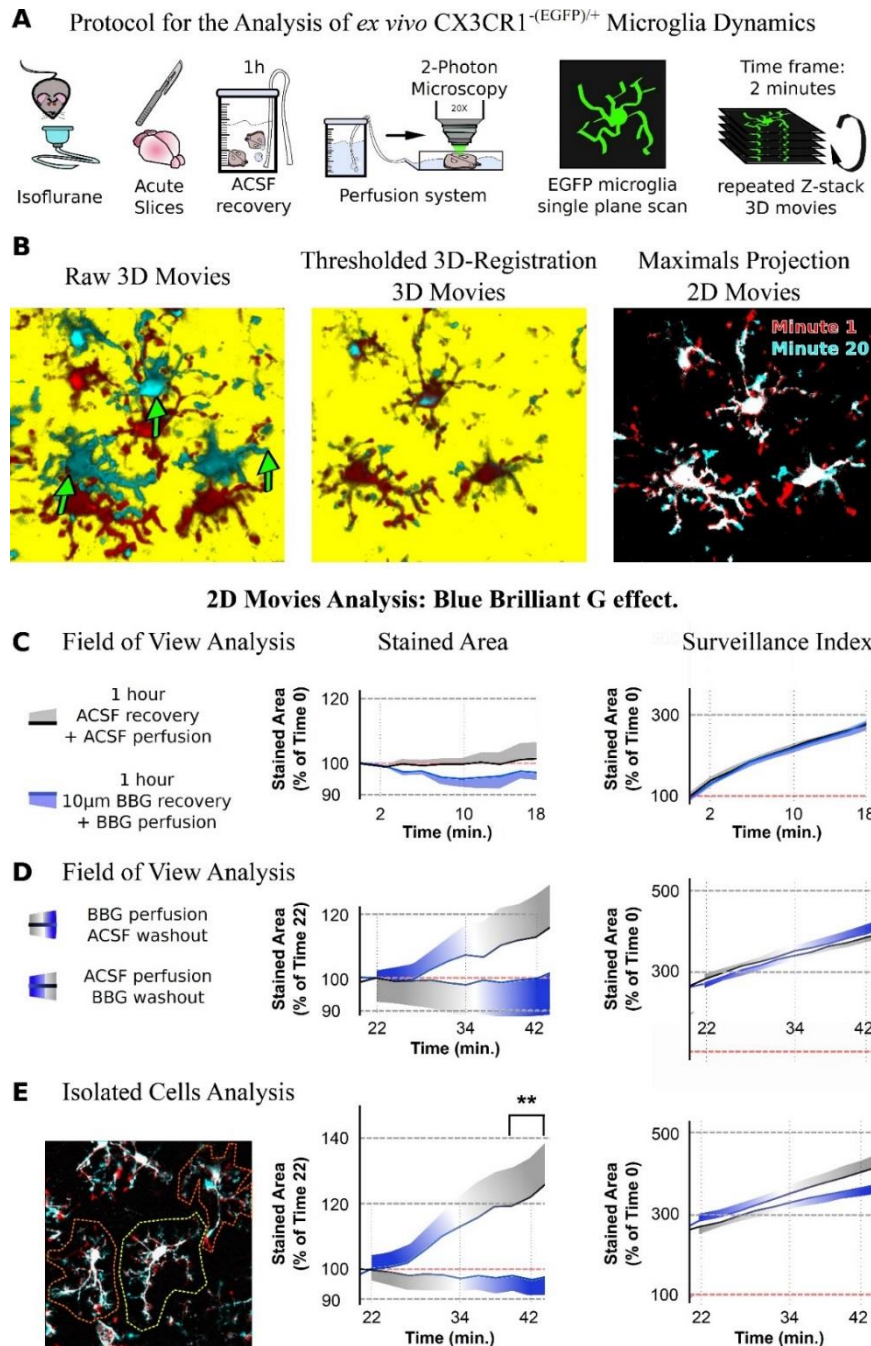


Figure 18. Two-Photon Microscopy analysis of fluorescent CX3CR^{Gfp/+} microglia and effects of 10 μ M BBG on CX3CR1^{-/+}EGFP^{-/+} on *ex vivo* mPFC slices. **A)** Schematic representation of the protocol. Imaging was performed between 1 and 3 hours after the recovery. **B)** Z-stacks repeated at a certain frequency, in this case two mins., were later transformed into quantifiable 2D movies. On the left, the three dimensional reconstruction of two different time-frames presents drifts along a 3D vector. After a series of graphical manipulation (center), it is possible to obtain 3D movies corrected by main drifts, therefore monitoring a fixed amount of volume. Eventually, maximal projection images (left) produced a 2D movie. **C)** After the recovery, slices were perfused with the respective recovery solutions. Left graphs represent the relative microglial stained area along time. Graphs on the right display the surveillance index. Field of view analysis N=3; number of slices: ACSF=8; BBG=4 (Stained Area), 5 (Surveillance Index). **D)** Slices presented in panel C subsequently underwent perfusion with the opposite BBG concentration, in order to study the effect of BBG application and washout. Field of view analysis. Movie total duration: 44 mins. N=3, number of slices: BBG perfusion (ACSF to BBG)=6; BBG washout (BBG to ACSF)=4. **E)** Manually isolated microglial cells analysis. In the picture, white represents no change over time; red shows retracted; cyan shows extended. N=3, number of cells: BBG perfusion = 16; BBG washout = 15. Shown is mean \pm SEM, curve comparison statistical analysis performed with Mann-Whitney U-test, *p*-value ** < 0.01 (**E**).

A deeper observation of the movies revealed an additional slow-drift component, therefore a further optimization of the volume quantification was needed (Figure 19). In figure 19A, white color represents portions of microglia which have not changed position in the two time-frames considered. The red color belongs to the 1st time-frame (1 to 2 mins.), while the cyan signal belongs to the 3rd time-frame (5 to 6 mins.). Therefore, red branches represent those cell portions which “disappeared” after the 1st time-frame (retracted). In cyan are those branches newly appeared (extended) from this cell before the 3rd time-frame. Microglia are very dynamic and the actual cellular motility raises the variability from time-frame to time-frame. To limit ulterior variability between data we corrected slow drift artifacts. First was calculated the total retracted and extended microglia area time-frame by time-frame and plotted (Figure 19B). In figure 19C the

schematic representation illustrates intuitively how, by subtracting the “retracted” volume from the “expanded” one, the small drifts get corrected. Eventually were calculated the averages of the net expansion along the BBG perfusion or washout periods (Figure 19D). Results of net expansion, obtained with field-of-view analysis, reproduced the findings previously revealed by the isolated cell analysis (Figure 18B): the washing from 10 μ M BBG significantly increased the volume of mPFC microglia in mPFC. Although not significantly different, it appears that pre-treatment and perfusion with BBG displays a tendency to lower microglial volume. There was no noticeable effect of BBG perfusion within this recording time window.

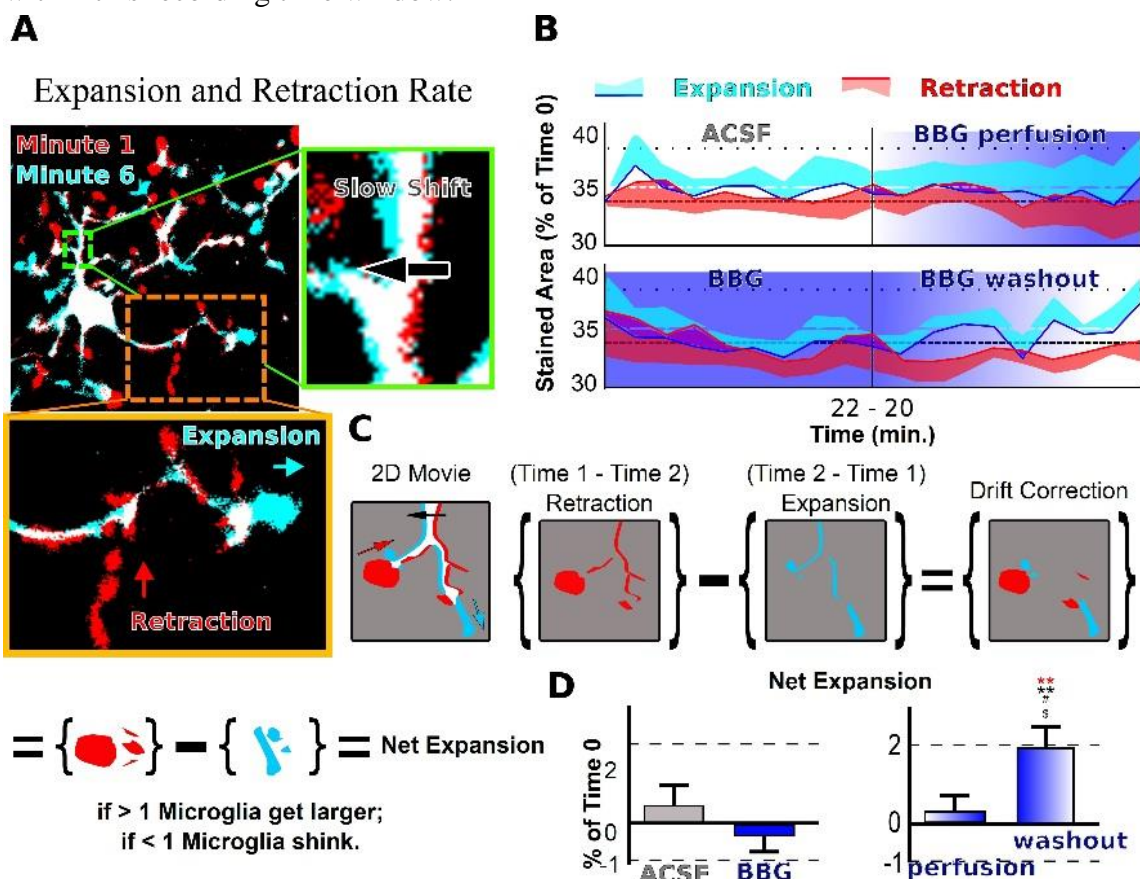


Figure 19. Slow drift correction of the field of view analysis, by calculation of microglial net expansion. **A)** Time-frames from a 3D registered maximal projection 2D movie of mPFC CX3CR1^{+/+}EGFP^{+/+} microglia during ACSF perfusion. Actual morphological rearrangement (expansion and retraction, down) and slow slice drift (right panel). **B)** Quantification of the field of view rate of expansion and of retraction, normalized over the respective first time-frame considered. **C)** Schematic representation of the operation done in calculating the average net expansion rate. **D)** Quantification of the average net expansion of field of views analyzed in B. Averages cover a period of 18 mins. N=3,

number of slices: BBG perfusion (ACSF to BBG)=6; BBG washout (BBG to ACSF)=4. Graph shows mean \pm SEM, statistical analysis performed with Tukey's test (red), p -value ** <0.01 vs BBG perfusion; Dunn's test (black), p -value ** <0.01 vs ACSF baseline; p -value # <0.05 vs BBG baseline; p -value $^{\$}$ <0.05 vs BBG perfusion.

4.16 Effect of 3 mM ATP on fluorescent microglia in *ex vivo* acute slices

Eventually, a last preliminary experiment assayed the effect of the non-physiological mM extracellular ATP concentration on microglia pre-treated with a P2X7R antagonist. Extracellular ATP has a very fast action, initially leading to a general protrusion of microglial branches and a cellular expansion, to later collapse its morphology if the signal persists (cytotoxic damages). In figure **20A** the pharmacological protocol applied is briefly schematized. Microglia movies during 3mM ATP application all show a sudden and pronounced change in the morphology (Figure **20B**). From the picture, it is possible to appreciate the shrinkage of the cell during perfusion of 3 mM ATP in ACSF. Interestingly, this ambient ATP signaling modifies the structure at the endings of the microglial branches, where the tip becomes larger and rounded (Figure **20B**, insert), as suggested in literature to be consequent of P2Y12R activation (**188**). As observed earlier, neither the ACSF nor the BBG baseline provoked significant microglial morphology changes, even if this time the surveillance index displayed a subtle non-significant difference (Figure **20C**). Perfusion with 3 mM ATP induced a rapid decrease in microglial volume of ACSF pretreated slices (Figure **20D**), while BBG pretreatment seems to buffer the cell shrinkage induced by ATP (Figure **20D**). However, it is important to note that due to high variability and low number of animals we were unable to find any significant difference.

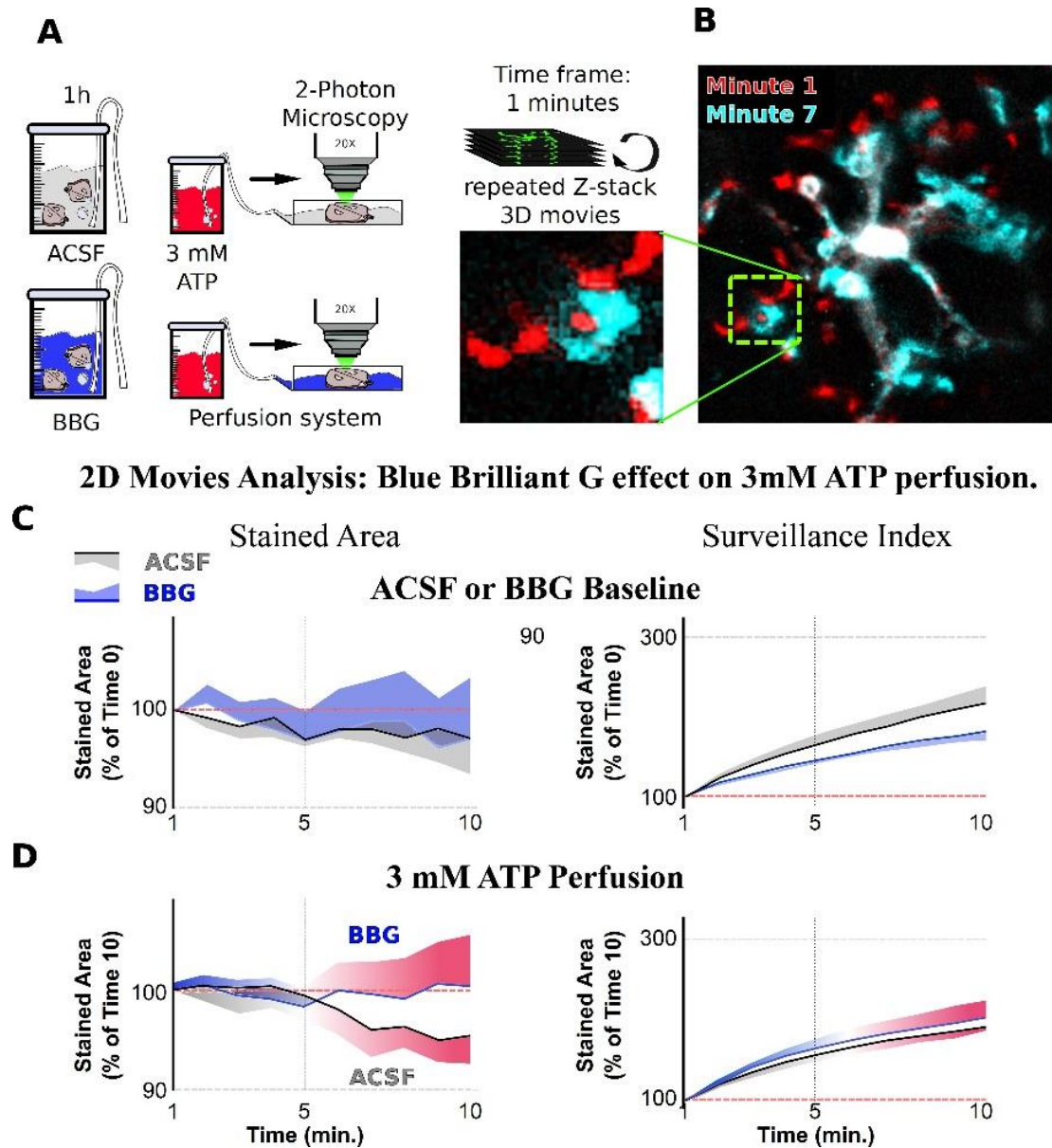


Figure 20. Analysis of fluorescent CX3CR1^{+/+}EGFP^{+/+} microglia, pre-treated with 10 μ M BBG-ACSF, and perfused with 3 mM ATP-ACSF or ATP-BBG-ACSF solution. **A)** Schematic representation of the experimental protocol. Movies time-frame of one minute. **B)** 2D movie of an ATP perfused slice. **C)** Results of relative microglial volume changes (left) and surveillance rate (right), along 10 mins. of ACSF or BBG perfusion. **D)** Effect of 10 mins. during which 3 mM ATP-ACSF, with or without 10 μ M BBG, was perfused on the slices. No significant differences were observed. N=3, number of slices: ACSF + ATP=4; BBG + ATP=4. Graph shows mean \pm SEM. Statistics: Student's *t*-test and Mann-Whitney U-test, not significant.

5. Discussion

5.1 Acute effect of PCP in P2rx7 genetically modified animals

The main finding of the present dissertation is that the positive- and cognitive-like symptoms induced by PCP in male mice is partly modulated by P2X7R functional expression. P2rx7^{-/-} animals were less susceptible to the psychotomimetic effects of the dissociative anesthetic, while P2X7R overexpression produced positive-like symptom responses with PCP dosage suboptimal to evoke psychosis-like activity (330), and exacerbated stereotypy with optimal doses. Moreover, after a subchronic PCP treatment, P2rx7^{-/-} mice did not display the typical impairment in a y-maze working memory task. Observed behaviors correlated with histological data: we found an alleviation of acute PCP-driven neuronal activation in a restricted area of the mPFC (layer V of PL and IL areas) in P2rx7^{-/-} mice, while P2rx7^{tg/+} displayed higher involvement of mPFC circuits. The c-Fos neuronal immunoreactivity can be considered an indirect measurement of *in vivo* neuronal activity (406). Comparing the same area, P2rx7^{-/-} and P2rx7^{tg/+} mice displayed a decreased and increased concentration of strongly activated neurons, respectively. These data suggest that P2X7R functional expression potentially modulates PCP-induced positive-like symptoms' expression prefrontal activity in male mice. We acknowledge that genetic manipulations in the strains studied could lead to unknown artifacts, such as altered protein c-Fos degradation dynamics.

5.2 Mechanisms involved in the acute effect of PCP in P2rx7^{-/-} animals

To identify possible protective mechanisms happening in the P2rx7^{-/-}, we analyzed different aspects of the mPFC layer V IL and PL cortices, where the PCP-driven c-Fos signal was identified. Considering data from double and triple immunostainings, [³H]-DA release experiments and electrophysiology, seem consistent with a pleiotropic role of P2rx7 gene (Figure 21). The lack of a differential PV interneuron activation between genotypes excluded a major preferential PCP-modulation of local GABAergic neurons. A c-Fos study, which extensively mapped the PCP-induced modulation of PV interneurons activity, already excluded the mPFC from such effects (225).

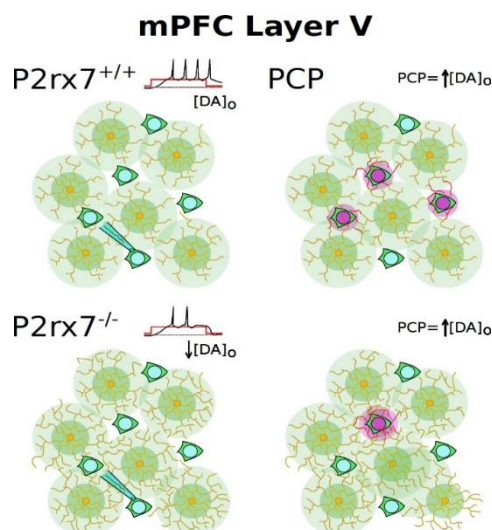


Figure 21. Cartoon summarizing the acute PCP findings in the P2rx7^{+/+} (up) and P2rx7^{-/-} (down) layer V of the mPFC. Data found in native or vehicle conditions (left). Acute PCP effects (increase extracellular dopamine **37**, **252**, **330**). Yellow cell: microglia; green cell: pyramidal neurons; green area: microglia cellular territory; light-green area: microglia intercellular territory; purple nuclei: activated neuron; purple area: peri-neuronal nucleus area; purple filaments: microglial branches towards neuronal nuclei.

Then we questioned the role of frontal dopamine release. A preliminary experiment ruled out gross anatomical developmental abnormalities in P2rx7^{-/-} strain. Both P2rx7^{-/-} and P2rx7^{tg/+} displayed no difference in the chemically stimulated local release of [³H]-DA. We confirmed a small but significant effect decrease in P2rx7^{-/-} PFC basal dopamine (**30**), while, in the P2rx7^{tg/+} PFC slices, we detected a lower dopamine uptake. These direct measurements may imply a functional role of P2X7R in regulating basal dopamine concentration. Anyway, subtle deregulation of the prefrontal dopaminergic tone leads to complex scenarios and speculation. We also observed subtle but interesting changes in the microglia morphology at the level of layer V PL and IL cortices, suggesting that P2X7R participate in the microglia-neuron interaction, thereby affecting neuronal activity. As expected, the number of microglial cells was not altered three hours after PCP administration, consistent with microglia displacement observations (**190**, **411**). In PCP-treated rodents, morphological signs of microglia pro-inflammatory shift in the literature were solely identified in retrosplenial cortices (**236**, **365**). The small decrease of P2Y12R immunoreactivity in P2rx7^{-/-} PCP-treated mPFC could reflect a slightly pro-inflammatory profile (**166**). Nevertheless, no difference was found between vehicle- and PCP-treated

groups. Using the software FIJI ImageJ, we obtained skeleton maps of the microglia reticule, which renders Sholl analysis mostly independent from immunoreactivity (**401**, **402**). The 30 μm thick slices imaging was undersized in the z-dimension to isolate entire microglial cells. We therefore applied the Sholl analysis on the non isolated microglia skeleton. Neither PCP administration nor P2rx7 gene deletion generated a general hyper- or hypo-ramified microglia phenotype, in the layer V of IL and PL cortices. It is important to point out that drops in cortical monoamines levels, following the majority of anesthesia types, induces expansion of microglial cells in matter of minutes (**412**). Since all animals underwent the same procedure, we acknowledge the systematic error. Moreover, while pentobarbital shall be considered a classical central anesthetic (**413**), PCP provokes an opposite acute and long-lasting increase of frontal monoamines concentration (**414**).

Microglia cell-centered analysis revealed that branches of saline-treated P2rx7^{-/-} mice displayed higher ramification after the first 20 μm of Sholl radius, compared to the saline-treated P2rx7^{+/+} ones. The PCP treatment of P2rx7^{-/-} mice dissolves this genotype-related difference. P2X7R may retain specific migration and phagocytic microglial functions, like the CX3CL1 chemoattraction (**373**), or the migration toward amyloid senile plaques (**415**). Interestingly, microglia ramification was reported to increase in the presence of a dopamine-3 receptor antagonist (**416**), a possible link to the lower dopaminergic frontal basal output of P2rx7^{-/-}. However, we could not find specific literature directly related to P2X7R expression and microglial morphology. Stainings against microglia and active neurons after acute treatments allowed to match the specific mPFC areas interested by PCP-driven hyper-activity. Recent findings demonstrated that around neuronal bodies, microglia contact neurons via a rather specialized communication route, found to be stable for tens of minutes (**183**) and proposed to function as a protective restraint of neuronal hyper-activation (**191**). From the PCP drive, leading to mPFC hyperactivity, until brain fixation (maximal cumulative c-Fos expression), passed 110 minutes in our experimental paradigm. The 2D Sholl analysis centered on neurons revealed that microglial branches were more abundant in the proximity of c-Fos positive neurons, respect to the less active neighboring neurons, in both genotypes. It is therefore possible that contacts between microglial branches and PCP-hyperactivated neurons *in vivo* might be stable for one-two hours, rather than tens of minutes. A series of 30 μm long z-stacks images from c-Fos and P2Y12R immunostainings were taken to perform a 15 μm Sholl

radius 3D analysis, centered in c-Fos⁺ nuclei, located in the central part of the stack z-axis. In PCP-treated P2rx7^{-/-} animals, mPFC layer V hyper-activated neurons were contacted by 1-2 more microglial branches (approximately 9-16%), with respect to wild-type. This small difference may also reflect an increased tendency of P2rx7^{-/-} c-Fos⁺ neuronal somata to be in direct contact with microglial somata. Eventually, we checked the intrinsic electrical properties of P2rx7^{-/-} neurons, since neuronal activity can directly attract microglial branches (191). Patch-clamp experiments of mPFC layer V neurons from young-adult mice did not identify functional differences between genotypes, with respect to resting membrane potential or rheobase. However, in the current clamp step protocol, a difference in spike accommodation and re-polarization were detected, suggesting lower excitability of P2rx7^{-/-} neurons. This suggests a subtle excitatory effect of P2X7R functional expression. The role of P2X7R in neuronal development remains unknown *in vivo* (417), as the majority of published studies focus mainly on adults and aged animals. To our knowledge, this is the first report of patch-clamp analysis on young adult P2rx7^{-/-} prefrontal cortical neurons. The electrophysiological profile emerging is in line with the c-Fos results, as P2rx7^{+/+} mPFC layer V neurons were prone to fire a higher number of action potential compared to P2rx7^{-/-} neurons.

Considering the microglia analysis, a diminished P2rx7^{-/-} neuronal excitability and a lower PCP-driven neuronal hyperactivity would suggest a lower, rather than a higher number of recruited microglial branches around P2rx7^{-/-} neuronal bodies. Indeed, microglia/neuron interaction is shown to be driven by ATP/ADP neuronal release, which depends at least partly on neuronal electrical activity (183, 191). Our RT-qPCR results confirmed the presence of P2rx7 RNA in the PFC of the Pfizer strain, yet the disrupted portion was detected only in wild-type tissue, suggesting that a COOH truncated isoform is expressed by the P2rx7^{-/-} tested animals. As discussed in the introduction, there is a general consensus that truncated P2X7R intracellular domain, in mice, generally present loss-of-function isoforms, with smaller ATP-driven currents, and unable to trigger “macropore” formation, among others intracellular pathways. Microglia-neuron contacts are intriguing phenomena, yet were only recently started to be characterized.

5.3 Hypothesis of P2X7R role in the mPFC microglial cells

Figure 22 aims to offer a closer, yet purely demonstrative, observation of the microglial organization around c-Fos⁺ nuclei. The analysis (Figure 9J, 22A) suggests that branches

reach the surface of the neuron and then multiply, surrounding the neuronal soma. It seems that branches run at a close distance to the soma, yet not quite touching it, while bulbous tips are very close to the neuronal soma (Figure 22B). In Figure 22C is shown a schematic representation of the inferred neuronal soma (c-Fos background, magenta-dashed line) with the map of the close microglial contact (patches P2Y12R signal, green dots). As mentioned in the introduction, in a very constricted extracellular environment, extracellular ATP concentration in special conditions could possibly overrun the threshold of P2X7R activation. This hypothesis is reinforced by the identification of P2X7R-EGFP protein at the interface of highly activated neuronal somata in PCP-treated $P2rx7^{tg/+}$ mice mPFC (Figure 2). Nonetheless, with the current data, we would not suggest further conclusions.

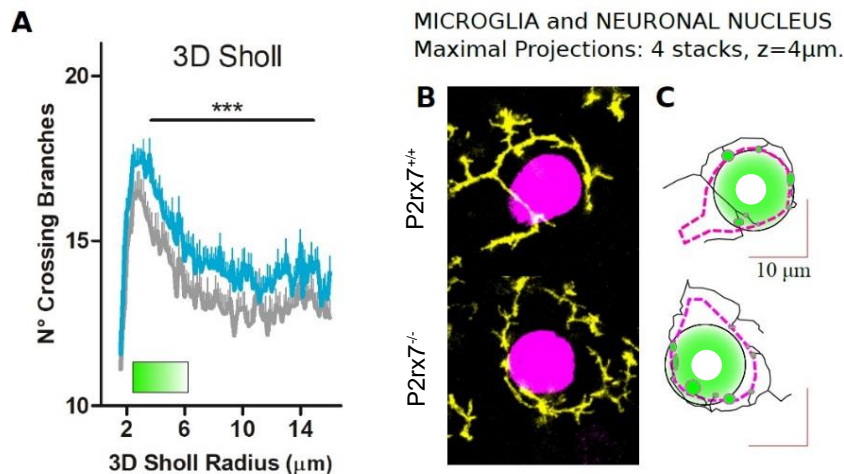


Figure 22. Microglia branches and neuronal body contacts in the PCP context. A) 3D Sholl analysis results (Figure 9J). Green bar: volume where microglia branches ramify over neuronal surface. B) Images from analyzed pictures, 4 μm z-stacks $\ast(30 \times 30 \mu\text{m}^2)$. C) Schematic representation of the manually inferred neuronal body (magenta-dashed line), volume of microglial debranching, centered at the c-Fos signal center (greenring), microglial branches (black line) and contacts (green points).

Data from the 2-photon preliminary analysis of layer V mPFC from two-months old $CX3CR1^{+/-}EGFP^{-/+}$ animals testing basic purinergic pharmacology, would suggest that P2X7R antagonist washout increased microglial territory. However, this was not achieved by increasing the surveillance index, therefore by exploring novel parenchymal territory.

It resulted that net microglia cellular volume linearly increased over twenty minutes washout, by an average 2% rate per minute. Since BBG is a dark dye, we verified that 10 μ M concentration was not interfering with our imaging, that was not influenced till BBG concentrations over 100 μ M, where signal decreased by 2-4% (data not shown). On one side, this data conflicts with the higher intercellular ramification found in P2rx7^{-/-} animals, since *ex vivo* gain-of-function of P2X7R correlated with microglia enlargement. But the results could also be interpreted as a compensation mechanisms, where P2X7R genetically induced loss-of-function that may antagonize microglial extension, could induce the adjustment of other pro-ramifying mechanisms, eventually leading to a more ramified microglia, like the phenotype observed in P2rx7^{-/-}. The working volume for microglia/neuron interaction studies falls in the field of super-resolution microscopy, since structures to resolve fall close to the point spread function limits of confocal, or 2-photon microscopy (180-250 nm for green fluorophores). Combining cell-biology functional assays with sub-diffraction microscopy could help in deciphering P2XR's pharmacology in microglia.

5.4 Acute effect of PCP in animals overexpressing P2X7R.

Our PCP study results confirm and extend our (30) and others (370, 371) previous observations, obtained with genetic deletion and pharmacological inhibition of P2X7R. For the first time, we tested P2rx7^{tg/+} young-adult animals with acute PCP systemic administration. Overexpressing heterozygous animals displayed exacerbated behavior, showing positive-like symptoms with low-dose PCP treatment, which may explain the milder effects of PCP on sociability scores during the circular open-field test. The pairs of P2rx7^{tg/+} mice often followed each other in circles, sniffing themselves more continuously than wild-type mice. With a fully psychotomimetic PCP dose, the P2rx7^{tg/+} mice performed accentuated stereotypical behavior, which correlates with values of concentration of strongly stained c-Fos neurons in the the layer V of IL and PL areas. The P2rx7^{tg/+} higher sensitivity to PCP, in terms of behavior and medial prefrontal neuronal hyperactivation, adds relevance to the model, as patients with schizophrenia also display increased response to arylcyclohexylamines anesthetics (418). Interestingly, the lower dopamine uptake of P2rx7^{tg/+} animals may indicate that the overexpressing strain has prefrontal hyperdopaminergia, consistent with the exacerbation of the PCP effect. The P2X7R-EGFP protein, expressed by heterozygous P2rx7^{tg/+} mice, was localized in the

layer V mPFC microglia and other cell types, throughout the mPFC. In summary, the implications of P2X7R expression upon acute PCP effect seems to indicate the sum of small cumulative effects leading to a positively correlated excitability of mPFC circuit.

5.5 Subchronic PCP treatment in P2rx7^{-/-} young adult mice

As aforementioned, while positive symptoms can be alleviated by available antipsychotic drugs, there is an unmet clinical need concerning cognitive deficits (419). We examined the working memory of P2rx7^{-/-} mice using an established subchronic PCP regimen that compromises memory performance (42). Along with the treatment, PCP normalized differences in the animal's weight, supposedly coming from metabolism differences in P2rx7^{-/-} mouse strains (409). Three days after the seven days treatment, animals were tested for the spontaneous alterations test in a y-maze. The lower locomotion displayed by P2rx7^{-/-} animals in the y-maze was contextual to this treatment protocol and test. Indeed, we could not detect other general locomotion-related differences outside the acute PCP-effect periods. Nonetheless, locomotor activity did not influence the total number of arm explorations. Subchronic PCP impaired the working memory performance of wild-type mice, respect to the P2rx7^{+/+} vehicle group and the P2rx7^{-/-} PCP treated group. The prefrontal cytokine levels, which followed the subchronic behavioral test battery, did not reveal any effects on the brain inflammatory profile in relation with PCP. These data confirm that NMDA-R antagonists directly modulate the neuronal activity without triggering a robust neuroinflammatory reaction in the mPFC circuit. Interestingly, the prefrontal level of fractalkine, or CX3CL1, was strongly upregulated in the P2rx7^{-/-} genotype. Fractalkine is an essential trophic factor of the brain and is strongly involved in microglial physiology (420). Since also P2X7R displayed trophic effect on microglia (197, 206), we cannot exclude the possibility that fractalkine upregulation could be a compensatory effect in a P2rx7 loss-of-function physiology to keep the microglia population in homeostatic conditions.

When the subchronic PCP and saline protocol was performed in group-caged mice, we observed the flattening of the average spatial working memory performances. Percentage of successful alternations of group-caged animals was unaffected by subchronic PCP. One explicit interpretation is that the social environment compensates some detrimental effects of PCP. On the other hand, this protocol fails to model schizophrenia cognitive-like symptoms (39). The difference in velocity, found between genotypes in single-cage

condition disappeared in group-caged experiments, normalizing to a lower distance covered by all groups. The number of same arm entries is a rarely used parameter, principally because of its difficult interpretation (421). The results point out that all groups of single-cage animals performed a significantly higher number of same arm entries with respect to group-caged animals, positively correlating with the respective velocity data. Indeed, single-cage wild-type animals cover a higher distance compared to P2rx7^{-/-} animals during the test, probably by poking and going in-and-out several times each arm they visit. PCP subchronic treatment exacerbates this tendency, making P2rx7^{+/+} more active and P2rx7^{-/-} less active, rendering to the genotypic differences of statistical significance. In conclusion, the group-caged condition buffers the detrimental effects of subchronic PCP on memory of wild-type animals, confirming the idea that enriched social environments can deeply modify the rodents' psychopathological cascades (422). Experiments done with further washout also displayed behavioral and treatment differences, though very subtle and of little translation potential. Interestingly, the slightly higher number in spontaneous rotations affecting P2rx7^{+/+} PCP-treated animals normalized with the repetition of the open-field experience after 24 hours from the previous test. It is therefore possible that PCP-treated P2rx7^{+/+} animals are likely to memorize the contextual experience of the day ten open-field test, and modulate their future behavior accordingly. Though the detrimental effect of subchronic PCP models on prefrontal GABAergic interneurons is well documented (423), with our protocol we could not properly identify the PV deficit in C57Bl/6 mice. This could be justified by differences between protocols regarding treatments, experiments and other complex environmental factors (422). While it is easy to spot where PCP exactly drives hyperactivation of the mPFC circuit during the acute effect, is more difficult to identify anatomical traces of subchronic PCP. Therefore, the current study's measurement of PV immunoreactivity may not be specific enough. A c-Fos subchronic PCP study on rats' mPFC, deciphering the disrupted working memory functions, found an increased recruitment of neurons at the level of the PL layer II/III correlated with poorer performance (286). We performed a c-Fos staining on subchronically treated animals monitoring the basal activity during the day-time, confirming that little if none induction of activity is observed in the mPFC superficial layers (254). We acknowledge the fact that a behavior-correlated c-Fos study could have been more interesting. In subchronically treated animals, counting of

microglial cells was checked with Iba-1 and P2Y12R markers in mPFC, resulting not suggestive of any pro-inflammatory shift, in line with the cytokine quantification. The broad analysis performed on the PFC underlined a general lower density of Iba-1 positive nuclei in PCP-treated P2rx7^{-/-} animals, likely corresponding to a lower intensity of the signal. Nonetheless, the P2Y12R manual quantification of microglial cells did not find this difference, either when considering large PFC areas (data not shown) or specific areas (cortical layering). The downregulation of Iba-1 while maintaining the same levels of P2Y12R may indicate an inflammation “resolutive” phenotype (109). Astrocytic stainings using GFAP marker resulted with a very poor signal, likely expressed by a minority of homeostatic astrocytes in the mouse PFC. Small differences in the numbers of astrocytes lay on a very sparse labeling, which makes the interpretation too speculative.

In summary, we propose that there exists a concrete possibility of a central P2X7R function able to modulate positive- and cognitive-like symptoms induced by PCP. In addition to the mechanisms inferred above, we cannot exclude alternative pharmacokinetic properties of PCP in the different genotypes. Acute PCP treatment is known also to trigger the stress response, affecting the hypothalamus-pituitary-adrenal axis by stimulating pituitary adrenocorticotrophic hormone release and consequently increasing plasma corticosterone levels (424, 425). After PCP subchronic treatment, stress induced by experimental procedures triggers greater stress responses in terms of behavior and plasma levels of adrenocorticotrophic hormone (426). As already mentioned, there is evidence that P2rx7^{-/-} animals display a basal “anti-depressed” profile, possibly dependent by reduced centrally-dependent HPA axis activation (25). This anti-stressed, therefore anti-depressed P2rx7 loss-of-function dependent phenotype, along with other evidence, points to a hypothetical cascade of neuroinflammatory-related events that would explain the protective role of P2X7R against repetitive stressful events (212). In addition, our previous study (30) indicated several subtle expression changes, in genes implicated in schizophrenia, in a small dose acute PCP model, which was partially reversed in P2rx7^{-/-} animals.

6. Conclusion

These results confirm the role of P2X7R in schizophrenia-like behaviors in an animal model, being proposed as a potential therapeutic target. A decrease of neuronal activation in a restricted area of the mPFC in response to PCP treatment in mice genetically deficient for P2rx7 was observed. Specifically, P2X7R gene deletion elicited a lower number of strongly activated neurons in the mPFC specific to the V layer of the PL and IL areas. Opposite results were found testing an P2X7R overexpressing line, which is more susceptible to PCP in terms of behavior and prefrontal specific circuits involvement. This finding identifies a potential primary site of action, whereby P2rx7 might affect PCP-induced behavior. Moreover, we observed a change in microglial morphology in the same area regarding the contact sites of microglia over the neuronal somata. This raises the possibility that P2X7 regulates microglia-neuron interaction and thereby affects animal behavior.

7. Summary

Schizophrenia is an invalidating psychiatric condition, still depleted of safe and effective treatments for its negative and cognitive symptoms. PCP is a dissociative anesthetic with psychotomimetic properties, mimicking pathological aspects of schizophrenia in humans and rodents. Non-human studies of PCP models revealed that the arylcyclohexylamines-dependent blockade of the glutamate NMDA-R mimics behavioral and neurological aspects of schizophrenia pathology. The murine models allow testing novel and safe drugs with the potential to counteract symptoms in the positive, negative and cognitive spectrum of psychosis. In this work we collected evidence of different nature, from behavioral observation to electrophysiological characterization of prefrontal neurons, trying to evaluate the effect of the ATP purinergic P2X7R functional expression in the PCP murine schizophrenia-model. In line with previously published results, we found that P2X7R loss-of-function confers a protective phenotype for what concern acute PCP psychotomimetic effects, both in terms of acute psychotic-like behavior (positive-like symptoms) and of subchronic PCP-derived working memory dysfunction (cognitive-like symptoms). We corroborated our observations by the study of a P2X7R overexpressing mouse line that presented exacerbated PCP-induced positive-like symptoms. The modulation of basal dopamine levels in the frontal brain, the increased acute PCP-induced layer-specific neuronal activation, the increased intrinsic excitability of neurons in the mPFC and the preferential interaction of microglia with hyperactive neurons in the mouse mPFC are features identified in the current study as P2X7R-expression dependent. Although we could not perform direct experiments interrogating the specific molecular mechanisms and cell types involved in the aforementioned P2X7R action, collectively, our findings support the notion that P2X7R exerts multiple pleiotropic roles. In summary, we find encouraging, and with a considerable degree of novelty, the revealed efficacy of the P2X7R loss-of-function in both categories of positive- and cognitive-like symptoms. However, the mechanism by which P2X7R is endogenously activated under these conditions needs to be further examined. Obvious advice on future directions would be to corroborate the current observations with P2X7R-antagonist studies in similar models. Moreover, scientific projects addressing the question about specific molecular pathways and mechanisms could be extremely interesting to further refine possible pharmacological strategies.

8. Összefoglalás

A szkizofrénia tartós munkaképtelenséghez vezető pszichiátriai kórkép, melynek negatív és kognitív tüneteit ma sem tudja kielégítően és biztonságosan kezelni az orvostudomány. A fenciklidin (PCP) egy jól ismert, disszociatív anesztéziát okozó anyag, amely a szkizofrénia patológiájának egyes aspektusait idézi elő rágcsálókban és emberben: állatkísérletek adatai szerint az NMDA receptorok arylciklohexilamin-függő blokádja reprodukálni képes a szkizofrénia viselkedési és neurológiai tüneteit. A rágcsáló modellek alkalmasak arra, hogy új farmakológiai útvonalak befolyásolását teszteljük a pszichózisok pozitív, negatív és kognitív tüneteinek ellensúlyozására.

Disszertációmban különböző, az elektrofiziológiai vizsgálatoktól a viselkedéskísérletekig terjedő módszerekkel kísérletet tettem az ATP érzékeny P2X7 purinoceptor (P2X7R) functionális expressziójának feltérképezésére a PCP által indukált szkizofrénia egérmodellben. Korábbi irodalmi előzményekkel összhangban azt tapasztaltam, hogy a P2X7 receptor funkció vesztése protektív hatású a PCP pszichotomimetikus hatásaira (pozitív tünetek), továbbá a PCP által kiváltott munkamemória deficitre (kognitív tünetek) is a szubkrónikus modellben. A bazális dopamin szintek modulációja, az akut, PCP által kiváltott réteg-specifikus neuronális aktiváció, a neuronok fokozott intrinszik excitabilitása, valamint a mikroglia preferenciális interakciója a hiperaktív neuronokkal az egér mediális prefrontális kéregben olyan jelenségek, amelyek P2X7 receptor függőnek bizonyultak kísérleteinkben. Bár olyan kísérleteket nem végeztünk, amelyek közvetlenül azonosították volna azokat a specifikus molekuláris mechanizmusokat és sejttípusokat, amelyek a P2X7 receptor aktiváció hatásait közvetítik a fent leírt megfigyelésekben, összességében véve eredményeink alátámasztják, hogy a P2X7 receptor sokrétű, pleiotrop szerepet tölt be.

Összefoglalva, a P2X7 receptorok funkcióvesztése segítségével újszerű és ígéretes hatásokat azonosítottunk, melyek alkalmasak lehetnek a pozitív és a kognitív tünetek kezelésére. Ugyanakkor az endogén P2X7 receptor aktiváció mechanizmusának feltárása ilyen körülmények között még további kutatásokat igényel. Ezek közül nyilvánvalóan érdemes a fenti megállapításokat specifikus P2X7 receptor antagonistá segítségével is alátámasztani hasonló modellekben. Ezen túlmenően, a hatásközvetítő molekuláris jelátviteli útvonalak és mechanizmusok feltérképezése is fontos feladat további lehetséges farmakológiai célpontok kidolgozása szempontjából.

9. References

1. Surís A, Holliday R, North CS. (2016) The Evolution of the Classification of Psychiatric Disorders. *Behav Sci (Basel)*, 18; 6(1):5.
2. Solmi M, Murru A, Pacchiarotti I, et al. (2017) Safety, tolerability, and risks associated with first- and second-generation antipsychotics: a state-of-the-art clinical review. *Ther Clin Risk Manag.* 13; 757-777.
3. Lieberman JA, Stroup TS, McEvoy JP, Swartz MS, Rosenheck RA, Perkins DO, Keefe RS, Davis SM, Davis CE, Lebowitz BD, Severe J, Hsiao JK; Clinical Antipsychotic Trials of Intervention Effectiveness (CATIE) Investigators.
4. Seeman, P., Wong, M., and Lee, T. (1974) Dopamine receptor block and nigral fiber impulse-blockade by major tranquilizers. *Fed Proc.* 33, 243.
5. Seeman, P., Chau-Wong, M., Tedesco, J., and Wong, K. (1975) Brain receptors for antipsychotic drugs and dopamine: direct binding assays. *Proc. Natl. Acad. Sci. U. S. A.* 72, 4376–4380.
6. Van Rossum, J. M. (1966) The significance of dopamine receptor blockade for the mechanism of action of neuroleptic drugs. *Arch Int. Pharmacodyn Ther* 160, 492–494.
7. Seeman, P. (1987) Dopamine receptors and the dopamine hypothesis of schizophrenia. *Synapse* 1, 133–152.
8. Lodge, D., and Anis, N. A. (1982) Effects of phencyclidine on excitatory amino acid activation of spinal interneurons in the cat. *Eur. J. Pharmacol.* 77, 203–204.
9. Anis, N., Berry, S., Burton, N., and Lodge, D. (1983) The dissociative anaesthetics, ketamine and phencyclidine, selectively reduce excitation of central mammalian neurones by N-methyl-D-aspartate. *Br. J. Pharmacol.* 79, 565–575.a
10. Javitt, D. C., and Zukin, S. R. (1991) Recent advances in the phencyclidine model of schizophrenia. *Am. J. Psychiatry* 148, 1301– 1308.
11. Morris, B. J., Cochran, S. M., and Pratt, J. A. (2005) PCP: from pharmacology to modelling schizophrenia. *Curr. Opin. Pharmacol.* 5, 101–106
12. Sperlagh B, Vizi ES. (1991) Effect of presynaptic P2 receptor stimulation on transmitter release. *J Neurochem.* 56(5); 1466-70.

13. Sperlách B, Kittel A, Lajtha A, Vizi ES. (1995) ATP acts as fast neurotransmitter in rat habenula: neurochemical and enzyme cytochemical evidence. *Neuroscience*. 66(4); 915-20.
14. Sperlách B, Mergl Z, Jurányi Z, Vizi ES, Makara GB. (1999) Local regulation of vasopressin and oxytocin secretion by extracellular ATP in the isolated posterior lobe of the rat hypophysis. *J Endocrinol*. 160(3); 343-50.
15. Sperlách B, Erdélyi F, Szabó G, Vizi ES. (2000) Local regulation of [(3)H]-noradrenaline release from the isolated guinea-pig right atrium by P(2X)-receptors located on axon terminals. *Br J Pharmacol*. 131(8); 1775-83.
16. Sperlách B, Haskó G, Németh Z, Vizi ES. (1998) ATP released by LPS increases nitric oxide production in raw 264.7 macrophage cell line via P2Z/P2X7 receptors. *Neurochem Int*. 33(3); 209-15.
17. Sperlách B, Köfalvi A, Deuchars J, Atkinson L, Milligan CJ, Buckley NJ, Vizi ES. (2002) Involvement of P2X7 receptors in the regulation of neurotransmitter release in the rat hippocampus. *J Neurochem*. 81(6); 1196-211.
18. Papp L, Vizi ES, Sperlách B. (2004) Lack of ATP-evoked GABA and glutamate release in the hippocampus of P2X7 receptor^{-/-} mice. *Neuroreport*. 25; 15(15):2387-.
19. Balázsa T, Bíró J, Gullai N, Ledent C, Sperlách B. (2008) CB1-cannabinoid receptors are involved in the modulation of non-synaptic [3H]serotonin release from the rat hippocampus. *Neurochem Int*. 52(1-2); 95-102.
20. Csölle C, Sperlách B. (2011) Endocannabinergic modulation of interleukin-1 β in mouse hippocampus under basal conditions and after in vivo systemic lipopolysaccharide stimulation. *Neuroimmunomodulation*. 18(4); 226-31.
21. Baranyi M, Porceddu PF, Gölöncsér F, Kulcsár S, Otrókoci L, Kittel Á, Pinna A, Frau L, Huleatt PB, Khoo ML, Chai CL, Dunkel P, Mátyus P, Morelli M, Sperlách B. (2016) Novel (Hetero)arylalkenyl propargylamine compounds are protective in toxin-induced models of Parkinson's disease. *Mol Neurodegener*. 13; 11:6.
22. Sperlách B, Illes P. (2014) P2X7 receptor: an emerging target in central nervous system diseases. *Trends Pharmacol Sci*. 35(10); 537-47.
23. Beamer E, Gölöncsér F, Horváth G, Bekő K, Otrókoci L, Koványi B, Sperlách B. (2016) Purinergic mechanisms in neuroinflammation: An update from molecules to behavior. *Neuropharmacology*. 104; 94-104.

24. Huang L, Otrókocsi L, Sperlágh B. (2019) Role of P2 receptors in normal brain development and in neurodevelopmental psychiatric disorders. *Brain Res Bull.* 151; 55-64.
25. Csölle C, Andó RD, Kittel Á, Gölöncsér F, Baranyi M, Soproni K, Zelena D, Haller J, Németh T, Mócsai A, Sperlágh B. (2013) The absence of P2X7 receptors (P2rx7) on non-haematopoietic cells leads to selective alteration in mood-related behaviour with dysregulated gene expression and stress reactivity in mice. *Int J Neuropsychopharmacol.* 16(1); 213-33.
26. Sperlagh B, Csolle C, Ando RD, Goloncser F, Kittel A, Baranyi M. (2012) The role of purinergic signaling in depressive disorders. *Neuropsychopharmacol Hung.* 14(4); 231-8.
27. Csölle C, Baranyi M, Zsilla G, Kittel A, Gölöncsér F, Illes P, Papp E, Vizi ES, Sperlágh B. (2013) Neurochemical Changes in the Mouse Hippocampus Underlying the Antidepressant Effect of Genetic Deletion of P2X7 Receptors. *PLoS One.* 21;8(6); e66547.
28. Otrókocsi L, Kittel Á, Sperlágh B. (2017) P2X7 Receptors Drive Spine Synapse Plasticity in the Learned Helplessness Model of Depression. *Int J Neuropsychopharmacol.* 1;20(10); 813-822.
29. Horváth G, Otrókocsi L, Beko K, Baranyi M, Kittel Á, Fritz-Ruenes PA, Sperlágh B. (2019) P2X7 Receptors Drive Poly(I:C) Induced Autism-like Behavior in Mice. *J Neurosci.* 27;39(13); 2542-2561.
30. Koványi B, Csölle C, Calovi S, Hanuska A, Kató E, Köles L, Bhattacharya A, Haller J, Sperlágh B. (2016) The role of P2X7 receptors in a rodent PCP-induced schizophrenia model. *Sci Rep.* 8; 6:36680.
31. Calovi S, Mut-Arbona P, Tod P, Iring A, Nicke A, Mato S, Vizi ES, Tønnesen J, Sperlagh B. (2020) P2X7 Receptor-Dependent Layer-Specific Changes in Neuron-Microglia Reactivity in the Prefrontal Cortex of a Phencyclidine Induced Mouse Model of Schizophrenia. *Front Mol Neurosci.* 11; 13:566251.
32. Beamer E, Kovács G, Sperlágh B. (2017) ATP released from astrocytes modulates action potential threshold and spontaneous excitatory postsynaptic currents in the neonatal rat prefrontal cortex. *Brain Res Bull.* 135; 129-142.

33. Göloncsér F, Baranyi M, Balázsfi D, Demeter K, Haller J, Freund TFF, Zelena D, Sperlág B. (2017) Regulation of Hippocampal 5-HT Release by P2X7 Receptors in Response to Optogenetic Stimulation of Median Raphe Terminals of Mice. *Front Mol Neurosci.* 12;10:325.
34. Kovács G, Környei Z, Tóth K, Baranyi M, Brunner J, Neubrandt M, Dénes Á, Sperlág B. (2018) Modulation of P2X7 purinergic receptor activity by extracellular Zn²⁺ in cultured mouse hippocampal astroglia. *Cell Calcium.* 75; 1-13.
35. Solle M, Labasi J, Perregaux DG, Stam E, Petrushova N, Koller BH, Griffiths RJ, Gabel CA. (2001) Altered cytokine production in mice lacking P2X(7) receptors. *J Biol Chem.* 5:276(1); 125-32.
36. Kaczmarek-Hajek K, Zhang J, Kopp R, Grosche A, Rissiek B, Saul A, Bruzzone S, Engel T, Jooss T, Krautloher A, Schuster S, Magnus T, Stadelmann C, Sirko S, Koch-Nolte F, Eulenburg V, Nicke A. (2018) Re-evaluation of neuronal P2X7 expression using novel mouse models and a P2X7-specific nanobody. *Elife.* 3;7; e36217.
37. Jentsch JD, Roth RH. (1999) The neuropsychopharmacology of phencyclidine: from NMDA receptor hypofunction to the dopamine hypothesis of schizophrenia. *Neuropsychopharmacology.* 20(3); 201-25.
38. Balla A, Koneru R, Smiley J, Sershen H, Javitt DC. (2001) Continuous phencyclidine treatment induces schizophrenia-like hyperreactivity of striatal dopamine release. *Neuropsychopharmacology.* 25(2); 157-64.
39. Jones CA, Watson DJ, Fone KC. (2011) Animal models of schizophrenia. *Br J Pharmacol.* 164(4); 1162-94.
40. Steeds H, Carhart-Harris RL, Stone JM. (2015) Drug models of schizophrenia. *Ther Adv Psychopharmacol.* 5(1); 43-58.
41. Mouri A, Koseki T, Narusawa S, Niwa M, Mamiya T, Kano S, Sawa A, Nabeshima T. (2012) Mouse strain differences in phencyclidine-induced behavioural changes. *Int J Neuropsychopharmacol.* 15(6); 767-79.
42. Zain MA, Rouhollahi E, Pandey V, Mani V, Majeed ABA, Wong WF, Mohamed Z. (2018) Phencyclidine dose optimisation for induction of spatial learning and memory deficits related to schizophrenia in C57BL/6 mice. *Exp Anim.* 1;67(4); 421-429.
43. Clayton JA, Collins FS. (2014) Policy: NIH to balance sex in cell and animal studies. *Nature.* 15;509(7500); 282-3.

44. Lewine RR, Gulley LR, Risch SC, Jewart R, Houpt JL. (1990) Sexual dimorphism, brain morphology, and schizophrenia. *Schizophr Bull.* 16(2); 195-203.
45. Mendrek A, Stip E. (2011) Sexual dimorphism in schizophrenia: is there a need for gender-based protocols? *Expert Rev Neurother.* 11(7); 951-9.
46. Crain JM, Nikodemova M, Watters JJ. (2009) Expression of P2 nucleotide receptors varies with age and sex in murine brain microglia. *J Neuroinflammation.* 25; 6:24.
47. Guneykaya D, Ivanov A, Hernandez DP, Haage V, Wojtas B, Meyer N, Maricos M, Jordan P, Buonfiglioli A, Gielniewski B, Ochocka N, Cömert C, Friedrich C, Artiles LS, Kaminska B, Mertins P, Beule D, Kettenmann H, Wolf SA. (2018) Transcriptional and Translational Differences of Microglia from Male and Female Brains. *Cell Rep.* 4;24(10); 2773-2783.e6.
48. Weinhard L, Neniskyte U, Vadisiute A, di Bartolomei G, Aygün N, Riviere L, Zonfrillo F, Dymecki S, Gross C. (2018) Sexual dimorphism of microglia and synapses during mouse postnatal development. *Dev Neurobiol.* 78(6); 618-626.
49. Turgeon SM, Anderson N, O'Loughlin K. (2010) Phencyclidine (PCP) produces sexually dimorphic effects on voluntary sucrose consumption and elevated plus maze behavior. *Pharmacol Biochem Behav.* 95(2); 173-8.
50. Snigdha S, Neill JC, McLean SL, Shemar GK, Cruise L, Shahid M, Henry B. (2011) Phencyclidine (PCP)-induced disruption in cognitive performance is gender-specific and associated with a reduction in brain-derived neurotrophic factor (BDNF) in specific regions of the female rat brain. *J Mol Neurosci.* 43(3); 337-45.
51. Miller DS and Horowitz SB. (1986) Intracellular compartmentalization of adenosine triphosphate. *J Biol Chem.* 261(30); 13911-5.
52. North RA. (2002) Molecular physiology of P2X receptors. *Physiol Rev.* 82(4); 1013-67.
53. Pankratov Y, Lalo U, Verkhratsky A, North RA. (2006) Vesicular release of ATP at central synapses. *Pflugers Arch.* 452(5); 589-97.
54. Melani A, Turchi D, Vannucchi MG, Cipriani S, Gianfriddo M, Pedata F. (2005) ATP extracellular concentrations are increased in the rat striatum during in vivo ischemia. *Neurochem Int.* 47(6); 442-8.

55. Dissing-Olesen L, LeDue JM, Rungta RL, Hefendehl JK, Choi HB, MacVicar BA. (2014) Activation of neuronal NMDA receptors triggers transient ATP-mediated microglial process outgrowth. *J Neurosci.* 6;34(32); 10511-27.
56. Taruno A. (2018) ATP Release Channels. *Int J Mol Sci.* 11;19(3); 808.
57. Pellegatti P, Raffaghello L, Bianchi G, Piccardi F, Pistoia V, Di Virgilio F. (2008) Increased level of extracellular ATP at tumor sites: in vivo imaging with plasma membrane luciferase. *PLoS One.* 9;3(7); e2599.
58. Wilhelm K, Ganesan J, Müller T, Dürr C, Grimm M, Beilhack A, Krempl CD, Sorichter S, Gerlach UV, Jüttner E, Zerweck A, Gärtner F, Pellegatti P, Di Virgilio F, Ferrari D, Kambham N, Fisch P, Finke J, Idzko M, Zeiser R. (2010) Graft-versus-host disease is enhanced by extracellular ATP activating P2X7R. *Nat Med.* 16(12); 1434-8.
59. Robson SC, Sévigny J, Zimmermann H. (2006) The E-NTPDase family of ectonucleotidases: Structure function relationships and pathophysiological significance. *Purinergic Signal.* 2(2); 409-30.
60. Chu S, Xiong W, Zhang D, Soylyu H, Sun C, Albensi BC, Parkinson FE. (2013) Regulation of adenosine levels during cerebral ischemia. *Acta Pharmacol Sin.* 34(1); 60-6.
61. Burnstock G, Verkhratsky A. (2009) Evolutionary origins of the purinergic signalling system. *Acta Physiol (Oxf).* 195(4); 415-47.
62. Verkhratsky A, Burnstock G. (2014) Biology of purinergic signalling: its ancient evolutionary roots, its omnipresence and its multiple functional significance. *Bioessays.* 36(7); 697-705.
63. Drury AN, Szent-Györgyi A. (1929) The physiological activity of adenine compounds with especial reference to their action upon the mammalian heart. *J Physiol.* 25;68(3); 213-37.
64. Holton FA. and Holton P. (1954) The capillary dilator substances in dry powders of spinal roots; a possible role of adenosine triphosphate in chemical transmission from nerve endings. *J Physiol.* 28;126(1); 124-40.
65. Holton P. (1959) The liberation of adenosine triphosphate on antidromic stimulation of sensory nerves. *J Physiol.* 12;145(3); 494-504.

66. Burnstock G, Campbell G, Satchell D, Smythe A. (1970) Evidence that adenosine triphosphate or a related nucleotide is the transmitter substance released by non-adrenergic inhibitory nerves in the gut. *Br J Pharmacol.* 40(4); 668-88.
67. Burnstock G, Satchell DG, Smythe A. (1972) A comparison of the excitatory and inhibitory effects of non-adrenergic, non-cholinergic nerve stimulation and exogenously applied ATP on a variety of smooth muscle preparations from different vertebrate species. *Br J Pharmacol.* 46(2); 234-42.
68. Burnstock G. (1972) Purinergic nerves. *Pharmacol Rev.* 24(3); 509-81.
69. Verkhatsky A, Zimmermann H, Abbracchio MP, Illes P, DiVirgilio F. (2020) In Memoriam Geoffrey Burnstock: Creator of Purinergic Signaling, *Function*, 1(1); zqaa006.
70. Abbracchio MP, Burnstock G. (1994) Purinoceptors: are there families of P2X and P2Y purinoceptors? *Pharmacol Ther.* 64(3);445-75.
71. Fredholm BB, Abbracchio MP, Burnstock G, Daly JW, Harden TK, Jacobson KA, Leff P, Williams M. (1994) Nomenclature and classification of purinoceptors. *Pharmacol Rev.* 46(2); 143-56.
72. Jacobson KA, Müller CE. (2016) Medicinal chemistry of adenosine, P2Y and P2X receptors. *Neuropharmacology.* 104; 31-49.
73. Ralevic V, Burnstock G. (1998) Receptors for purines and pyrimidines. *Pharmacol Rev.* 50(3); 413-92.
74. Robinson LE, Murrell-Lagnado RD. (2013) The trafficking and targeting of P2X receptors. *Front Cell Neurosci.* 22:7:233.
75. Koshimizu T, Koshimizu M, Stojilkovic SS. (1999) Contributions of the C-terminal domain to the control of P2X receptor desensitization. *J Biol Chem.* 31;274(53); 37651-7.
76. Jarvis MF, Khakh BS. (2009) ATP-gated P2X cation-channels. *Neuropharmacology.* 56(1); 208-15.
77. Coddou C, Yan Z, Obsil T, Huidobro-Toro JP, Stojilkovic SS. (2011) Activation and regulation of purinergic P2X receptor channels. *Pharmacol Rev.* 63(3); 641-83.
78. Di Virgilio F, Schmalzing G, Markwardt F. (2018) The Elusive P2X7 Macropore. *Trends Cell Biol.* 28(5); 392-404.

79. Habermacher C, Dunning K, Chataigneau T, Grutter T. (2016) Molecular structure and function of P2X receptors. *Neuropharmacology*. 104; 18-30.
80. Surprenant A, North RA. (2009) Signaling at purinergic P2X receptors. *Annu Rev Physiol*. 71; 333-59.
81. Dreisig K, Kornum BR. (2016) A critical look at the function of the P2Y11 receptor. *Purinergic Signal*. 12(3); 427-37.
82. Herold CL, Qi AD, Harden TK, Nicholas RA.(2004) Agonist versus antagonist action of ATP at the P2Y4 receptor is determined by the second extracellular loop. *J Biol Chem*. 279(12); 11456-64.
83. von Kügelgen I, Hoffmann K. (2016) Pharmacology and structure of P2Y receptors. *Neuropharmacology*. 104; 50-61.
84. Cunha RA. (2016) How does adenosine control neuronal dysfunction and neurodegeneration? *J Neurochem*. 139(6); 1019-1055.
85. Kawate T, Michel JC, Birdsong WT, Gouaux E. (2009) Crystal structure of the ATP-gated P2X(4) ion channel in the closed state. *Nature*. 30;460(7255); 592-8.
86. Hattori M, Gouaux E. (2012) Molecular mechanism of ATP binding and ion channel activation in P2X receptors. *Nature*. 10;485(7397); 207-12.
87. Kasuya G, Fujiwara Y, Takemoto M, Dohmae N, Nakada-Nakura Y, Ishitani R, Hattori M, Nureki O. (2016) Structural Insights into Divalent Cation Modulations of ATP-Gated P2X Receptor Channels. *Cell Rep*. 14(4); 932-944.
88. Mansoor SE, Lü W, Oosterheert W, Shekhar M, Tajkhorshid E, Gouaux E. (2016) X-ray structures define human P2X(3) receptor gating cycle and antagonist action. *Nature*. 6;538(7623); 66-71.
89. Li M, Wang Y, Banerjee R, Marinelli F, Silberberg S, Faraldo-Gómez JD, Hattori M, Swartz KJ. (2019) Molecular mechanisms of human P2X3 receptor channel activation and modulation by divalent cation bound ATP. *Elife*. 24;8; e47060.
90. Karasawa A, Kawate T. (2016) Structural basis for subtype-specific inhibition of the P2X7 receptor. *Elife*. 9;5; e22153.
91. Chataigneau T, Lemoine D, Grutter T. (2013) Exploring the ATP-binding site of P2X receptors. *Front Cell Neurosci*. 30; 7:273.
92. Coddou C, Stojilkovic SS, Huidobro-Toro JP. (2011) Allosteric modulation of ATP-gated P2X receptor channels. *Rev Neurosci*. 22(3); 335-54.

93. Müller CE. (2015) Medicinal chemistry of P2X receptors: allosteric modulators. *Curr Med Chem.* 22(7); 929-41.
94. De Roo M, Rodeau JL, Schlichter R. (2003) Dehydroepiandrosterone potentiates native ionotropic ATP receptors containing the P2X2 subunit in rat sensory neurones. *J Physiol.* 1;552(Pt 1); 59-71.
95. Bernier LP, Ase AR, Séguéla P. (2013) Post-translational regulation of P2X receptor channels: modulation by phospholipids. *Front Cell Neurosci.* 25; 7:226.
96. Kopp R, Krautloher A, Ramírez-Fernández A, Nicke A. (2019) P2X7 Interactions and Signaling - Making Head or Tail of It. *Front Mol Neurosci.* 12; 183.
97. Surprenant A. (1996) Functional properties of native and cloned P2X receptors. *Ciba Found Symp.* 198; 208-22.
98. Brake AJ, Wagenbach MJ, Julius D. (1994) New structural motif for ligand-gated ion channels defined by an ionotropic ATP receptor. *Nature.* 371(6497); 519-23.
99. Giniatullin R, Nistri A. (2013) Desensitization properties of P2X3 receptors shaping pain signaling. *Front Cell Neurosci.* 7; 245.
100. McCarthy AE, Yoshioka C, Mansoor SE. (2019) Full-Length P2X7 Structures Reveal How Palmitoylation Prevents Channel Desensitization. *Cell.* 179(3); 659-670.e13.
101. Gonnord P, Delarasse C, Auger R, Benihoud K, Prigent M, Cuif MH, Lamaze C, Kanellopoulos JM. (2009) Palmitoylation of the P2X7 receptor, an ATP-gated channel, controls its expression and association with lipid rafts. *FASEB J.* 23(3); 795-805.
102. Liu X, Surprenant A, Mao HJ, Roger S, Xia R, Bradley H, Jiang LH. (2008) Identification of key residues coordinating functional inhibition of P2X7 receptors by zinc and copper. *Mol Pharmacol.* 73(1); 252-9.
103. Moore SF, Mackenzie AB. (2008) Species and agonist dependent zinc modulation of endogenous and recombinant ATP-gated P2X7 receptors. *Biochem Pharmacol.* 76(12); 1740-7.
104. Coutinho-Silva R, Persechini PM. (1997) P2Z purinoceptor-associated pores induced by extracellular ATP in macrophages and J774 cells. *Am J Physiol.* 273(6); C1793-800.
105. Cockcroft S, Gomperts BD. (1980) The ATP4- receptor of rat mast cells. *Biochem J.* 188(3); 789-98.

106. Surprenant A, Rassendren F, Kawashima E, North RA, Buell G. (1996) The cytolytic P2Z receptor for extracellular ATP identified as a P2X receptor (P2X7). *Science*. 272 (5262); 735-8.
107. Di Virgilio F, Dal Ben D, Sarti AC, Giuliani AL, Falzoni S. (2017) The P2X7 Receptor in Infection and Inflammation. *Immunity*. 47(1); 15-31.
108. Sluyter R. (2017) The P2X7 Receptor. *Adv Exp Med Biol*. 1051; 17-53.
109. Calovi S, Mut-Arbona P, Sperlágh B. (2019) Microglia and the Purinergic Signaling System. *Neuroscience*. 405; 137-147.
110. Wareham K, Vial C, Wykes RC, Bradding P, Seward EP. (2009) Functional evidence for the expression of P2X1, P2X4 and P2X7 receptors in human lung mast cells. *Br J Pharmacol*. 157(7); 1215-24.
111. Kurashima Y, Amiya T, Nochi T, Fujisawa K, Haraguchi T, Iba H, Tsutsui H, Sato S, Nakajima S, Iijima H, Kubo M, Kunisawa J, Kiyono H. (2012) Extracellular ATP mediates mast cell-dependent intestinal inflammation through P2X7 purinoceptors. *Nat Commun*. 3; 1034.
112. Cockcroft S, Gomperts BD. (1979) ATP induces nucleotide permeability in rat mast cells. *Nature*. 279(5713); 541-2.
113. Klapperstück M, Büttner C, Schmalzing G, Markwardt F. (2001) Functional evidence of distinct ATP activation sites at the human P2X(7) receptor. *J Physiol*. 534(Pt 1); 25-35.
114. Pippel A, Stolz M, Woltersdorf R, Kless A, Schmalzing G, Markwardt F. (2017) Localization of the gate and selectivity filter of the full-length P2X7 receptor. *Proc Natl Acad Sci U S A*. 114(11); E2156-E2165.
115. Miller CM, Boulter NR, Fuller SJ, Zakrzewski AM, Lees MP, Saunders BM, (2011) Wiley JS, Smith NC. The role of the P2X₇ receptor in infectious diseases. *PLoS Pathog*. 7(11); e1002212.
116. Rissiek B, Haag F, Boyer O, Koch-Nolte F, Adriouch S. (2015) ADP-ribosylation of P2X7: a matter of life and death for regulatory T cells and natural killer T cells. *Curr Top Microbiol Immunol*. 384; 107-26.
117. Yang D, He Y, Muñoz-Planillo R, Liu Q, Núñez G. (2015) Caspase-11 Requires the Pannexin-1 Channel and the Purinergic P2X7 Pore to Mediate Pyroptosis and Endotoxic Shock. *Immunity*. 43(5); 923-32.

118. Pelegrin P, Surprenant A. (2006) Pannexin-1 mediates large pore formation and interleukin-1beta release by the ATP-gated P2X7 receptor. *EMBO J.* 25(21); 5071-82.
119. Steinberg TH, Newman AS, Swanson JA, Silverstein SC. (1987) ATP4-permeabilizes the plasma membrane of mouse macrophages to fluorescent dyes. *J Biol Chem.* 262(18); 8884-8.
120. Virginio C, MacKenzie A, Rassendren FA, North RA, Surprenant A.(1999) Pore dilation of neuronal P2X receptor channels. *Nat Neurosci.* 2(4); 315-21.
121. Cheewatrakoolpong B, Gilchrest H, Anthes JC, Greenfeder S. (2005) Identification and characterization of splice variants of the human P2X7 ATP channel. *Biochem Biophys Res Commun.* 332(1); 17-27.
122. Adinolfi E, Cirillo M, Woltersdorf R, Falzoni S, Chiozzi P, Pellegatti P, Callegari MG, Sandonà D, Markwardt F, Schmalzing G, Di Virgilio F. (2010) Trophic activity of a naturally occurring truncated isoform of the P2X7 receptor. *FASEB J.* 24(9); 3393-404.
123. Kaczmarek-Hájek K, Lörinczi E, Hausmann R, Nicke A. (2012) Molecular and functional properties of P2X receptors--recent progress and persisting challenges. *Purinergic Signal.* 8(3); 375-417.
124. Sikora A, Liu J, Brosnan C, Buell G, Chessel I, Bloom BR. (1999) Cutting edge: purinergic signaling regulates radical-mediated bacterial killing mechanisms in macrophages through a P2X7-independent mechanism. *J Immunol.* 163(2); 558-61.
125. Taylor SR, Gonzalez-Begne M, Dewhurst S, Chimini G, Higgins CF, Melvin JE, Elliott JI. (2008) Sequential shrinkage and swelling underlie P2X7-stimulated lymphocyte phosphatidylserine exposure and death. *J Immunol.* 180(1); 300-8.
126. Masin M, Young C, Lim K, Barnes SJ, Xu XJ, Marschall V, Brutkowski W, Mooney ER, Gorecki DC, Murrell-Lagnado R. (2012) Expression, assembly and function of novel C-terminal truncated variants of the mouse P2X7 receptor: re-evaluation of P2X7 knockouts. *Br J Pharmacol.* 165(4); 978-93.
127. Taylor SR, Gonzalez-Begne M, Sojka DK, Richardson JC, Sheardown SA, Harrison SM, Pusey CD, Tam FW, Elliott JI. (2009) Lymphocytes from P2X7-deficient mice exhibit enhanced P2X7 responses. *J Leukoc Biol.* 85(6);978-86.

128. Sánchez-Nogueiro J, Marín-García P, Miras-Portugal MT. (2005) Characterization of a functional P2X(7)-like receptor in cerebellar granule neurons from P2X(7) knockout mice. *FEBS Lett.* 579(17); 3783-8.
129. Marín-García P, Sánchez-Nogueiro J, Gómez-Villafuertes R, León D, Miras-Portugal MT. (2008) Synaptic terminals from mice midbrain exhibit functional P2X7 receptor. *Neuroscience.* 151(2); 361-73.
130. Nicke A, Kuan YH, Masin M, Rettinger J, Marquez-Klaka B, Bender O, Górecki DC, Murrell-Lagnado RD, Soto F. (2009) A functional P2X7 splice variant with an alternative transmembrane domain 1 escapes gene inactivation in P2X7 knock-out mice. *J Biol Chem.* 284(38); 25813-22.
131. Adriouch S, Dox C, Welge V, Seman M, Koch-Nolte F, Haag F. (2002) Cutting edge: a natural P451L mutation in the cytoplasmic domain impairs the function of the mouse P2X7 receptor. *J Immunol.* 169(8); 4108-12.
132. Syberg S, Schwarz P, Petersen S, Steinberg TH, Jensen JE, Teilmann J, Jørgensen NR. (2012) Association between P2X7 Receptor Polymorphisms and Bone Status in Mice. *J Osteoporos.* 2012; 637986.
133. Todd JN, Poon W, Lyssenko V, Groop L, Nichols B, Wilmot M, Robson S, Enjyoji K, Herman MA, Hu C, Zhang R, Jia W, Ma R, Florez JC, Friedman DJ. (2015) Variation in glucose homeostasis traits associated with P2RX7 polymorphisms in mice and humans. *J Clin Endocrinol Metab.* 100(5); E688-96.
134. Wilson HL, Wilson SA, Surprenant A, North RA. (2002) Epithelial membrane proteins induce membrane blebbing and interact with the P2X7 receptor C terminus. *J Biol Chem.* 277(37); 34017-23.
135. Bartlett R, Stokes L, Sluyter R. (2014) The P2X7 receptor channel: recent bhattdevelopments and the use of P2X7 antagonists in models of disease. *Pharmacol Rev.* 66(3); 638-75.
136. Chrovian CC, Rech JC, Bhattacharya A, Letavic MA. (2014) P2X7 antagonists as potential therapeutic agents for the treatment of CNS disorders. *Prog Med Chem.* 53; 65-100.
137. Burnstock G, Di Virgilio F. (2013) Purinergic signalling and cancer. *Purinergic Signal.* 9(4); 491-540.

138. Arulkumaran N, Unwin RJ, Tam FW. (2011) A potential therapeutic role for P2X7 receptor (P2X7R) antagonists in the treatment of inflammatory diseases. *Expert Opin Investig Drugs*. 20(7); 897-915.
139. Eser A, Colombel JF, Rutgeerts P, Vermeire S, Vogelsang H, Braddock M, Persson T, Reinisch W. (2015) Safety and Efficacy of an Oral Inhibitor of the Purinergic Receptor P2X7 in Adult Patients with Moderately to Severely Active Crohn's Disease: A Randomized Placebo-controlled, *Double-blind, Phase IIa Study*. *Inflamm Bowel Dis*. 21(10); 2247-53.
140. Bhattacharya A and Ceusters M. (2020) Targeting neuroinflammation with brain penetrant P2X7 antagonists as novel therapeutics for neuropsychiatric disorders. *Neuropsychopharmacology*. 45(1); 234-235.
141. Territo PR, Meyer JA, Peters JS, Riley AA, McCarthy BP, Gao M, Wang M, Green MA, Zheng QH, Hutchins GD. (2017) Characterization of 11C-GSK1482160 for Targeting the P2X7 Receptor as a Biomarker for Neuroinflammation. *J Nucl Med*. 58(3);458-465.
142. Fantoni ER, Dal Ben D, Falzoni S, Di Virgilio F, Lovestone S, Gee A. (2017) Design, synthesis and evaluation in an LPS rodent model of neuroinflammation of a novel 18F-labelled PET tracer targeting P2X7. *EJNMMI Res*. 7(1); 31.
143. Fuller SJ, Stokes L, Skarratt KK, Gu BJ, Wiley JS. (2009) Genetics of the P2X7 receptor and human disease. *Purinergic Signal*. 5(2); 257-62.
144. Gunosewoyo H, Kassiou M. (2010) P2X purinergic receptor ligands: recently patented compounds. *Expert Opin Ther Pat*. 20(5); 625-46.
145. Lenertz LY, Gavala ML, Zhu Y, Bertics PJ. (2011) Transcriptional control mechanisms associated with the nucleotide receptor P2X7, a critical regulator of immunologic, osteogenic, and neurologic functions. *Immunol Res*. 50(1); 22-38.
146. Kuhny M, Hochdörfer T, Ayata CK, Idzko M, Huber M. (2014) CD39 is a negative regulator of P2X7-mediated inflammatory cell death in mast cells. *Cell Commun Signal*. 12; 40.
147. Illes P, Khan TM, Rubini P. (2017) Neuronal P2X7 Receptors Revisited: Do They Really Exist? *J Neurosci*. 37(30); 7049-7062.

148. Miras-Portugal MT, Sebastián-Serrano Á, de Diego García L, Díaz-Hernández M. (2017) Neuronal P2X7 Receptor: Involvement in Neuronal Physiology and Pathology. *J Neurosci.* 37(30); 7063-7072.
149. Wei L, Syed Mortadza SA, Yan J, Zhang L, Wang L, Yin Y, Li C, Chalon S, Emond P, Belzung C, Li D, Lu C, Roger S, Jiang LH. (2018) ATP-activated P2X7 receptor in the pathophysiology of mood disorders and as an emerging target for the development of novel antidepressant therapeutics. *Neurosci Biobehav Rev.* 87; 192-205.
150. He Y, Taylor N, Fourgeaud L, Bhattacharya A. (2017) The role of microglial P2X7: modulation of cell death and cytokine release. *J Neuroinflammation.* 14(1); 135.
151. Masuch A, Shieh CH, van Rooijen N, van Calker D, Biber K. (2016) Mechanism of microglia neuroprotection: Involvement of P2X7, TNF α , and valproic acid. *Glia.* 64(1); 76-89.
152. Choi HB, Ryu JK, Kim SU, McLarnon JG. (2007) Modulation of the purinergic P2X7 receptor attenuates lipopolysaccharide-mediated microglial activation and neuronal damage in inflamed brain. *J Neurosci.* 27(18); 4957-68.
153. Diamant B and Dahlquist R. (1970) The inhibitory action of adenosine-5'-triphosphate (ATP) on histamine release and mast cell degranulation induced by compound 48-80. *Acta Pharmacol Toxicol (Copenh).* 28(1); 44.
154. Gong T, Liu L, Jiang W, Zhou R. (2020) DAMP-sensing receptors in sterile inflammation and inflammatory diseases. *Nat Rev Immunol.* 20(2); 95-112.
155. Cohen HB, Briggs KT, Marino JP, Ravid K, Robson SC, Mosser DM. (2013) TLR stimulation initiates a CD39-based autoregulatory mechanism that limits macrophage inflammatory responses. *Blood.* 122(11); 1935-45.
156. Kahlenberg JM, Lundberg KC, Kertesy SB, Qu Y, Dubyak GR. (2005) Potentiation of caspase-1 activation by the P2X7 receptor is dependent on TLR signals and requires NF-kappaB-driven protein synthesis. *J Immunol.* 175(11); 7611-22.
157. Ferrari D, Chiozzi P, Falzoni S, Dal Susino M, Collo G, Buell G, Di Virgilio F. (1997) ATP-mediated cytotoxicity in microglial cells. *Neuropharmacology.* 36(9); 1295-301.
158. Ferrari D, Pizzirani C, Adinolfi E, Lemoli RM, Curti A, Idzko M, Panther E, Di Virgilio F. (2006) The P2X7 receptor: a key player in IL-1 processing and release. *J Immunol.* 176(7); 3877-83.

159. Qu Y, Franchi L, Nunez G, Dubyak GR. (2007) Nonclassical IL-1 beta secretion stimulated by P2X7 receptors is dependent on inflammasome activation and correlated with exosome release in murine macrophages. *J Immunol.* 179(3); 1913-25.
160. Pelegrin P, Barroso-Gutierrez C, Surprenant A. (2008) P2X7 receptor differentially couples to distinct release pathways for IL-1beta in mouse macrophage. *J Immunol.* 180(11); 7147-57.
161. Cruz CM, Rinna A, Forman HJ, Ventura AL, Persechini PM, Ojcius DM. (2006) ATP activates a reactive oxygen species-dependent oxidative stress response and secretion of proinflammatory cytokines in macrophages. *J Biol Chem.* 282(5); 2871-9.
162. Martin E, Amar M, Dalle C, Youssef I, Boucher C, Le Duigou C, Brückner M, Prigent A, Sazdovitch V, Halle A, Kanellopoulos JM, Fontaine B, Delatour B, Delarasse C. (2019) New role of P2X7 receptor in an Alzheimer's disease mouse model. *Mol Psychiatry.* 24(1); 108-125.
163. Savio LEB, de Andrade Mello P, da Silva CG, Coutinho-Silva R. (2018) The P2X7 Receptor in Inflammatory Diseases: Angel or Demon? *Front Pharmacol.* 9; 52.
164. Izquierdo P, Attwell D, Madry C. Ion Channels and Receptors as Determinants of Microglial Function. (2019) *Trends Neurosci.* 42(4); 278-292.
165. Davalos D, Grutzendler J, Yang G, Kim JV, Zuo Y, Jung S, Littman DR, Dustin ML, Gan WB. (2005) ATP mediates rapid microglial response to local brain injury in vivo. *Nat Neurosci.* 8(6); 752-8.
166. Haynes SE, Hollopeter G, Yang G, Kurpius D, Dailey ME, Gan WB, Julius D. (2006) The P2Y12 receptor regulates microglial activation by extracellular nucleotides. *Nat Neurosci.* 9(12); 1512-9.
167. Braun N, Sévigny J, Robson SC, Enjyoji K, Guckelberger O, Hammer K, Di Virgilio F, Zimmermann H. (2000) Assignment of ecto-nucleoside triphosphate diphosphohydrolase-1/cd39 expression to microglia and vasculature of the brain. *Eur J Neurosci.* 12(12); 4357-66.
168. Färber K, Markworth S, Pannasch U, Nolte C, Prinz V, Kronenberg G, Gertz K, Endres M, Bechmann I, Enjyoji K, Robson SC, Kettenmann H. (2008) The ectonucleotidase cd39/ENTPDase1 modulates purinergic-mediated microglial migration. *Glia.* 56(3); 331-41.

169. Bulavina L, Szulzewsky F, Rocha A, Krabbe G, Robson SC, Matyash V, Kettenmann H. (2013) NTPDase1 activity attenuates microglial phagocytosis. *Purinergic Signal*. 9(2); 199-205.
170. Matyash M, Zabiegalov O, Wendt S, Matyash V, Kettenmann H. (2017) The adenosine generating enzymes CD39/CD73 control microglial processes amification in the mouse brain. *PLoS One*. 12(4); e0175012.
171. Arnoux I, Hoshiko M, Mandavy L, Avignone E, Yamamoto N, Audinat E. (2013) Adaptive phenotype of microglial cells during the normal postnatal development of the somatosensory "Barrel" cortex. *Glia*. 61(10);1582-94.
172. Crain JM, Nikodemova M, Watters JJ. (2009) Expression of P2 nucleotide receptors varies with age and sex in murine brain microglia. *J Neuroinflammation*. 6; 24.
173. Illes P, Nörenberg W, Gebicke-Haerter PJ. (1996) Molecular mechanisms of microglial activation. B. Voltage- and purinoceptor-operated channels in microglia. *Neurochem Int*. 29(1); 13-24.
174. Kurpius D, Wilson N, Fuller L, Hoffman A, Dailey ME. (2006) Early activation, motility, and homing of neonatal microglia to injured neurons does not require protein synthesis. *Glia*. 54(1); 58-70.
175. Cătălin B, Stopper L, Bălșeanu TA, Scheller A. (2017) The in situ morphology of microglia is highly sensitive to the mode of tissue fixation. *J Chem Neuroanat*. 86; 59-66.
176. Schilling T, Eder C. (2015) Microglial K(+) channel expression in young adult and aged mice. *Glia*. 63(4); 664-72.
177. Madry C, Arancibia-Cárcamo IL, Kyrargyri V, Chan VTT, Hamilton NB, Attwell D. (2018) Effects of the ecto-ATPase apyrase on microglial ramification and surveillance reflect cell depolarization, not ATP depletion. *Proc Natl Acad Sci U S A*. 115(7); E1608-E1617.
178. Madry C, Kyrargyri V, Arancibia-Cárcamo IL, Jolivet R, Kohsaka S, Bryan RM, Attwell D. (2018) Microglial Ramification, Surveillance, and Interleukin-1 β Release Are Regulated by the Two-Pore Domain K⁺ Channel THIK-1. *Neuron*. 97(2); 299-312.e6.

179. Koizumi S, Shigemoto-Mogami Y, Nasu-Tada K, Shinozaki Y, Ohsawa K, Tsuda M, Joshi BV, Jacobson KA, Kohsaka S, Inoue K. (2007) UDP acting at P2Y6 receptors is a mediator of microglial phagocytosis. *Nature*. 446(7139); 1091-5.
180. Neher JJ, Neniskyte U, Hornik T, Brown GC. (2014) Inhibition of UDP/P2Y6 purinergic signaling prevents phagocytosis of viable neurons by activated microglia in vitro and in vivo. *Glia*. 62(9); 1463-75.
181. Pannell M, Meier MA, Szulzewsky F, Matyash V, Endres M, Kronenberg G, Prinz V, Waiczies S, Wolf SA, Kettenmann H. (2016) The subpopulation of microglia expressing functional muscarinic acetylcholine receptors expands in stroke and Alzheimer's disease. *Brain Struct Funct*. 221(2); 1157-72.
182. Mildner A, Huang H, Radke J, Stenzel W, Priller J. (2017) P2Y12 receptor is expressed on human microglia under physiological conditions throughout development and is sensitive to neuroinflammatory diseases. *Glia*. 65(2); 375-387.
183. Cserép C, Pósfai B, Lénárt N, Fekete R, László ZI, Lele Z, Orsolits B, Molnár G, Heindl S, Schwarcz AD, Ujvári K, Környei Z, Tóth K, Szabadits E, Sperlágh B, Baranyi M, Csiba L, Hortobágyi T, Maglóczky Z, Martinecz B, Szabó G, Erdélyi F, Szipócs R, Tamkun MM, Gesierich B, Duering M, Katona I, Liesz A, Tamás G, Dénes Á. (2020) Microglia monitor and protect neuronal function through specialized somatic purinergic junctions. *Science*. 367(6477); 528-537.
184. Ohsawa K, Irino Y, Sanagi T, Nakamura Y, Suzuki E, Inoue K, Kohsaka S. (2010) P2Y12 receptor-mediated integrin-beta1 activation regulates microglial process extension induced by ATP. *Glia*. 58(7):790-801.
185. Abiega O, Beccari S, Diaz-Aparicio I, Nadjar A, Layé S, Leyrolle Q, Gómez-Nicola D, Domercq M, Pérez-Samartín A, Sánchez-Zafra V, Paris I, Valero J, Savage JC, Hui CW, Tremblay MÈ, Deudero JJ, Brewster AL, Anderson AE, Zaldumbide L, Galbarriatu L, Marinas A, Vivanco Md, Matute C, Maletic-Savatic M, Encinas JM, Sierra A. (2016) Neuronal Hyperactivity Disturbs ATP Microgradients, Impairs Microglial Motility, and Reduces Phagocytic Receptor Expression Triggering Apoptosis/Microglial Phagocytosis Uncoupling. *PLoS Biol*. 14(5); e1002466.
186. Wu LJ, Vadakkan KI, Zhuo M. (2007) ATP-induced chemotaxis of microglial processes requires P2Y receptor-activated initiation of outward potassium currents. *Glia*. 55(8); 810-21.

187. Irino Y, Nakamura Y, Inoue K, Kohsaka S, Ohsawa K. (2008) Akt activation is involved in P2Y₁₂ receptor-mediated chemotaxis of microglia. *J Neurosci Res.* 86(7); 1511-9.
188. Bernier LP, Bohlen CJ, York EM, Choi HB, Kamyabi A, Dissing-Olesen L, Hefendehl JK, Collins HY, Stevens B, Barres BA, MacVicar BA. (2019) Nanoscale Surveillance of the Brain by Microglia via cAMP-Regulated Filopodia. *Cell Rep.* 27(10); 2895-2908.e4.
189. Kato G, Inada H, Wake H, Akiyoshi R, Miyamoto A, Eto K, Ishikawa T, Moorhouse AJ, Strassman AM, Nabekura J. (2016) Microglial Contact Prevents Excess Depolarization and Rescues Neurons from Excitotoxicity. *eNeuro.* 3(3); ENEURO.0004-16.2016.
190. Fekete R, Cserép C, Lénárt N, Tóth K, Orsolits B, Martinecz B, Méhes E, Szabó B, Németh V, Gönci B, Sperlág B, Boldogkői Z, Kittel Á, Baranyi M, Ferenczi S, Kovács K, Szalay G, Rózsa B, Webb C, Kovacs GG, Hortobágyi T, West BL, Környei Z, Dénes Á. (2018) Microglia control the spread of neurotropic virus infection via P2Y₁₂ signalling and recruit monocytes through P2Y₁₂-independent mechanisms. *Acta Neuropathol.* 136(3); 461-482.
191. Sharma K, Wu LJ, Eyo UB. (2020) Calming Neurons with a Microglial Touch. *Trends Neurosci.* 43(4); 197-199.
192. Suurväli J, Boudinot P, Kanellopoulos J, Rüütel Boudinot S. (2017) P2X₄: A fast and sensitive purinergic receptor. *Biomed J.* 40(5); 245-256.
193. Jimenez-Pacheco A, Mesuret G, Sanz-Rodriguez A, Tanaka K, Mooney C, Conroy R, Miras-Portugal MT, Diaz-Hernandez M, Henshall DC, Engel T. (2013) Increased neocortical expression of the P2X₇ receptor after status epilepticus and anticonvulsant effect of P2X₇ receptor antagonist A-438079. *Epilepsia.* 54(9); 1551-61.
194. Rigato C, Swinnen N, Buckinx R, Couillin I, Mangin JM, Rigo JM, Legendre P, Le Corrionc H. (2012) Microglia proliferation is controlled by P2X₇ receptors in a Pannexin-1-independent manner during early embryonic spinal cord invasion. *J Neurosci.* 32(34); 11559-73.
195. Sanz JM, Di Virgilio F. (2000) Kinetics and mechanism of ATP-dependent IL-1 beta release from microglial cells. *J Immunol.* 164(9); 4893-8.

196. Boche D, Perry VH, Nicoll JA. (2013) Review: activation patterns of microglia and their identification in the human brain. *Neuropathol Appl Neurobiol.* 39(1); 3-18.
197. Monif M, Burnstock G, Williams DA. (2010) Microglia: proliferation and activation driven by the P2X7 receptor. *Int J Biochem Cell Biol.* 42(11); 1753-6.
198. Jurga AM, Paleczna M, Kuter KZ. (2020) Overview of General and Discriminating Markers of Differential Microglia Phenotypes. *Front Cell Neurosci.* 14; 198.
199. Mesquida-Veny F, Del Río JA, Hervera A. (2020) Macrophagic and microglial complexity after neuronal injury. *Prog Neurobiol.* 101970.
200. Takenouchi T, Nakai M, Iwamaru Y, Sugama S, Tsukimoto M, Fujita M, Wei J, Sekigawa A, Sato M, Kojima S, Kitani H, Hashimoto M. (2009) The activation of P2X7 receptor impairs lysosomal functions and stimulates the release of autophagolysosomes in microglial cells. *J Immunol.* 182(4); 2051-62.
201. Yue N, Huang H, Zhu X, Han Q, Wang Y, Li B, Liu Q, Wu G, Zhang Y, Yu J. (2017) Activation of P2X7 receptor and NLRP3 inflammasome assembly in hippocampal glial cells mediates chronic stress-induced depressive-like behaviors. *J Neuroinflammation.* 14(1); 102.
202. Munoz FM, Gao R, Tian Y, Henstenburg BA, Barrett JE, Hu H. (2017) Neuronal P2X7 receptor-induced reactive oxygen species production contributes to nociceptive behavior in mice. *Sci Rep.* 7(1); 3539.
203. Turola E, Furlan R, Bianco F, Matteoli M, Verderio C. (2012) Microglial microvesicle secretion and intercellular signaling. *Front Physiol.* 3; 149.
204. Colombo F, Bastoni M, Nigro A, Podini P, Finardi A, Casella G, Ramesh M, Farina C, Verderio C, Furlan R. (2018) Cytokines Stimulate the Release of Microvesicles from Myeloid Cells Independently from the P2X7 Receptor/Acid Sphingomyelinase Pathway. *Front Immunol.* 9; 204.
205. Seeland S, Kettiger H, Murphy M, Treiber A, Giller J, Kiss A, Sube R, Krähenbühl S, Hafner M, Huwyler J. (2015) ATP-induced cellular stress and mitochondrial toxicity in cells expressing purinergic P2X7 receptor. *Pharmacol Res Perspect.* 3(2); e00123.

206. Monif M, Reid CA, Powell KL, Drummond KJ, O'Brien TJ, Williams DA. (2016) Interleukin-1 β has trophic effects in microglia and its release is mediated by P2X7R pore. *J Neuroinflammation*. 13(1); 173.
207. Tronel C, Largeau B, Santiago Ribeiro MJ, Guilloteau D, Dupont AC, Arlicot N. (2017) Molecular Targets for PET Imaging of Activated Microglia: The Current Situation and Future Expectations. *Int J Mol Sci*. 18(4); 802.
208. Ou A, Gu BJ, Wiley JS. (2018) The scavenger activity of the human P2X7 receptor differs from P2X7 pore function by insensitivity to antagonists, genetic variation and sodium concentration: Relevance to inflammatory brain diseases. *Biochim Biophys Acta Mol Basis Dis*. 1864(4 Pt A); 1051-59.
209. Beamer E, Fischer W, Engel T. (2017) The ATP-Gated P2X7 Receptor As a Target for the Treatment of Drug-Resistant Epilepsy. *Front Neurosci*. 11; 21.
210. Bhattacharya A. (2018) Recent Advances in CNS P2X7 Physiology and Pharmacology: Focus on Neuropsychiatric Disorders. *Front Pharmacol*. 9; 30.
211. Eyo UB, Peng J, Swiatkowski P, Mukherjee A, Bispo A, Wu LJ. (2014) Neuronal hyperactivity recruits microglial processes via neuronal NMDA receptors and microglial P2Y12 receptors after status epilepticus. *J Neurosci*. 34(32); 10528-40.
212. Illes P, Verkhratsky A, Tang Y. (2020) Pathological ATPergic Signaling in Major Depression and Bipolar Disorder. *Front Mol Neurosci*. 12; 331.
213. Jung S, Aliberti J, Graemmel P, Sunshine MJ, Kreutzberg GW, Sher A, Littman DR. (2000) Analysis of fractalkine receptor CX(3)CR1 function by targeted deletion and green fluorescent protein reporter gene insertion. *Mol Cell Biol*. 20(11); 4106-14.
214. Bin Dayel A, Evans RJ, Schmid R. (2019) Mapping the Site of Action of Human P2X7 Receptor Antagonists AZ11645373, Brilliant Blue G, KN-62, Calmidazolium, and ZINC58368839 to the Intersubunit Allosteric Pocket. *Mol Pharmacol*. 96(3); 355-363.
215. Saha S, Chant D, Welham J, McGrath J. (2005) A systematic review of the prevalence of schizophrenia. *PLoS Med*. 2(5); e141.
216. Tandon R, Nasrallah HA, Keshavan MS. (2009) Schizophrenia, "just the facts" 4. Clinical features and conceptualization. *Schizophr Res*. 110(1-3); 1-23.

217. Lesh TA, Niendam TA, Minzenberg MJ, Carter CS. (2011) Cognitive control deficits in schizophrenia: mechanisms and meaning. *Neuropsychopharmacology*. 36(1); 316-38.
218. Palmer BA, Pankratz VS, Bostwick JM. (2005) The lifetime risk of suicide in schizophrenia: a reexamination. *Arch Gen Psychiatry*. 62(3); 247-253.
219. Millier A, Schmidt U, Angermeyer MC, Chauhan D, Murthy V, Toumi M, Cadi-Soussi N. (2014) Humanistic burden in schizophrenia: a literature review. *J Psychiatr Res*. 54; 85-93.
220. Guma E, Plitman E, Chakravarty MM. (2019) The role of maternal immune activation in altering the neurodevelopmental trajectories of offspring: A translational review of neuroimaging studies with implications for autism spectrum disorder and schizophrenia. *Neurosci Biobehav Rev*. 104; 141-157.
221. Haddad FL, Patel SV, Schmid S. (2020) Maternal Immune Activation by Poly I:C as a preclinical Model for Neurodevelopmental Disorders: A focus on Autism and Schizophrenia. *Neurosci Biobehav Rev*. 113; 546-567.
222. Kay SR, Fiszbein A, Opler LA. (1987) The positive and negative syndrome scale (PANSS) for schizophrenia. *Schizophr Bull*. 13(2); 261-76.
223. Nuechterlein KH, Barch DM, Gold JM, Goldberg TE, Green MF, Heaton RK. (2004) Identification of separable cognitive factors in schizophrenia. *Schizophr Res*. 72(1); 29-39.
224. Fuxe K, Ferré S, Genedani S, Franco R, Agnati LF. (2007) Adenosine receptor-dopamine receptor interactions in the basal ganglia and their relevance for brain function. *Physiol Behav*. 92(1-2); 210-7.
225. Moghaddam B, Javitt D. (2012) From revolution to evolution: the glutamate hypothesis of schizophrenia and its implication for treatment. *Neuropsychopharmacology*. 37(1); 4-15.
226. Krystal AD, Weiner RD, Dean MD, Lindahl VH, Tramontozzi LA 3rd, Falcone G, Coffey CE. (2003) Comparison of seizure duration, ictal EEG, and cognitive effects of ketamine and methohexital anesthesia with ECT. *J Neuropsychiatry Clin Neurosci*. 15(1); 27-34.
227. Marcotte ER, Pearson DM, Srivastava LK. (2001) Animal models of schizophrenia: a critical review. *J Psychiatry Neurosci*. 26(5); 395-410.

228. Bubeníková-Valesová V, Horáček J, Vrajová M, Höschl C. (2008) Models of schizophrenia in humans and animals based on inhibition of NMDA receptors. *Neurosci Biobehav Rev.* 32(5); 1014-23.
229. McCutcheon RA, Krystal JH, Howes OD. (2020) Dopamine and glutamate in schizophrenia: biology, symptoms and treatment. *World Psychiatry.* 19(1); 15-33.
230. Lear E. Intravenous anesthesia. (1968) A survey of newer agents. *Anesth Analg.* 47(2); 154-9.
231. Domino EF. (1992) Chemical dissociation of human awareness: focus on non-competitive NMDA receptor antagonists. *J Psychopharmacol.* 6(3); 418-24.
232. Morris H, Wallach J. (2014) From PCP to MXE: a comprehensive review of the non-medical use of dissociative drugs. *Drug Test Anal.* 6(7-8); 614-32.
233. Wallach J, Kang H, Colestock T, Morris H, Bortolotto ZA, Collingridge GL, Lodge D, Halberstadt AL, Brandt SD, Adejare A. (2016) Pharmacological Investigations of the Dissociative 'Legal Highs' Diphenidine, Methoxphenidine and Analogues. *PLoS One.* 11(6):e0157021.
234. Lodge D, Mercier MS. (2015) Ketamine and phencyclidine: the good, the bad and the unexpected. *Br J Pharmacol.* 172(17); 4254-76.
235. Lewis DA, Gonzalez-Burgos G. (2006) Pathophysiologically based treatment interventions in schizophrenia. *Nat Med.* 12(9); 1016-22.
236. Olney JW, Labruyere J, Price MT. (1989) Pathological changes induced in cerebrocortical neurons by phencyclidine and related drugs. *Science.* 244(4910); 1360-2.
237. Bakshi VP, Geyer MA. (1995) Antagonism of phencyclidine-induced deficits in prepulse inhibition by the putative atypical antipsychotic olanzapine. *Psychopharmacology (Berl).* 122(2); 198-201.
238. Geyer MA, Krebs-Thomson K, Braff DL, Swerdlow NR. (2001) Pharmacological studies of prepulse inhibition models of sensorimotor gating deficits in schizophrenia: a decade in review. *Psychopharmacology (Berl).* 156(2-3); 117-54.
239. Bourne GW, Théorêt Y, Esplin B, Capek R. (1983) Effect of phencyclidine on inhibition in the hippocampal slice. *Naunyn Schmiedebergs Arch Pharmacol.* 323(2); 168-72.

240. Wang RY, Liang X. (1998) M100907 and clozapine, but not haloperidol or raclopride, prevent phencyclidine-induced blockade of NMDA responses in pyramidal neurons of the rat medial prefrontal cortical slice. *Neuropsychopharmacology*. 19(1); 74-85.
241. Suzuki Y, Jodo E, Takeuchi S, Niwa S, Kayama Y. (2002) Acute administration of phencyclidine induces tonic activation of medial prefrontal cortex neurons in freely moving rats. *Neuroscience*. 114(3); 769-79.
242. Monaghan DT, Jane DE. (2009) Pharmacology of NMDA Receptors. In: Van Dongen AM, editor. *Biology of the NMDA Receptor*. Boca Raton (FL): CRC Press/Taylor & Francis;. Chapter 12.
243. Hirai H, Kirsch J, Laube B, Betz H, Kuhse J. (1996) The glycine binding site of the N-methyl-D-aspartate receptor subunit NR1: identification of novel determinants of co-agonist potentiation in the extracellular M3-M4 loop region. *Proc Natl Acad Sci U S A*. 93(12); 6031-6.
244. Cavara NA, Hollmann M. (2008) Shuffling the deck anew: how NR3 tweaks NMDA receptor function. *Mol Neurobiol*. 38(1); 16-26.
245. Lodge D, Johnson KM. (1990) Noncompetitive excitatory amino acid receptor antagonists. *Trends Pharmacol Sci*. 11(2); 81-6.
246. Huettner JE, Bean BP. (1988) Block of N-methyl-D-aspartate-activated current by the anticonvulsant MK-801: selective binding to open channels. *Proc Natl Acad Sci U S A*. 85(4); 1307-11.
247. Wong EH, Kemp JA, Priestley T, Knight AR, Woodruff GN, Iversen LL. (1986) The anticonvulsant MK-801 is a potent N-methyl-D-aspartate antagonist. *Proc Natl Acad Sci U S A*. 83(18); 7104-8.
248. Gill R, Foster AC, Woodruff GN. (1987) Systemic administration of MK-801 protects against ischemia-induced hippocampal neurodegeneration in the gerbil. *J Neurosci*. 7(10); 3343-9.
249. Monaghan DT, Larsen H. (1997) NR1 and NR2 subunit contributions to N-methyl-D-aspartate receptor channel blocker pharmacology. *J Pharmacol Exp Ther*. 280(2); 614-20.

250. Anastasio NC, Xia Y, O'Connor ZR, Johnson KM. (2009) Differential role of N-methyl-D-aspartate receptor subunits 2A and 2B in mediating phencyclidine-induced perinatal neuronal apoptosis and behavioral deficits. *Neuroscience*. 163(4); 1181-91.
251. Ishmael JE, Franklin PH, Murray TF. (1998) Dextrorotatory opioids induce stereotyped behavior in Sprague-Dawley and Dark Agouti rats. *Psychopharmacology (Berl)*. 140(2); 206-16.
252. French ED. (1994) Phencyclidine and the midbrain dopamine system: electrophysiology and behavior. *Neurotoxicol Teratol*. 16(4); 355-62.
253. Kargieman L, Riga MS, Artigas F, Celada P. (2012) Clozapine Reverses Phencyclidine-Induced Desynchronization of Prefrontal Cortex through a 5-HT(1A) Receptor-Dependent Mechanism. *Neuropsychopharmacology*. 37(3); 723-33.
254. Castañé A, Santana N, Artigas F. (2015) PCP-based mice models of schizophrenia: differential behavioral, neurochemical and cellular effects of acute and subchronic treatments. *Psychopharmacology (Berl)*. 232(21-22); 4085-97.
255. Hervig ME, Thomsen MS, Kalló I, Mikkelsen JD. (2016) Acute phencyclidine administration induces c-Fos-immunoreactivity in interneurons in cortical and subcortical regions. *Neuroscience*. 334; 13-25.
256. Kalinichev M, Robbins MJ, Hartfield EM, Maycox PR, Moore SH, Savage KM, Austin NE, Jones DN. (2008) Comparison between intraperitoneal and subcutaneous phencyclidine administration in Sprague-Dawley rats: a locomotor activity and gene induction study. *Prog Neuropsychopharmacol Biol Psychiatry*.;32(2); 414-22.
257. Balla A, Sershen H, Serra M, Koneru R, Javitt DC. (2003) Subchronic continuous phencyclidine administration potentiates amphetamine-induced frontal cortex dopamine release. *Neuropsychopharmacology*. 28(1);34-44.
258. Hammarlund-Udenaes M, Fridén M, Syvänen S, Gupta A. (2008) On the rate and extent of drug delivery to the brain. *Pharm Res*. 25(8); 1737-50.
259. Kemp JA, Foster AC, Wong EH, Middlemiss DN. (1988) A comment on the classification and nomenclature of phencyclidine and sigma receptor sites. *Trends Neurosci*. 11(9); 388-9.

260. Proksch JW, Gentry WB, Owens SM. (2000) The effect of rate of drug administration on the extent and time course of phencyclidine distribution in rat brain, testis, and serum. *Drug Metab Dispos.* 28(7); 742-7.
261. Javitt DC, Sweet RA. (2015) Auditory dysfunction in schizophrenia: integrating clinical and basic features. *Nat Rev Neurosci.* 16(9):535-50.
262. Javitt DC. (2008) Phenomenology, aetiology and treatment of schizophrenia. *Novartis Found Symp.* 289:4-16; discussion 17-22; 87-93.
263. Clementz BA, Sweeney JA, Hamm JP, Ivleva EI, Ethridge LE, Pearlson GD, Keshavan MS, Tamminga CA. (2016) Identification of Distinct Psychosis Biotypes Using Brain-Based Biomarkers. *Am J Psychiatry.* 173(4); 373-84.
264. Rabinowicz EF, Silipo G, Goldman R, Javitt DC. (2000) Auditory sensory dysfunction in schizophrenia: imprecision or distractibility? *Arch Gen Psychiatry.* 57(12); 1149-55.
265. Brekke J, Kay DD, Lee KS, Green MF. (2005) Biosocial pathways to functional outcome in schizophrenia. *Schizophr Res.* 80(2-3); 213-25.
266. Gold R, Butler P, Revheim N, Leitman DI, Hansen JA, Gur RC, Kantrowitz JT, Laukka P, Juslin PN, Silipo GS, Javitt DC. (2012) Auditory emotion recognition impairments in schizophrenia: relationship to acoustic features and cognition. *Am J Psychiatry.* 169(4); 424-32.
267. Umbricht D, Schmid L, Koller R, Vollenweider FX, Hell D, Javitt DC. (2000) Ketamine-induced deficits in auditory and visual context-dependent processing in healthy volunteers: implications for models of cognitive deficits in schizophrenia. *Arch Gen Psychiatry.* 57(12); 1139-47.
268. Rosburg T, Kreitschmann-Andermahr I. (2016) The effects of ketamine on the mismatch negativity (MMN) in humans - A meta-analysis. *Clin Neurophysiol.* 127(2); 1387-1394.
269. Javitt DC, Steinschneider M, Schroeder CE, Arezzo JC. (1996) Role of cortical N-methyl-D-aspartate receptors in auditory sensory memory and mismatch negativity generation: implications for schizophrenia. *Proc Natl Acad Sci U S A.* 93(21); 11962-7.
270. Gil-da-Costa R, Stoner GR, Fung R, Albright TD. (2013) Nonhuman primate model of schizophrenia using a noninvasive EEG method. *Proc Natl Acad Sci U S A.* 110(38):15425-30.

271. Celada P, Lladó-Pelfort L, Santana N, Kargieman L, Troyano-Rodriguez E, Riga MS, Artigas F. (2013) Disruption of thalamocortical activity in schizophrenia models: relevance to antipsychotic drug action. *Int J Neuropsychopharmacol.* 16(10); 2145-63.
272. Uramura K, Maejima Y, Shimomura K, Santoso P, Katsuda S, Kobayashi D, Jodo E, Kodaira M, Otgon-Uul Z, Yang Y, Sakuma K, Takigawa M, Hazama A, Yada T. (2014) Chronic phencyclidine treatment induces long-lasting glutamatergic activation of VTA dopamine neurons. *Neurosci Lett.* 564; 72-7.
273. Jodo E, Suzuki Y, Katayama T, Hoshino KY, Takeuchi S, Niwa S, Kayama Y. (2005) Activation of medial prefrontal cortex by phencyclidine is mediated via a hippocampo-prefrontal pathway. *Cereb Cortex.* 15(5); 663-9.
274. Adams B, Moghaddam B. (1998) Corticolimbic dopamine neurotransmission is temporally dissociated from the cognitive and locomotor effects of phencyclidine. *J Neurosci.* 18(14); 5545-54.
275. Björklund A, Dunnett SB. (2007) Dopamine neuron systems in the brain: an update. *Trends Neurosci.* 30(5); 194-202.
276. Rolls ET, Loh M, Deco G, Winterer G. (2008) Computational models of schizophrenia and dopamine modulation in the prefrontal cortex. *Nat Rev Neurosci.* 9(9); 696-709.
277. Arnsten AF, Wang M, Paspalas CD. (2015) Dopamine's Actions in Primate Prefrontal Cortex: Challenges for Treating Cognitive Disorders. *Pharmacol Rev.* 67(3); 681-96.
278. Balla A, Schneider S, Sershen H, Javitt DC. (2012) Effects of novel, high affinity glycine transport inhibitors on frontostriatal dopamine release in a rodent model of schizophrenia. *Eur Neuropsychopharmacol.* 22(12); 902-10.
279. Yavas E, Young AM. (2017) N-Methyl-d-aspartate Modulation of Nucleus Accumbens Dopamine Release by Metabotropic Glutamate Receptors: Fast Cyclic Voltammetry Studies in Rat Brain Slices in Vitro. *ACS Chem Neurosci.* 8(2); 320-328.
280. Xu P, Chen A, Li Y, Xing X, Lu H. (2019) Medial prefrontal cortex in neurological diseases. *Physiol Genomics.* 51(9); 432-442.
281. Seamans JK, Laphis CC, Durstewitz D. (2008) Comparing the prefrontal cortex of rats and primates: insights from electrophysiology. *Neurotox Res.* 14(2-3); 249-62.

282. Chai WJ, Abd Hamid AI, Abdullah JM. (2018) Working Memory From the Psychological and Neurosciences Perspectives: A Review. *Front Psychol.* 9; 401.
283. Forbes NF, Carrick LA, McIntosh AM, Lawrie SM. (2009) Working memory in schizophrenia: a meta-analysis. *Psychol Med.* 39(6); 889-905.
284. Lee J, Park S. (2005) Working memory impairments in schizophrenia: a meta-analysis. *J Abnorm Psychol.* 114(4); 599-611.
285. Insel TR. (2010) Rethinking schizophrenia. *Nature.* 468(7321); 187-93.
286. Arime Y, Akiyama K. (2017) Abnormal neural activation patterns underlying working memory impairment in chronic phencyclidine-treated mice. *PLoS One* 12(12); e0189287.
287. Breier A, Malhotra AK, Pinals DA, Weisenfeld NI, Pickar D. (1997) Association of ketamine-induced psychosis with focal activation of the prefrontal cortex in healthy volunteers. *Am J Psychiatry.* 154(6); 805-11.
288. Fuster, J. (2015) *The Prefrontal Cortex*; Academic Press: London, UK,
289. Smaers JB, Gómez-Robles A, Parks AN, Sherwood CC. (2017) Exceptional Evolutionary Expansion of Prefrontal Cortex in Great Apes and Humans. *Curr Biol.* 27(5); 714-720.
290. Mesulam MM. (2015) Fifty years of disconnection syndromes and the Geschwind legacy. *Brain.* 138(Pt 9); 2791-9
291. Uylings HB, van Eden CG. (1990) Qualitative and quantitative comparison of the prefrontal cortex in rat and in primates, including humans. *Prog Brain Res.* 85; 31-62.
292. Preuss TM. (1995) Do rats have prefrontal cortex? The rose-woolsey-akert program reconsidered. *J Cogn Neurosci.* 7(1); 1-24.
293. Van De Werd HJ, Rajkowska G, Evers P, Uylings HB. (2010) Cytoarchitectonic and chemoarchitectonic characterization of the prefrontal cortical areas in the mouse. *Brain Struct Funct.* 214(4); 339-53.
294. Muralidhar S, Wang Y, Markram H. (2014) Synaptic and cellular organization of layer 1 of the developing rat somatosensory cortex. *Front Neuroanat.* 7; 52.
295. Miller KD, Pinto DJ, Simons DJ. (2001) Processing in layer 4 of the neocortical circuit: new insights from visual and somatosensory cortex. *Curr Opin Neurobiol.* 11(4); 488-97.

296. Radnikow G, Feldmeyer D. (2018) Layer- and Cell Type-Specific Modulation of Excitatory Neuronal Activity in the Neocortex. *Front Neuroanat.* 12; 1.
297. Defelipe J, Fariñas I. (1992) The pyramidal neuron of the cerebral cortex: morphological and chemical characteristics of the synaptic inputs. *Prog Neurobiol.* 39(6); 563-607.
298. Gabbott PL, Dickie BG, Vaid RR, Headlam AJ, Bacon SJ. (1997) Local-circuit neurones in the medial prefrontal cortex (areas 25, 32 and 24b) in the rat: morphology and quantitative distribution. *J Comp Neurol.* 377(4); 465-99.
299. Kawaguchi Y, Kubota Y. (1997) GABAergic cell subtypes and their synaptic connections in rat frontal cortex. *Cereb Cortex.* 7(6); 476-86.
300. Kvitsiani D, Ranade S, Hangya B, Taniguchi H, Huang JZ, Kepecs A. (2013) Distinct behavioural and network correlates of two interneuron types in prefrontal cortex. *Nature.* 498(7454); 363-6.
301. Heidbreder CA, Groenewegen HJ. (2003) The medial prefrontal cortex in the rat: evidence for a dorso-ventral distinction based upon functional and anatomical characteristics. *Neurosci Biobehav Rev.* 27(6); 555-79.
302. Kummer KK, Mitrić M, Kalpachidou T, Kress M. (2020) The Medial Prefrontal Cortex as a Central Hub for Mental Comorbidities Associated with Chronic Pain. *Int J Mol Sci.* 21(10); 3440.
303. Green SA, Hernandez L, Bookheimer SY, Dapretto M. (2017) Reduced modulation of thalamocortical connectivity during exposure to sensory stimuli in ASD. *Autism Res.* 10(5); 801-809.
304. Mazade R, Alonso JM. (2017) Thalamocortical processing in vision. *Vis Neurosci.* 34; E007.
305. Beierlein M, Connors BW. (2002) Short-term dynamics of thalamocortical and intracortical synapses onto layer 6 neurons in neocortex. *J Neurophysiol.* 88(4); 1924-32.
306. Aston-Jones G, Cohen JD. (2005) Adaptive gain and the role of the locus coeruleus-norepinephrine system in optimal performance. *J Comp Neurol.* 493(1); 99-110.

307. Bloem B, Poorthuis RB, Mansvelder HD. (2014) Cholinergic modulation of the medial prefrontal cortex: the role of nicotinic receptors in attention and regulation of neuronal activity. *Front Neural Circuits*. 8; 17.
308. Glantz LA, Lewis DA. (2000) Decreased dendritic spine density on prefrontal cortical pyramidal neurons in schizophrenia. *Arch Gen Psychiatry*. 57(1); 65-73.
309. Toriumi K, Oki M, Muto E, Tanaka J, Mouri A, Mamiya T, Kim HC, Nabeshima T. (2016) Prenatal phencyclidine treatment induces behavioral deficits through impairment of GABAergic interneurons in the prefrontal cortex. *Psychopharmacology (Berl)*. 233(12); 2373-81.
310. McKibben CE, Jenkins TA, Adams HN, Harte MK, Reynolds GP. (2010) Effect of pretreatment with risperidone on phencyclidine-induced disruptions in object recognition memory and prefrontal cortex parvalbumin immunoreactivity in the rat. *Behav Brain Res*. 208(1); 132-6.
311. Hu H, Gan J, Jonas P. (2014) Interneurons. Fast-spiking, parvalbumin⁺ GABAergic interneurons: from cellular design to microcircuit function. *Science*. 345(6196); 1255263.
312. Howard MW, Rizzuto DS, Caplan JB, Madsen JR, Lisman J, Aschenbrenner-Scheibe R, Schulze-Bonhage A, Kahana MJ. (2003) Gamma oscillations correlate with working memory load in humans. *Cereb Cortex*. 13(12); 1369-74.
313. Lundqvist M, Rose J, Herman P, Brincat SL, Buschman TJ, Miller EK. (2016) Gamma and Beta Bursts Underlie Working Memory. *Neuron*. 90(1); 152-164.
314. Cardin JA, Carlén M, Meletis K, Knoblich U, Zhang F, Deisseroth K, Tsai LH, Moore CI. (2009) Driving fast-spiking cells induces gamma rhythm and controls sensory responses. *Nature*. 459(7247); 663-7.
315. Rojas DC, Wilson LB. (2014) γ -band abnormalities as markers of autism spectrum disorders. *Biomark Med*. 8(3); 353-68.
316. McNally JM, McCarley RW. (2016) Gamma band oscillations: a key to understanding schizophrenia symptoms and neural circuit abnormalities. *Curr Opin Psychiatry*. 29(3); 202-10.
317. Carlén M, Meletis K, Siegle JH, Cardin JA, Futai K, Vierling-Claassen D, Rühlmann C, Jones SR, Deisseroth K, Sheng M, Moore CI, Tsai LH. (2012) A critical

- role for NMDA receptors in parvalbumin interneurons for gamma rhythm induction and behavior. *Mol Psychiatry*. 17(5); 537-48.
318. Cochran SM, Fujimura M, Morris BJ, Pratt JA. (2002) Acute and delayed effects of phencyclidine upon mRNA levels of markers of glutamatergic and GABAergic neurotransmitter function in the rat brain. *Synapse*. 46(3); 206-14.
319. Steullet P, Cabungcal JH, Coyle J, Didriksen M, Gill K, Grace AA, Hensch TK, LaMantia AS, Lindemann L, Maynard TM, Meyer U, Morishita H, O'Donnell P, Puhl M, Cuenod M, Do KQ. (2017) Oxidative stress-driven parvalbumin interneuron impairment as a common mechanism in models of schizophrenia. *Mol Psychiatry*. 22(7); 936-943.
320. Lewis DA, Curley AA, Glausier JR, Volk DW. (2012) Cortical parvalbumin interneurons and cognitive dysfunction in schizophrenia. *Trends Neurosci*. 35(1); 57-67.
321. Rossier J, Bernard A, Cabungcal JH, Perrenoud Q, Savoye A, Gallopin T, Hawrylycz M, Cuénod M, Do K, Urban A, Lein ES. (2015) Cortical fast-spiking parvalbumin interneurons enwrapped in the perineuronal net express the metalloproteinases Adamts8, Adamts15 and Neprilysin. *Mol Psychiatry*. 20(2); 154-61.
322. Do KQ, Cuenod M, Hensch TK. Targeting Oxidative Stress and Aberrant Critical Period Plasticity in the Developmental Trajectory to Schizophrenia. *Schizophr Bull*. 41(4); 835-46.
323. Bernard C, Prochiantz A. (2016) Otx2-PNN Interaction to Regulate Cortical Plasticity. *Neural Plast*. 2016; 7931693.
324. Kwok JC, Dick G, Wang D, Fawcett JW. (2011) Extracellular matrix and perineuronal nets in CNS repair. *Dev Neurobiol*. 71(11); 1073-89.
325. Cabungcal JH, Steullet P, Morishita H, Kraftsik R, Cuenod M, Hensch TK, Do KQ. (2013) Perineuronal nets protect fast-spiking interneurons against oxidative stress. *Proc Natl Acad Sci U S A*. 110(22); 9130-5.
326. Mauney SA, Athanas KM, Pantazopoulos H, Shaskan N, Passeri E, Berretta S, Woo TU. (2013) Developmental pattern of perineuronal nets in the human prefrontal cortex and their deficit in schizophrenia. *Biol Psychiatry*. 74(6); 427-35.

327. Gandal MJ, Nesbitt AM, McCurdy RM, Alter MD. (2012) Measuring the maturity of the fast-spiking interneuron transcriptional program in autism, schizophrenia, and bipolar disorder. *PLoS One*. 7(8); e41215.
328. Nakatani-Pawlak A, Yamaguchi K, Tatsumi Y, Mizoguchi H, Yoneda Y. (2009) Neonatal phencyclidine treatment in mice induces behavioral, histological and neurochemical abnormalities in adulthood. *Biol Pharm Bull*. 32(9); 1576-83.
329. Homayoun H, Moghaddam B. (2007) NMDA receptor hypofunction produces opposite effects on prefrontal cortex interneurons and pyramidal neurons. *J Neurosci*. 27(43); 11496-500.
330. Paasonen J, Salo RA, Ihalainen J, Leikas JV, Savolainen K, Lehtonen M, Forsberg MM, Gröhn O. (2017) Dose-response effect of acute phencyclidine on functional connectivity and dopamine levels, and their association with schizophrenia-like symptom classes in rat. *Neuropharmacology*. 119; 15-25.
331. Monyer H, Burnashev N, Laurie DJ, Sakmann B, Seeburg PH. (1994) Developmental and regional expression in the rat brain and functional properties of four NMDA receptors. *Neuron*. 12(3); 529-40.
332. Karavanova I, Vasudevan K, Cheng J, Buonanno A. (2007) Novel regional and developmental NMDA receptor expression patterns uncovered in NR2C subunit-beta-galactosidase knock-in mice. *Mol Cell Neurosci*. 34(3); 468-80.
333. Santana N, Troyano-Rodriguez E, Mengod G, Celada P, Artigas F. (2011) Activation of thalamocortical networks by the N-methyl-D-aspartate receptor antagonist phencyclidine: reversal by clozapine. *Biol Psychiatry*. 69(10); 918-27.
334. Cadinu D, Grayson B, Podda G, Harte MK, Doostdar N, Neill JC. (2018) NMDA receptor antagonist rodent models for cognition in schizophrenia and identification of novel drug treatments, an update. *Neuropharmacology*. 142; 41-62.
335. Gigg J, McEwan F, Smausz R, Neill J, Harte MK. (2020) Synaptic biomarker reduction and impaired cognition in the sub-chronic PCP mouse model for schizophrenia. *J Psychopharmacol*. 34(1); 115-124.
336. Seshadri S, Klaus A, Winkowski DE, Kanold PO, Plenz D. (2018) Altered avalanche dynamics in a developmental NMDA-R hypofunction model of cognitive impairment. *Transl Psychiatry*. 8(1); 3.

337. Lisman JE, Pi HJ, Zhang Y, Otmakhova NA. (2010) A thalamo-hippocampal-ventral tegmental area loop may produce the positive feedback that underlies the psychotic break in schizophrenia. *Biol Psychiatry*. 68(1); 17-24.
338. Santana N, Mengod G, Artigas F. (2009) Quantitative analysis of the expression of dopamine D1 and D2 receptors in pyramidal and GABAergic neurons of the rat prefrontal cortex. *Cereb Cortex*. 19(4); 849-60.
339. de Almeida J, Mengod G. (2007) Quantitative analysis of glutamatergic and GABAergic neurons expressing 5-HT(2A) receptors in human and monkey prefrontal cortex. *J Neurochem*. 103(2); 475-86.
340. Kargieman L, Santana N, Mengod G, Celada P, Artigas F. (2007) Antipsychotic drugs reverse the disruption in prefrontal cortex function produced by NMDA receptor blockade with phencyclidine. *Proc Natl Acad Sci U S A*. 104(37); 14843-8.
341. Kuroda M. (1998) Synaptic connections between the prefrontal cortex and the mediodorsal nucleus of the thalamus. *Kaibogaku Zasshi*. 73(2); 93-106.
342. Zhang Y, Llinas RR, Lisman JE. (2009) Inhibition of NMDA-Rs in the Nucleus Reticularis of the Thalamus Produces Delta Frequency Bursting. *Front Neural Circuits*. 3; 20.
343. Zhang Y, Yoshida T, Katz DB, Lisman JE. (2012) NMDA-R antagonist action in thalamus imposes δ oscillations on the hippocampus. *J Neurophysiol*. 107(11); 3181-9.
344. Kiss T, Hoffmann WE, Hajós M. (2011) Delta oscillation and short-term plasticity in the rat medial prefrontal cortex: modelling NMDA dysfunction of schizophrenia. *Int J Neuropsychopharmacol*. 14(1); 29-42.
345. López Hill X, Scorza MC. (2012) Role of the anterior thalamic nucleus in the motor hyperactivity induced by systemic MK-801 administration in rats. *Neuropharmacology*. 62(7); 2440-6.
346. López-Gil X, Babot Z, Amargós-Bosch M, Suñol C, Artigas F, Adell A. (2007) Clozapine and haloperidol differently suppress the MK-801-increased glutamatergic and serotonergic transmission in the medial prefrontal cortex of the rat. *Neuropsychopharmacology*. 32(10); 2087-97.
347. Steriade M. (2001) The GABAergic reticular nucleus: a preferential target of corticothalamic projections. *Proc Natl Acad Sci U S A*. 98(7); 3625-7.

348. Jones EG. (2002) Thalamic circuitry and thalamocortical synchrony. *Philos Trans R Soc Lond B Biol Sci.* 357(1428); 1659-73.
349. Camchong J, MacDonald AW 3rd, Bell C, Mueller BA, Lim KO. (2011) Altered functional and anatomical connectivity in schizophrenia. *Schizophr Bull.* 37(3); 640-50.
350. Hudson MR, Sokolenko E, O'Brien TJ, Jones NC. (2020) NMDA receptors on parvalbumin-positive interneurons and pyramidal neurons both contribute to MK-801 induced gamma oscillatory disturbances: Complex relationships with behaviour. *Neurobiol Dis.* 134; 104625.
351. Llinás RR, Steriade M. (2006) Bursting of thalamic neurons and states of vigilance. *J Neurophysiol.* 95(6); 3297-308
352. González-Maeso J, Sealfon SC. (2009) Psychedelics and schizophrenia. *Trends Neurosci.* 32(4); 225-32.
353. Nichols CD, Sanders-Bush E. (2004) Molecular genetic responses to lysergic acid diethylamide include transcriptional activation of MAP kinase phosphatase-1, C/EBP-beta and ILAD-1, a novel gene with homology to arrestins. *J Neurochem.* 90(3); 576-84.
354. Meltzer HY, Park S, Kessler R. (1999) Cognition, schizophrenia, and the atypical antipsychotic drugs. *Proc Natl Acad Sci U S A.* 96(24); 13591-3.
355. Khandaker GM, Dantzer R. (2016) Is there a role for immune-to-brain communication in schizophrenia? *Psychopharmacology (Berl).* 233(9); 1559-73.
356. Miller BJ, Goldsmith DR. (2020) Evaluating the Hypothesis That Schizophrenia Is an Inflammatory Disorder. *Focus (Am Psychiatr Publ).* 18(4); 391-401.
357. Müller N. (2018) Inflammation in Schizophrenia: Pathogenetic Aspects and Therapeutic Considerations. *Schizophr Bull.* 44(5); 973-982.
358. Kubicki M, McCarley R, Westin CF, Park HJ, Maier S, Kikinis R, Jolesz FA, Shenton ME. (2007) A review of diffusion tensor imaging studies in schizophrenia. *J Psychiatr Res.* 41(1-2); 15-30.
359. Uranova NA, Vostrikov VM, Vikhрева OV, Zimina IS, Kolomeets NS, Orlovskaya DD. (2007) The role of oligodendrocyte pathology in schizophrenia. *Int J Neuropsychopharmacol.* 10(4); 537-45.
360. Pasternak O, Westin CF, Bouix S, Seidman LJ, Goldstein JM, Woo TU, Petryshen TL, Mesholam-Gately RI, McCarley RW, Kikinis R, Shenton ME, Kubicki M. (2012)

- Excessive extracellular volume reveals a neurodegenerative pattern in schizophrenia onset. *J Neurosci.* 32(48); 17365-72.
361. Pasternak O, Sochen N, Gur Y, Intrator N, Assaf Y. (2009) Free water elimination and mapping from diffusion MRI. *Magn Reson Med.* 62(3); 717-30.
362. Najjar S, Pearlman DM. (2015) Neuroinflammation and white matter pathology in schizophrenia: systematic review. *Schizophr Res.* 161(1); 102-12.
363. Bernstein HG, Steiner J, Guest PC, Dobrowolny H, Bogerts B. (2015) Glial cells as key players in schizophrenia pathology: recent insights and concepts of therapy. *Schizophr Res.* 161(1); 4-18.
364. Mattei D, Djodari-Irani A, Hadar R, Pelz A, de Cossío LF, Goetz T, Matyash M, Kettenmann H, Winter C, Wolf SA. (2014) Minocycline rescues decrease in neurogenesis, increase in microglia cytokines and deficits in sensorimotor gating in an animal model of schizophrenia. *Brain Behav Immun.* 38; 175-84.
365. Zhu S, Wang H, Shi R, Zhang R, Wang J, Kong L, Sun Y, He J, Kong J, Wang JF, Li XM. (2014) Chronic phencyclidine induces inflammatory responses and activates GSK3 β in mice. *Neurochem Res.* 39(12); 2385-93.
366. Krügel U. (2016) Purinergic receptors in psychiatric disorders. *Neuropharmacology.* 104; 212-25.
367. Basso AM, Bratcher NA, Harris RR, Jarvis MF, Decker MW, Rueter LE. (2009) Behavioral profile of P2X7 receptor knockout mice in animal models of depression and anxiety: relevance for neuropsychiatric disorders. *Behav Brain Res.* 198(1); 83-90.
368. Boucher AA, Arnold JC, Hunt GE, Spiro A, Spencer J, Brown C, McGregor IS, Bennett MR, Kassiou M. (2011) Resilience and reduced c-Fos expression in P2X7 receptor knockout mice exposed to repeated forced swim test. *Neuroscience.* 189; 170-7.
369. Bhattacharya A, Wang Q, Ao H, Shoblock JR, Lord B, Aluisio L, Fraser I, Nepomuceno D, Neff RA, Welty N, Lovenberg TW, Bonaventure P, Wickenden AD, Letavic MA. (2013) Pharmacological characterization of a novel centrally permeable P2X7 receptor antagonist: JNJ-47965567. *Br J Pharmacol.* 170(3); 624-40.
370. Lord B, Aluisio L, Shoblock JR, Neff RA, Varlinskaya EI, Ceusters M, Lovenberg TW, Carruthers N, Bonaventure P, Letavic MA, Deak T, Drinkenburg W, Bhattacharya

- A. (2014) Pharmacology of a novel central nervous system-penetrant P2X7 antagonist JNJ-42253432. *J Pharmacol Exp Ther.* 351(3); 628-41.
371. Gubert C, Fries GR, Pfaffenseller B, Ferrari P, Coutinho-Silva R, Morrone FB, Kapczinski F, Battastini AMO. (2016) Role of P2X7 Receptor in an Animal Model of Mania Induced by D-Amphetamine. *Mol Neurobiol.* 53(1); 611-620.
372. Gubert C, Andrejew R, Leite CE, Moritz CEJ, Scholl J, Figueiro F, Kapczinski F, da Silva Magalhães PV, Battastini AMO. (2020) P2X7 Purinergic Receptor Is Involved in the Pathophysiology of Mania: a Preclinical Study. *Mol Neurobiol.* 57(3); 1347-1360.
373. Fernandes NC, Sriram U, Gofman L, Cenna JM, Ramirez SH, Potula R. (2016) Methamphetamine alters microglial immune function through P2X7R signaling. *J Neuroinflammation.* 13(1); 91.
374. Rubio-Araiz A, Perez-Hernandez M, Urrutia A, Porcu F, Borcel E, Gutierrez-Lopez MD, O'Shea E, Colado MI. (2014) 3,4-Methylenedioxymethamphetamine (MDMA, ecstasy) disrupts blood-brain barrier integrity through a mechanism involving P2X7 receptors. *Int J Neuropsychopharmacol.* 17(8); 1243-55.
375. Pérez-Hernández M, Fernández-Valle ME, Rubio-Araiz A, Vidal R, Gutiérrez-López MD, O'Shea E, Colado MI. (2017) 3,4-Methylenedioxymethamphetamine (MDMA, ecstasy) produces edema due to BBB disruption induced by MMP-9 activation in rat hippocampus. *Neuropharmacology.* 118; 157-166.
376. Inoue K, Koizumi S, Ueno S. (1996) Implication of ATP receptors in brain functions. *Prog Neurobiol.* 50(5-6); 483-92.
377. Khakh BS, Gittermann D, Cockayne DA, Jones A. (2003) ATP modulation of excitatory synapses onto interneurons. *J Neurosci.* 23(19); 7426-37.
378. Bowser DN, Khakh BS. (2007) Vesicular ATP is the predominant cause of intercellular calcium waves in astrocytes. *J Gen Physiol.* 129(6); 485-91.
379. Mahmoud S, Gharagozloo M, Simard C, Gris D. (2019) Astrocytes Maintain Glutamate Homeostasis in the CNS by Controlling the Balance between Glutamate Uptake and Release. *Cells.* 8(2);184.
380. Cunha RA. (2005) Neuroprotection by adenosine in the brain: From A(1) receptor activation to A (2A) receptor blockade. *Purinergic Signal.* 1(2); 111-34.
381. Ciruela F, Casadó V, Rodrigues RJ, Luján R, Burgueño J, Canals M, Borycz J, Rebola N, Goldberg SR, Mallol J, Cortés A, Canela EI, López-Giménez JF, Milligan G,

- Lluis C, Cunha RA, Ferré S, Franco R. (2006) Presynaptic control of striatal glutamatergic neurotransmission by adenosine A1-A2A receptor heteromers. *J Neurosci.* 26(7); 2080-7.
382. Marchi M, Raiteri L, Risso F, Vallarino A, Bonfanti A, Monopoli A, Ongini E, Raiteri M. (2002) Effects of adenosine A1 and A2A receptor activation on the evoked release of glutamate from rat cerebrocortical synaptosomes. *Br J Pharmacol.* 136(3); 434-40.
383. Sarantis K, Tsiamaki E, Kouvaros S, Papatheodoropoulos C, Angelatou F. (2015) Adenosine A₂A receptors permit mGluR5-evoked tyrosine phosphorylation of NR2B (Tyr1472) in rat hippocampus: a possible key mechanism in NMDA receptor modulation. *J Neurochem.* 135(4); 714-26.
384. Borycz J, Pereira MF, Melani A, Rodrigues RJ, Köfalvi A, Panlilio L, Pedata F, Goldberg SR, Cunha RA, Ferré S. (2007) Differential glutamate-dependent and glutamate-independent adenosine A1 receptor-mediated modulation of dopamine release in different striatal compartments. *J Neurochem.* 101(2); 355-63.
385. Brunstein MG, Ghisolfi ES, Ramos FL, Lara DR. (2005) A clinical trial of adjuvant allopurinol therapy for moderately refractory schizophrenia. *J Clin Psychiatry.* 66(2); 213-9.
386. Wonodi I, Gopinath HV, Liu J, Adami H, Hong LE, Allen-Emerson R, McMahon RP, Thaker GK. (2011) Dipyridamole monotherapy in schizophrenia: pilot of a novel treatment approach by modulation of purinergic signaling. *Psychopharmacology (Berl).* 218(2); 341-5.
387. Villar-Menéndez I, Díaz-Sánchez S, Blanch M, Albasanz JL, Pereira-Veiga T, Monje A, Planchat LM, Ferrer I, Martín M, Barrachina M. (2014) Reduced striatal adenosine A2A receptor levels define a molecular subgroup in schizophrenia. *J Psychiatr Res.* 51; 49-59.
388. Moscoso-Castro M, Gracia-Rubio I, Ciruela F, Valverde O. (2016) Genetic blockade of adenosine A2A receptors induces cognitive impairments and anatomical changes related to psychotic symptoms in mice. *Eur Neuropsychopharmacol.* 26(7); 1227-40.
389. Matos M, Shen HY, Augusto E, Wang Y, Wei CJ, Wang YT, Agostinho P, Boison D, Cunha RA, Chen JF. (2015) Deletion of adenosine A2A receptors from

- astrocytes disrupts glutamate homeostasis leading to psychomotor and cognitive impairment: relevance to schizophrenia. *Biol Psychiatry*. 78(11); 763-74.
390. Aliagas E, Villar-Menéndez I, Sévigny J, Roca M, Romeu M, Ferrer I, Martín-Satué M, Barrachina M. (2013) Reduced striatal ecto-nucleotidase activity in schizophrenia patients supports the "adenosine hypothesis". *Purinergic Signal*. 9(4); 599-608.
391. Cheffer A, Castillo ARG, Corrêa-Velloso J, Gonçalves MCB, Naaldijk Y, Nascimento IC, Burnstock G, Ulrich H. (2018) Purinergic system in psychiatric diseases. *Mol Psychiatry*. 23(1); 94-106.
392. Luthardt J, Borvendeg SJ, Sperlagh B, Poelchen W, Wirkner K, Illes P. (2003) P2Y(1) receptor activation inhibits NMDA receptor-channels in layer V pyramidal neurons of the rat prefrontal and parietal cortex. *Neurochem Int*. 42(2); 161-72.
393. Guzman SJ, Schmidt H, Franke H, Krügel U, Eilers J, Illes P, Gerevich Z. (2010) P2Y1 receptors inhibit long-term depression in the prefrontal cortex. *Neuropharmacology*. 59(6); 406-15.
394. Koch H, Bernalov A, Drescher K, Franke H, Krügel U. (2015) Impaired cognition after stimulation of P2Y1 receptors in the rat medial prefrontal cortex. *Neuropsychopharmacology*. 40(2); 305-14.
395. Franke H, Kittner H, Grosche J, Illes P. (2003) Enhanced P2Y1 receptor expression in the brain after sensitisation with d-amphetamine. *Psychopharmacology (Berl)*. 167(2); 187-94.
396. Zhang YX, Yamashita H, Ohshita T, Sawamoto N, Nakamura S. (1995) ATP increases extracellular dopamine level through stimulation of P2Y purinoceptors in the rat striatum. *Brain Res*. 691(1-2); 205-12.
397. Hempel C, Nörenberg W, Sobottka H, Urban N, Nicke A, Fischer W, Schaefer M. (2013) The phenothiazine-class antipsychotic drugs prochlorperazine and trifluoperazine are potent allosteric modulators of the human P2X7 receptor. *Neuropharmacology*. 75; 365-79.
398. Nabeshima T, Ishikawa K, Yamaguchi K, Furukawa H, and Kameyama T. (1987) Phencyclidine-induced head-weaving observed in mice after ritanserin treatment. *Eur. J. Pharmacol*. 139; 171-178.

399. Sams-Dodd F. (1995) Automation of the social interaction test by a video-tracking system: behavioural effects of repeated phencyclidine treatment. *J. Neurosci. Methods.* 59; 157-167.
400. Chaudhuri A, Zangenehpour S, Rahbar-Dehgan F, and Ye F. (2000) Molecular maps of neural activity and quiescence. in *Acta Neurobiologiae Experimentalis.* 60(3); 403-410.
401. Schindelin J, Arganda-Carreras I, Frise E, Kaynig V, Longair M, Pietzsch T, Preibisch S, Rueden C, Saalfeld S, Schmid B, Tinevez JY, White DJ, Hartenstein V, Eliceiri K, Tomancak P, Cardona A. (2012) Fiji: an open-source platform for biological-image analysis. *Nat. Methods.* 9(7): 676-682.
402. Ferreira TA, Blackman AV, Oyrer J, Jayabal S, Chung AJ, Watt AJ, Sjöström PJ, van Meyel DJ (2014) Neuronal morphometry directly from bitmap images. *Nat. Methods.* 11(10); 982–984.
403. Dénes Á, Humphreys N, Lane TE, Grecis R, Rothwell N. (2010) Chronic systemic infection exacerbates ischemic brain damage via a CCL5 (regulated on activation, normal T-cell expressed and secreted)-mediated proinflammatory response in mice. *J. Neurosci.* 30; 10086-10095.
404. Franklin KBJ., & Paxinos G. (1997) The mouse brain in stereotaxic coordinates.
405. Day HE, Kryskow EM, Nyhuis TJ, Herlihy L, Campeau S. (2008) Conditioned fear inhibits c-fos mRNA expression in the central extended amygdala. *Brain Res.* 1229; 137-146.
406. Chung L. (2015) A brief introduction to the transduction of neural activity into fos signal. *Dev. Reprod.* 19; 61-67.
407. Fekete Á, Franklin L, Ikemoto T, Rózsa B, Lendvai B, Sylvester Vizi E, Zelles T. (2009) Mechanism of the persistent sodium current activator veratridine-evoked Ca²⁺ elevation: Implication for epilepsy. *J. Neurochem.* 111(3); 745-756.
408. Butovsky O, Jedrychowski MP, Moore CS, Cialic R, Lanser AJ, Gabriely G, Koeglsperger T, Dake B, Wu PM, Doykan CE, Fanek Z, Liu L, Chen Z, Rothstein JD, Ransohoff RM, Gygi SP, Antel JP, Weiner HL. (2014) Identification of a unique TGF- β -dependent molecular and functional signature in microglia. *Nat. Neurosci.* 17; 131-143.

409. Giacobazzo G, Apolloni S, Coccorello R. (2018) Loss of P2X7 receptor function dampens whole body energy expenditure and fatty acid oxidation. *Purinergic Signal.* 14; 299-305.
410. Elsworth JD, Groman SM, Jentsch JD, Leranath C, Redmond DE Jr, Kim JD, Diano S, Roth RH. (2014) Primate phencyclidine model of schizophrenia: sex-specific effects on cognition, brain derived neurotrophic factor, spine synapses, and dopamine turnover in prefrontal cortex. *Int. J. Neuropsychopharmacol.* 18(6); pyu048.
411. Eyo UB, Mo M, Yi MH, Murugan M, Liu J, Yarlagadda R, Margolis DJ, Xu P, Wu LJ. (2018) P2Y12R-dependent translocation mechanisms gate the changing microglial landscape. *Cell Rep.* 23(4); 959-966.
412. Liu YU, Ying Y, Li Y, Eyo UB, Chen T, Zheng J, Umpierre AD, Zhu J, Bosco DB, Dong H, Wu LJ. (2019) Neuronal network activity controls microglial process surveillance in awake mice via norepinephrine signaling. *Nat. Neurosci.* 22(11); 1771-1781.
413. Pan WHT and Lai YJ. (1995) Anesthetics decreased the microdialysis extraction fraction of norepinephrine but not dopamine in the medial prefrontal cortex. *Synapse.* 21; 85-92.
414. Kehr J, Yoshitake T, Ichinose F, Yoshitake S, Kiss B, Gyertyán I, Adham N. (2018) Effects of cariprazine on extracellular levels of glutamate, GABA, dopamine, noradrenaline and serotonin in the medial prefrontal cortex in the rat phencyclidine model of schizophrenia studied by microdialysis and simultaneous recordings of locomotor activity. *Psychopharmacology (Berl).* 235; 1593-1607.
415. Martínez-Frailes C, Di Lauro C, Bianchi C, de Diego-García L, Sebastián-Serrano Á, Boscá L, Díaz-Hernández M. (2019) Amyloid peptide induced neuroinflammation increases the P2X7 receptor expression in microglial cells, impacting on its functionality. *Front. Cell. Neurosci.* 13; 143.
416. Elgueta D, Aymerich MS, Contreras F, Montoya A, Celorrio M, Rojo-Bustamante E, Riquelme E, González H, Vásquez M, Franco R, Pacheco R. (2017) Pharmacologic antagonism of dopamine receptor D3 attenuates neurodegeneration and motor impairment in a mouse model of parkinson's disease. *Neuropharmacology.* 113(Pt A); 110-123.

417. Díaz-Hernandez M, del Puerto A, Díaz-Hernandez JI, Diez-Zaera M, Lucas JJ, Garrido JJ, Miras-Portugal MT. (2008) Inhibition of the ATP-gated P2X7 receptor promotes axonal growth and branching in cultured hippocampal neurons. *J. Cell Sci.* 121; 3717-28.
418. Lahti AC, Weiler MA, Michaelidis T, Parwani A, Tamminga CA. (2001) Effects of ketamine in normal and schizophrenic volunteers. *Neuropsychopharmacology.* 25; 455-467.
419. Tripathi A, Kar SK, Shukla R. (2018) Cognitive deficits in schizophrenia: understanding the biological correlates and remediation strategies. *Clin.Psychopharmacol. Neurosci.* 16; 7-17.
420. Arnoux I and Audinat E. (2015) Fractalkine signaling and microglia functions in the developing brain. *Neural Plast.* 2015; 689404.
421. Walrave L, Vinken M, Albertini G, De Bundel D, Leybaert L, Smolders IJ. (2016) Inhibition of Connexin43 Hemichannels Impairs Spatial Short-Term Memory without Affecting Spatial Working Memory. *Front Cell Neurosci.* 10; 288.
422. Murueta-Goyena A, Ortuzar N, Lafuente JV, Bengoetxea H. (2020) Enriched Environment Reverts Somatostatin Interneuron Loss in MK-801 Model of Schizophrenia. *Mol Neurobiol.* 57(1):125-134.
423. Piyabhan P, Tingpej P, Duansak N. (2019) Effect of pre- and post-treatment with bacopa monnieri (brahmi) on phencyclidine-induced disruptions in object recognition memory and cerebral calbindin, parvalbumin, and calretinin immunoreactivity in rats. *Neuropsychiatr. Dis. Treat.* 15; 1103-1117.
424. Pechnick RN, Bresee CJ, Poland RE. (2006) The role of antagonism of NMDA receptor-mediated neurotransmission and inhibition of the dopamine reuptake in the neuroendocrine effects of phencyclidine. *Life Sci.* 78; 2006-2011.
425. Pechnick RN, Chun BM, George R, Hanada K, Poland RE. (1990) Determination of the loci of action of phencyclidine on the CNS-pituitary-adrenal axis. *J. Pharmacol. Exp. Ther.* 254, 344-9.
426. Tejedor-Real P, Sahagún M, Biguet NF, Mallet J. (2007) Neonatal handling prevents the effects of phencyclidine in an animal model of negative symptoms of schizophrenia. *Biol. Psychiatry.* 61; 865-872.

10. List of publications

Publications related to this thesis:

Original research articles:

Koványi B¹, Csölle C, Calovi S, Hanuska A, Kató E, Köles L, Bhattacharya A, Haller J, Sperlágh B. (2016) *The role of P2X7 receptors in a rodent PCP-induced schizophrenia model*. **Scientific Reports** Nov 8;6:36680.

Calovi S¹, Mut-Arbona P, Tod P, Iring A, Nicke A, Mato S, Vizi ES, Tønnesen J, Sperlagh B. (2020) *P2X7 Receptor-Dependent Layer-Specific Changes in Neuron-Microglia Reactivity in the Prefrontal Cortex of a Phencyclidine Induced Mouse Model of Schizophrenia*. **Frontiers in Molecular Neuroscience**. Nov 11;13:566251.

Review published in the context of the PhD studies:

Calovi S¹, Mut-Arbona P, Sperlágh B. (2019) *Microglia and the Purinergic Signaling System*. **Neuroscience**. May 1;405:137-147.

11. Acknowledgements

I would like to express my special gratitude to my supervisor, Beáta Sperlág. I am thankful for the opportunity she gave me to develop in her laboratory, transmitting her mentality of patience and scientific optimism that characterizes her successful work, and, especially, for the generosity and human traits that she displayed. I am thankful to all the past and present members of the lab for always being helpful and supportive. Tunde, Gergo, Lilla, Flora, the post doc, Lumei and especially to Paulita, an unsubstitutable peer generous in the most needed moments. Maria, a calm and safe spot of inexhaustible curiosity and good vibrations. I feel ultimately grateful to Jan and his laboratory, at the Achucarro center of Bilbao. He helped me beyond what I would have possibly imagined, and played a key role during a crucial and delicate period with absolute professionalism and humanity. Being an Italian student in the Semmelweis University and MTA KOKI Hungarian institutions, my greatest gratitude goes to the people that are forming this special environment. Beyond the internationally recognized prestige that confers this PhD title and the curricular value of working in this research center, I feel truly honoured for having been part for five years into a unique students' society. Ringrazio i miei amati genitori, papà e mammy, perchè sono le pietre fondanti di tutti e quattro gli angoli. Solo in questi anni di lontananza penso di aver realmente compreso la magnitudine dell'amore che provano per me, e mi mancano. Ogni giorno di più. Voglio che lo sappiano, sebbene io dimostri riluttanza in ammetterlo. Li ringrazio perché questo traguardo è frutto di una educazione orientata alla curiosità più pura e naturale, alla fiducia in me stesso, all'onestà e alla giustizia come valori imprescindibili. Ringrazio mio fratello perchè, dopo tutta la vita, è il migliore amico che chiunque potrebbe desiderare, e la persona che più d'ogni altra gode del mio intimo rispetto e alla quale auguro un futuro brillante, e di farmi a lungo compagnia. Eventually, and most importantly, there is you. My love. I find it so unfair you are appearing just now, just so little, just so silently. You represent a before and after in my life. You found me and I found you, and just this shook a few of my fundamental beliefs. From the moment I started feeling your commitment for you, its depth, my life perspective changed. I hope I will be able to return a fraction of the happiness you provoked.